Quantum mechanics of the fractional-statistics gas: Random-phase approximation

Q. Dai, J. L. Levy, and A. L. Fetter

Department of Physics, Stanford University, Stanford, California 94305

C. B. Hanna

IBM Research Division, Thomas J. Watson Research Center, P.O. Box 218, Yorktown Heights, New York 10598

R. B. Laughlin

Department of Physics, Stanford University, Stanford, California 94305
and Lawrence Livermore National Laboratory, P.O. Box 808, Livermore, California 94550

(Received 4 October 1991)

A description of the fractional-statistics gas based on the complete summation of Hartree, Fock, ladder and bubble diagrams is presented. The superfluid properties identified previously in the random-phase-approximation (RPA) calculation of Fetter, Hanna, and Laughlin [Phys. Rev. B **39**, 9679 (1989)] are substantially confirmed. The discrepancy between the RPA sound speed and the Hartree-Fock bulk modulus is found to be eliminated. The unusual Hall-effect behavior is found to vanish for the Bose gas test case but not for the fractional-statistics gas, implying that it is physically correct. Excellent agreement is obtained with the collective-mode dispersion obtained numerically by Xie, He, and Das Sarma [Phys. Rev. Lett. **65**, 649 (1990)].

I. INTRODUCTION

In this last of three papers on the fractional-statistics gas, we describe in detail the random-phase-approximation (RPA) procedure by which the superfluid properties of this system are explicitly demonstrated. In the two previous papers, we studied the Hartree-Fock ground state[1] of the fractional-statistics gas and the collective-mode spectrum[2] associated with it, and found several behaviors characteristic of a system with a preferred particle density. We attributed this result, which is unphysical because the underlying equations of motion are scale invariant, to the presence of long-range interactions in the Hamiltonian that are handled incorrectly by the Hartree-Fock solution. This is well known from the theory of metals:[3] the Hartree-Fock ground state is not sufficiently accurate at long wavelengths to account for plasma oscillations, which are true quantum-mechanical excitations of the metal. The necessary modification of this ground state, namely, the virtual excitation of macroscopic numbers of long-wavelength compressional sound waves in pairs, is efficiently achieved using the random-phase approximation. The basic premise of this paper is that the formal problems we encounter in the anyon gas are similar to those in an ordinary metal and, thus, have an analogous solution.

The work reported in this paper goes considerably beyond the simple RPA calculation[4] reported previously by us, including exchange, ladder, and three-body RPA graphs. All of these are essential for fully understanding the behavior of the system, particularly at finite temperature. The exchange diagrams, which are formally infinite, must be included to account for the physical behavior of isolated quasiparticles described in our first pa-

per. The ladder diagrams, which are also infinite, must be included because they are required to maintain gauge invariance and because they cancel the divergent exchange energies. The three-body RPA graphs are the same size as the two-body graphs included in our previous calculation and thus are equally relevant. In this expanded form the calculation becomes both consistent with our previous variational work and more logical. However, it also becomes more complex. For this reason we include in this paper a detailed discussion of the relevant Feynman rules and examples of their application.

Let us begin our discussion by restating the problem. By an ideal gas of particles obeying ν fractional statistics we mean a set of spinless fermions confined to move in the x-y plane and described by the Hamiltonian

$$\mathcal{H} = \sum_{i=1}^{N} \frac{1}{2m} \left| \mathbf{P}_i + \frac{e}{c} \mathbf{A}_i \right|^2 , \tag{1.1}$$

where $\mathbf{r}_i$ denotes the two-dimensional vector locating the ith particle in the plane and

$$\mathbf{A}_i = \sum_{j \neq i}^{N} \mathbf{A}_{ij} = (1-\nu) \frac{\hbar c}{e} \hat{\mathbf{z}} \times \sum_{j \neq i}^{N} \frac{\mathbf{r}_i - \mathbf{r}_j}{|\mathbf{r}_i - \mathbf{r}_j|^2} . \tag{1.2}$$

Equation (1.1) has the physical interpretation that each particle interacts with all the others through the vector potential generated by a set of rigidly attached solenoids. We wish to evaluate the ground state and elementary excitations for the case of $\nu = \frac{1}{2}$, which we have argued is appropriate for describing the spinless charged excitation of a Mott insulator. The starting point of our calculations is a Hartree-Fock ground state, which is a single

Slater determinant of the form[1]

$$\Phi_0(\mathbf{r}_1, \ldots, \mathbf{r}_N)$$

$$= \frac{1}{\sqrt{N!}} \sum_\sigma \text{sgn}(\sigma) \varphi_{\sigma(1)}(\mathbf{r}_1) \times \cdots \times \varphi_{\sigma(N)}(\mathbf{r}_N) ,$$

$$(1.3)$$

with orbitals taken to be

$$\varphi_{nk}(z) = \frac{(\frac{1}{2}z - 2\partial/\partial z^*)^n}{(2^n n!)^{1/2}} \frac{(\frac{1}{2}z^* - 2\partial/\partial z)^k}{(2^k k!)^{1/2}} \frac{e^{-|z|^2/4}}{(2\pi)^{1/2}} ,$$

$$(1.4)$$

where k indexes the state's angular momentum, $n \geq 0$ is its Landau-level index, and $z = x + iy$ is $\mathbf{r}$ expressed as a complex number. In writing Eq. (1.4) we have used dimensionless units in which the effective cyclotron energy

$$\hbar\omega_c = \hbar\frac{eB}{mc} = 2\pi(1-\nu)\frac{\hbar^2}{m}\bar{\rho} = (1-\nu)E_f ,$$

$$(1.5)$$

where $\bar{\rho}$ is the mean particle density and E_f is the Fermi energy of a gas of spinless fermions at this density, and the corresponding magnetic length

$$a_0 = \left[\frac{hc/e}{2\pi B}\right]^{1/2} = [2\pi(1-\nu)\bar{\rho}]^{-1/2}$$

$$(1.6)$$

is set to unity. In the Hartree-Fock ground state, orbitals with $n < (1-\nu)^{-1}$ are occupied, and the rest are empty. The special values of ν we associate with superfluidity are those for which $(1-\nu)^{-1}$ is an integer.

Let us now introduce the particle density,

$$\rho(\mathbf{r}) = \sum_{i=1}^N \delta(\mathbf{r} - \mathbf{r}_i) ,$$

$$(1.7)$$

and current density,

$$\mathbf{J}(\mathbf{r}) = \sum_{i=1}^N \frac{1}{2m}\left\{\mathbf{P}_i + \frac{e}{c}\mathbf{A}_i, \delta(\mathbf{r} - \mathbf{r}_i)\right\} ,$$

$$(1.8)$$

operators through which externally applied scalar and vector potentials couple to the system. Our main objective in this paper will be to compute the linear response of the system to such perturbations. The current-density operator includes a term proportional to the two-body vector potential $\mathbf{A}_i$, as required by gauge invariance and compatibility with the continuity equation

$$[\mathcal{H}, \rho(\mathbf{r})] = i\hbar\nabla\cdot\mathbf{J}(\mathbf{r}) .$$

$$(1.9)$$

Let us also introduce a "mean-field" current-density operator

$$\mathbf{j}(\mathbf{r}) = \sum_{i=1}^N \frac{1}{2m}\left\{\mathbf{P}_i + \frac{e}{c}\overline{\mathbf{A}}_i, \delta(\mathbf{r} - \mathbf{r}_i)\right\} ,$$

$$(1.10)$$

where

$$\overline{\mathbf{A}} = (1-\nu)\frac{hc}{2e}\bar{\rho}\hat{z}\times\mathbf{r} = \frac{1}{2}\mathbf{B}\times\mathbf{r} ,$$

$$(1.11)$$

which does *not* satisfy Eq. (1.9), but which will appear re-

peatedly in perturbative expansions. The Fourier transforms of these operators are given as usual by

$$\rho_\mathbf{q} = \int \rho(\mathbf{r})e^{-i\mathbf{q}\cdot\mathbf{r}}d\mathbf{r} = \sum_{j=1}^N e^{-i\mathbf{q}\cdot\mathbf{r}_j} ,$$

$$(1.12)$$

$$\mathbf{J}_\mathbf{q} = \int \mathbf{J}(\mathbf{r})e^{-i\mathbf{q}\cdot\mathbf{r}}d\mathbf{r}$$

$$= \sum_{j=1}^N \frac{1}{2m}\left\{\mathbf{P}_j + \frac{e}{c}\mathbf{A}_j, e^{-i\mathbf{q}\cdot\mathbf{r}_j}\right\} ,$$

$$(1.13)$$

and

$$\mathbf{j}_\mathbf{q} = \int \mathbf{j}(\mathbf{r})e^{-i\mathbf{q}\cdot\mathbf{r}}d\mathbf{r}$$

$$= \sum_{j=1}^N \frac{1}{2m}\left\{\mathbf{P}_j + \frac{e}{c}\overline{\mathbf{A}}_j, e^{-i\mathbf{q}\cdot\mathbf{r}_j}\right\} .$$

$$(1.14)$$

II. PHONON ANALOGY

In our previous work[2] we found that the state $\rho_\mathbf{q}|\Phi_0\rangle$, with $|\Phi_0\rangle$ and $\rho_\mathbf{q}$ defined as in Eqs. (1.3) and (1.12), which represents a compressional sound wave, had a finite positive expected excitation energy in the $\mathbf{q}\to 0$ limit. To understand the physical origin of this gap and its subsequent destruction by the RPA, which are central to our description of anyon superfluidity, it is helpful to consider the analogous error that occurs if the ground state $|\Phi_P\rangle$ of the phonon Hamiltonian

$$\mathcal{H}_P = \sum_j \left\{-\frac{\hbar^2}{2M}\left[\frac{\partial}{\partial x_j}\right]^2 + \frac{1}{2}K(x_j - x_{j+1})^2\right\}$$

$$(2.1)$$

is approximated by the ground state $|\Phi_E\rangle$ of the Einstein Hamiltonian

$$\mathcal{H}_E = \sum_j \left\{-\frac{\hbar^2}{2M}\left[\frac{\partial}{\partial x_j}\right]^2 + Kx_j^2\right\} ,$$

$$(2.2)$$

which lacks translational invariance.[5] For convenience, let us define the coordinates

$$x_q = \sum_j^N e^{-iqr_j}x_j ,$$

$$(2.3)$$

where N is the number of particles and r_j is the quiescent location of the jth particle, in terms of which we may write

$$\mathcal{H}_P = \sum_q \left\{-\frac{N}{2}\frac{\hbar^2}{M}\left[\frac{\partial}{\partial x_q}\right]\left[\frac{\partial}{\partial x_{-q}}\right] + \frac{1}{2}\frac{M}{N}\omega_q^2 x_q x_{-q}\right\}$$

$$(2.4)$$

and

$$\mathcal{H}_E = \sum_q \left\{-\frac{N}{2}\frac{\hbar^2}{M}\left[\frac{\partial}{\partial x_q}\right]\left[\frac{\partial}{\partial x_{-q}}\right] + \frac{1}{2}\frac{M}{N}\omega_E^2 x_q x_{-q}\right\} ,$$

$$(2.5)$$

where

$$\omega_E = \left[2\frac{K}{M} \right]^{1/2} , \quad \omega_q = \omega_E \sqrt{1 - \cos(qb_0)} , \qquad (2.6)$$

with b_0 denoting the bond length. This decouples the harmonic oscillators and enables us to express the ground states as the Gaussian products

$$|\Phi_E\rangle = \prod_{q>0} \left[\frac{2}{\pi\lambda^2} \right]^{1/2} \exp\left\{ -\frac{1}{\lambda^2} x_q x_{-q} \right\} \qquad (2.7)$$

and

$$|\Phi_P\rangle = \prod_{q>0} \left[\frac{2}{\pi\lambda^2}(\omega_q/\omega_E) \right]^{1/2}$$

$$\times \exp\left\{ -\frac{1}{\lambda^2}(\omega_q/\omega_E)x_q x_{-q} \right\} , \qquad (2.8)$$

where

$$\lambda = \left[\frac{N\hbar}{M\omega_E} \right]^{1/2} . \qquad (2.9)$$

The wave functions $x_q|\Phi_E\rangle$ and $x_q|\Phi_P\rangle$ are exact eigenstates of $\mathcal{H}_E$ and $\mathcal{H}_P$, respectively, describing a single phonon of momentum q. Thus, if $|\Phi_P\rangle$ is approximated by $|\Phi_E\rangle$, we obtain, for the expected energy to make the phonon,

$$\frac{\langle \Phi_E|x_{-q}\mathcal{H}_P x_q|\Phi_E\rangle}{\langle \Phi_E|x_{-q}x_q|\Phi_E\rangle} - \frac{\langle \Phi_E|\mathcal{H}_P|\Phi_E\rangle}{\langle \Phi_E|\Phi_E\rangle}$$

$$= \frac{1}{2}\hbar\omega_E\left[1 + \left[\frac{\omega_q}{\omega_E} \right]^2 \right] . \qquad (2.10)$$

The energy gap of $\frac{1}{2}\hbar\omega_E$ produced by this calculation is evidently attributable to the poor choice of ground state. More specifically, $|\Phi_E\rangle$ fails to exhibit long-wavelength density fluctuations necessarily present in the true ground state and symptomatic of its continuous broken symmetry.

Let us now expand the true ground state of $\mathcal{H}_P$ in terms of the ground and excited states of $\mathcal{H}_E$. Representing the latter by means of the usual Einstein oscillator ladder operators

$$a_q^\dagger = \frac{1}{\sqrt{2}}\left[\frac{1}{\lambda}x_q - \lambda\frac{\partial}{\partial x_{-q}} \right] , \qquad (2.11)$$

which create phonons, we obtain

$$|\Phi_P\rangle = \prod_{q>0} \frac{2\sqrt{\omega_q\omega_E}}{\omega_q + \omega_E}\exp\left\{ \left[\frac{\omega_E - \omega_q}{\omega_E + \omega_q} \right]a_q^\dagger a_{-q}^\dagger \right\}|\Phi_E\rangle , \qquad (2.12)$$

exactly. Thus restoration of translational invariance of the underlying Hamiltonian and expression of the broken symmetry are achieved by hybridizing macroscopic numbers of phonon pairs of opposite momenta into the unperturbed ground state, just as it is in superfluid helium, and are associated fundamentally with the softness of the Goldstone mode[6] ω_q at long wavelengths.

Let us now solve the problem again using the random-phase approximation. Recall that the expected displacement of the kth particle resulting from external forces F_j is given to linear order by

$$\langle \Psi(t)|x_k|\Psi(t)\rangle = -\sum_j (i\hbar)^{-1}\int_{-\infty}^t \langle \Phi|[\hat{x}_k(t),\hat{x}_j(t')]|\Phi\rangle F_j(t')dt' , \qquad (2.13)$$

where $|\Psi(t)\rangle$ is the many-body wave function in the Schrödinger representation,[7] the bracket denotes commutator, and

$$\hat{x}_j(t) = e^{(i/\hbar)\mathcal{H}t}x_j e^{(-i/\hbar)\mathcal{H}t} \qquad (2.14)$$

is the Heisenberg version of the operator x_j, with $\mathcal{H}$ denoting either $\mathcal{H}_E$ or $\mathcal{H}_P$. To implement the RPA, we approximate the difference between $\mathcal{H}_P$ and $\mathcal{H}_E$ as an additional external force on the jth particle caused by the displacement of its near neighbors. We then obtain the equations

$$\langle \Psi(t)|x_k|\Psi(t)\rangle^P \cong -\sum_j (i\hbar)^{-1}\int_{-\infty}^t \langle \Phi|[\hat{x}_k(t),\hat{x}_j(t')]|\Phi\rangle^E\{F_j(t') + \Delta F_j(t')\}dt' \qquad (2.15)$$

and

$$\Delta F_j(t) = K\{\langle \Psi(t)|x_{j-1}|\Psi(t)\rangle^P + \langle \Psi(t)|x_{j+1}|\Psi(t)\rangle^P\} , \qquad (2.16)$$

which we solve simultaneously to obtain an approximate expression for $\langle \Phi|[\hat{x}_k(t),\hat{x}_j(t')]|\Phi\rangle^P$. Following the usual convention, we shall express these kernels, the displacement-displacement response functions, as the Fourier transforms

$$\langle x_q x_{-q}\rangle_\omega = N\sum_k^N (i\hbar)^{-1}\int_0^\infty \langle \Phi|[\hat{x}_k(t),\hat{x}_0(0)]|\Phi\rangle e^{-i(qr_k - \omega t)}e^{(-\eta/\hbar)t}dt$$

$$= \sum_l |\langle l|x_q|\Phi\rangle|^2\left\{ \frac{1}{\hbar\omega - [E_l - E_0] + i\eta} + \frac{1}{-\hbar\omega - [E_l - E_0] - i\eta} \right\} , \qquad (2.17)$$

where

$$\mathcal{H}|l\rangle = E_l|l\rangle \ . \tag{2.18}$$

Written in terms of these, the solution of Eqs. (2.15) and (2.16) is

$$\langle x_q x_{-q}\rangle_\omega^P \cong [1 - \langle x_q x_{-q}\rangle_\omega^E K_q]^{-1}\langle x_q x_{-q}\rangle_\omega^E \ , \tag{2.19}$$

where

$$K_q = -2\frac{K}{N}\cos(qb_0) \ . \tag{2.20}$$

However, Eq. (2.17) may also be explicitly evaluated for the two cases, giving

$$\langle x_q x_{-q}\rangle_\omega^P = \frac{N}{M[(\omega + i\eta/\hbar)^2 - \omega_q^2]} \tag{2.21}$$

and

$$\langle x_q x_{-q}\rangle_\omega^E = \frac{N}{M[(\omega + i\eta/\hbar)^2 - \omega_E^2]} \ . \tag{2.22}$$

Comparing this result with Eq. (2.19), we find that the RPA here is *exact*. Evidently, the ground and excited states implicit in the RPA are the correct ones. Furthermore, it may be seen from our analysis that any phonon Hamiltonian, and by inference any Hamiltonian reducing to decoupled harmonic oscillators, is exactly solved by the RPA. It follows that the ground-state correction of Eq. (2.12) is implicit in the random-phase approximation and that symmetry breaking is also implicit, provided that the collective-mode frequency, as defined by the pole in the response function, disperses to zero as $q \to 0$.

The modification of the ground state by the RPA occurs through the agency of the antiresonant terms in the unperturbed response function. This is easily demonstrated in the case of phonons by evaluating Eq. (2.19) without these contributions. Thus, substituting

$$\langle x_q x_{-q}\rangle_\omega^E \cong \frac{1}{2M\omega_E}\frac{N}{\omega - \omega_E + i\eta/\hbar} \ , \tag{2.23}$$

into Eq. (2.19), we obtain

$$\langle x_q x_{-q}\rangle_\omega^P \cong \frac{1}{2M\omega_E}\frac{N}{\omega - \frac{1}{2}\omega_E[1 + (\omega_q/\omega_E)^2] + i\eta/\hbar} \ , \tag{2.24}$$

which is equivalent to the variational result of Eq. (2.10). This occurs because hybridization of phonons into the ground state $|\Phi_E\rangle$ enables the operator x_q to absorb a phonon already present and thus lower the unperturbed energy rather than raise it. Elimination of the antiresonant terms forbids such absorptions and thus effectively prevents the ground state from being modified. This is, of course, precisely the deficiency of our previous calculation of the collective mode of the fractional-

statistics gas based on the wave function $\rho_q|\Phi_0\rangle^2$.

The perturbation can affect the broken symmetry only if it diverges sufficiently strongly at long wavelengths. Let us associate with the bond between sites j and $j + 1$ a density operator

$$\rho(r_{j+1/2}) = \frac{x_j - x_{j+1}}{b_0^2} \ , \tag{2.25}$$

like that defined in Eq. (1.7). Since the Fourier transform of this operator,

$$\rho_q = b_0\sum_j \rho(r_{j+1/2})e^{-i(q/2)[r_j + r_{j+1}]}$$

$$= -i\frac{2}{b_0}\sin\left[\frac{1}{2}qb_0\right]x_q \ , \tag{2.26}$$

is equivalent to x_q, we may substitute it into Eq. (2.19) to obtain

$$\langle \rho_q \rho_{-q}\rangle_\omega^P \cong [1 - \langle \rho_q \rho_{-q}\rangle_\omega^E V_q]^{-1}\langle \rho_q \rho_{-q}\rangle_\omega^E \ , \tag{2.27}$$

with

$$V_q = -\frac{b_0^2 K}{N}\left\{\frac{\cos(qb_0)}{1 - \cos(qb_0)}\right\} \ . \tag{2.28}$$

This expression is identical to the formula for dielectric screening in a metal[3] and differs functionally from it only in working in reverse. Rather than opening up a gap at the plasma frequency, the random-phase approximation collapses a gap already present. However, since Eq. (2.27) may be inverted to give

$$\langle \rho_q \rho_{-q}\rangle_\omega^E \cong [1 + \langle \rho_q \rho_{-q}\rangle_\omega^P V_q]^{-1}\langle \rho_q \rho_{-q}\rangle_\omega^P \ , \tag{2.29}$$

the ability of V_q to collapse a gap is equivalent to its ability to create one.

III. DIELECTRIC RESPONSE

Let us now review our previous arguments[4,8] for superfluidity in the fractional-statistics gas based on the random-phase approximation. These arguments omit the effects of exchange and thus lead to the wrong behavior at finite temperature. However, they treat the modification of the ground state by the long-range forces correctly and are a good introduction to the more thorough analysis beginning in Sec. V.

Following the discussion of the previous section, we anticipate that the Hartree-Fock ground state $|\Phi_0\rangle$ defined by Eq. (1.3) will be strongly modified at long wavelengths if a sufficiently divergent perturbation can be found. Since $|\Phi_0\rangle$ is the exact ground state of the Hamiltonian

$$\mathcal{H}_0 = \sum_{i=1}^N \frac{1}{2m}\left|\mathbf{P}_i + \frac{e}{c}\overline{\mathbf{A}}_i\right|^2 \ , \tag{3.1}$$

with $\overline{\mathbf{A}}$ defined as in Eq. (1.11), let us take the perturbation to be

$$\mathcal{H}_1 = \mathcal{H} - \mathcal{H}_0 = \sum_{i=1}^{N} \frac{1}{2m} \left[2\frac{e}{c} \left[\mathbf{P}_i + \frac{e}{c} \overline{\mathbf{A}}_i \right] \cdot (\mathbf{A}_i - \overline{\mathbf{A}}_i) + \left[\frac{e}{c} \right]^2 |\mathbf{A}_i - \overline{\mathbf{A}}_i|^2 \right]$$

$$= \frac{e}{c} \sum_{\mathbf{q} \neq 0} \mathbf{V}(\mathbf{q}) \cdot \mathbf{j}_{-\mathbf{q}} \rho_{\mathbf{q}} - \frac{1}{2m} \left[\frac{e}{c} \right]^2 \sum_{\mathbf{q} \neq 0} \sum_{\mathbf{p} \neq 0} \mathbf{V}(\mathbf{q}) \cdot \mathbf{V}(\mathbf{p}) \rho_{\mathbf{p}-\mathbf{q}} \rho_{\mathbf{q}} \rho_{-\mathbf{p}} , \tag{3.2}$$

where $\rho_{\mathbf{q}}$ and $\mathbf{j}_{\mathbf{q}}$ are defined as in Eqs. (1.12) and (1.14) and

$$\mathbf{V}(\mathbf{q}) = \frac{1}{L^2} \int \mathbf{A}_{12} e^{-i\mathbf{q}\cdot(\mathbf{r}_1 - \mathbf{r}_2)} d\mathbf{r}_1$$

$$= (1-\nu) \frac{1}{iL^2} \frac{hc}{eq} (\hat{\mathbf{z}} \times \hat{\mathbf{q}}) = V(\mathbf{q})(\hat{\mathbf{z}} \times \hat{\mathbf{q}}) . \tag{3.3}$$

We note that

$$\mathbf{A}_j - \overline{\mathbf{A}}_j = \sum_{\mathbf{q} \neq 0} \mathbf{V}(\mathbf{q}) e^{i\mathbf{q}\cdot\mathbf{r}_j} \rho_{\mathbf{q}} . \tag{3.4}$$

$\mathcal{H}_1$ may be seen to contain terms diverging as $|\mathbf{q}|^{-2}$, which is the same as a Coulomb interaction or the interaction of Eq. (2.28), and thus to have the requisite strength.

We shall now work out the linear response of the systems described by $\mathcal{H}$ and $\mathcal{H}_0$ to externally applied potentials $\mathbf{A}(\mathbf{r},t)$ and $\varphi(\mathbf{r},t)$. Since gauge invariance requires that $\mathcal{H}$ be modified in the manner

$$\mathcal{H} \rightarrow \sum_{i=1}^{N} \left\{ \frac{1}{2m} \left| \mathbf{P}_i + \frac{e}{c} [\mathbf{A}_i + \mathbf{A}(\mathbf{r}_i, t)] \right|^2 - e\varphi(\mathbf{r}_i, t) \right\} , \tag{3.5}$$

in the presence of potentials, we obtain

$$\Delta\mathcal{H}(t) = \int \left\{ \frac{e}{c} \mathbf{A}(\mathbf{r},t) \cdot \mathbf{J}(\mathbf{r}) - e\varphi(\mathbf{r},t)\rho(\mathbf{r}) \right\} d\mathbf{r} , \tag{3.6}$$

to linear order, where $\rho(\mathbf{r})$ and $\mathbf{J}(\mathbf{r})$ are defined as in Eqs. (1.7) and (1.8). Evaluating the linear response to this perturbation, we obtain, with Φ denoting the true ground state,

$$\left\langle \Psi(t) \left| \begin{bmatrix} \rho(\mathbf{r}) \\ J_x(\mathbf{r}) \\ J_y(\mathbf{r}) \end{bmatrix} \right| \Psi(t) \right\rangle = \int (i\hbar)^{-1} \int_{-\infty}^{t} \left\langle \Phi \left| \begin{bmatrix} [\hat{\rho}(\mathbf{r},t),\hat{\rho}(\mathbf{r}',t')] & [\hat{\rho}(\mathbf{r},t),\hat{J}^x(\mathbf{r}',t')] & [\hat{\rho}(\mathbf{r},t),\hat{J}^y(\mathbf{r}',t')] \\ [\hat{J}^x(\mathbf{r},t),\hat{\rho}(\mathbf{r}',t')] & [\hat{J}^x(\mathbf{r},t),\hat{J}^x(\mathbf{r}',t')] & [\hat{J}^x(\mathbf{r},t),\hat{J}^y(\mathbf{r}',t')] \\ [\hat{J}^y(\mathbf{r},t),\hat{\rho}(\mathbf{r}',t')] & [\hat{J}^y(\mathbf{r},t),\hat{J}^x(\mathbf{r}',t')] & [\hat{J}^y(\mathbf{r},t),\hat{J}^y(\mathbf{r}',t')] \end{bmatrix} \right| \Phi \right\rangle$$

$$\times \begin{bmatrix} -e\varphi(\mathbf{r}',t') \\ \frac{e}{c} A_x(\mathbf{r}',t') \\ \frac{e}{c} A_y(\mathbf{r}',t') \end{bmatrix} dt' d\mathbf{r}' . \tag{3.7}$$

The paramagnetic response kernel is given explicitly by

$$\Delta = L^2 \int (i\hbar)^{-1} \int_0^{\infty} e^{-i(\mathbf{q}\cdot\mathbf{r}-\omega t)} e^{(-\eta/\hbar)t} \left\langle \Phi \left| \begin{bmatrix} [\hat{\rho}(\mathbf{r},t),\hat{\rho}(0,0)] & [\hat{\rho}(\mathbf{r},t),\hat{J}^x(0,0)] & [\hat{\rho}(\mathbf{r},t),\hat{J}^y(0,0)] \\ [\hat{J}^x(\mathbf{r},t),\hat{\rho}(0,0)] & [\hat{J}^x(\mathbf{r},t),\hat{J}^x(0,0)] & [\hat{J}^x(\mathbf{r},t),\hat{J}^y(0,0)] \\ [\hat{J}^y(\mathbf{r},t),\hat{\rho}(0,0)] & [\hat{J}^y(\mathbf{r},t),\hat{J}^x(0,0)] & [\hat{J}^y(\mathbf{r},t),\hat{J}^y(0,0)] \end{bmatrix} \right| \Phi \right\rangle dt \, d\mathbf{r}$$

$$= \begin{bmatrix} \langle \rho_{\mathbf{q}}\rho_{-\mathbf{q}} \rangle_\omega & \langle \rho_{\mathbf{q}} J^x_{-\mathbf{q}} \rangle_\omega & \langle \rho_{\mathbf{q}} J^y_{-\mathbf{q}} \rangle_\omega \\ \langle J^x_{\mathbf{q}}\rho_{-\mathbf{q}} \rangle_\omega & \langle J^x_{\mathbf{q}} J^x_{-\mathbf{q}} \rangle_\omega & \langle J^x_{\mathbf{q}} J^y_{-\mathbf{q}} \rangle_\omega \\ \langle J^y_{\mathbf{q}}\rho_{-\mathbf{q}} \rangle_\omega & \langle J^y_{\mathbf{q}} J^x_{-\mathbf{q}} \rangle_\omega & \langle J^y_{\mathbf{q}} J^y_{-\mathbf{q}} \rangle_\omega \end{bmatrix} , \tag{3.8}$$

where

$$\langle \mathcal{O}\mathcal{O}' \rangle_\omega = \sum_l \left\{ \frac{\langle \Phi|\mathcal{O}|l \rangle \langle l|\mathcal{O}'|\Phi \rangle}{\hbar\omega - [E_l - E_0] + i\eta} + \frac{\langle \Phi|\mathcal{O}'|l \rangle \langle l|\mathcal{O}|\Phi \rangle}{-\hbar\omega - [E_l - E_0] - i\eta} \right\} , \tag{3.9}$$

for any two operators $\mathcal{O}$ and $\mathcal{O}'$, with $|l\rangle$ and E_l denoting the exact eigenstate and eigenvalue of $\mathcal{H}$. In order to account correctly for the measured current induced by these potentials, we must correct Δ for the modification of the current operator,

$$\mathbf{J}(\mathbf{r})\rightarrow\mathbf{J}(\mathbf{r})+\frac{1}{m}\frac{e}{c}\rho(\mathbf{r})\,\mathbf{A}(\mathbf{r},t)\;,\tag{3.10}$$

by the potential. This gives

$$\mathcal{H}=\frac{1}{L^2}\Delta+\frac{\bar{p}}{m}\begin{bmatrix}0&0&0\\0&1&0\\0&0&1\end{bmatrix}\;,\tag{3.11}$$

with $\bar{p}$ defined as in Eq. (1.5), for the full response kernel. The calculation proceeds identically in the unperturbed system, except that the mean-field current $\mathbf{j}(\mathbf{r})$ defined by Eq. (1.10) must replace $\mathbf{J}(\mathbf{r})$, as the former is the true current of the system described by $\mathcal{H}_0$.

Let us now implement the RPA by drawing an analogy with dielectric screening in a metal. In an electron gas, screening arises because density fluctuations $\rho(\mathbf{r})$ generate an effective scalar potential $\Delta\varphi(\mathbf{r})$ according to the Poisson equation

$$\Delta\varphi(\mathbf{r},t)=-\int\frac{e}{|\mathbf{r}-\mathbf{r}'|}\langle\Psi(t)|\rho(\mathbf{r}')|\Psi(t)\rangle d\mathbf{r}'\;,\tag{3.12}$$

where $|\Psi(t)\rangle$ is the time-dependent electron-gas wave function. In contrast to our phonon example, however, this expression is not exact, but is rather an approximation made valid by the long-range nature of the Coulomb interaction. We shall now make the same approximation for the anyon gas. To simplify the derivation, we first observe that the $\mathbf{p}=\mathbf{q}$ term in Eq. (3.2) dominates the sum because it has matrix elements connecting the ground state with itself. Replacing $\rho_{\mathbf{p}-\mathbf{q}}$ in this expression with its ground-state expectation value N, we obtain

$$\mathcal{H}_1^{\text{RPA}}=\frac{e}{c}\sum_{\mathbf{q}\neq0}\mathbf{V}(\mathbf{q})\cdot\mathbf{j}_{-\mathbf{q}}\rho_{\mathbf{q}}$$

$$+\frac{N}{2m}\left[\frac{e}{c}\right]^2\sum_{\mathbf{q}\neq0}|\mathbf{V}(\mathbf{q})|^2\rho_{\mathbf{q}}\rho_{-\mathbf{q}}\;.\tag{3.13}$$

The perturbation Hamiltonian is now similar to that of an ideal metal, except for the presence of a current operator in the expression for the "Coulomb" interaction between particles. This requires us to consider the scalar and vector potentials generated by both density and current density fluctuations. Linearizing $\mathcal{H}_1$, we obtain

$$e\,\Delta\varphi(\mathbf{r},t)\cong-\frac{1}{L^2}\sum_{\mathbf{q}}\left\langle\Psi(t)\left|\frac{\delta\mathcal{H}_1^{\text{RPA}}}{\delta\rho_{\mathbf{q}}^\dagger}\right|\Psi(t)\right\rangle e^{i\mathbf{q}\cdot\mathbf{r}}$$

$$=-\frac{1}{L^2}\sum_{\mathbf{q}}\left\langle\Psi(t)\left|\left\{\left[\frac{e}{c}\right]\mathbf{V}(-\mathbf{q})\cdot\mathbf{j}_{\mathbf{q}}+\frac{N}{m}\left[\frac{e}{c}\right]^2|\mathbf{V}(\mathbf{q})|^2\rho_{\mathbf{q}}\right\}\right|\Psi(t)\right\rangle e^{i\mathbf{q}\cdot\mathbf{r}}\tag{3.14}$$

and

$$\frac{e}{c}\Delta\,\mathbf{A}(\mathbf{r},t)\cong\frac{1}{L^2}\sum_{\mathbf{q}}\left\langle\Psi(t)\left|\frac{\delta\mathcal{H}_1^{\text{RPA}}}{\delta\mathbf{j}_{\mathbf{q}}^\dagger}\right|\Psi(t)\right\rangle e^{i\mathbf{q}\cdot\mathbf{r}}$$

$$=\frac{1}{L^2}\sum_{\mathbf{q}}\left\langle\Psi(t)\left|\left\{\left[\frac{e}{c}\right]\mathbf{V}(\mathbf{q})\rho_{\mathbf{q}}\right\}\right|\Psi(t)\right\rangle e^{i\mathbf{q}\cdot\mathbf{r}}\;,\tag{3.15}$$

where $|\Psi(t)\rangle$ is now the time-dependent wave function of the anyon gas. Then we implement the RPA by writing, approximately,

$$\left\langle\Psi(t)\left|\begin{bmatrix}\rho(\mathbf{r})\\j_x(\mathbf{r})\\j_y(\mathbf{r})\end{bmatrix}\right|\Psi(t)\right\rangle\cong\int(i\hbar)^{-1}\int_{-\infty}^{t}\left\langle\Phi_0\left|\begin{bmatrix}[\hat{\rho}(\mathbf{r},t),\hat{\rho}(\mathbf{r}',t')]&[\hat{\rho}(\mathbf{r},t),\hat{j}^{x}(\mathbf{r}',t')]&[\hat{\rho}(\mathbf{r},t),\hat{j}^{y}(\mathbf{r}',t')]\\ [\hat{j}^{x}(\mathbf{r},t),\hat{\rho}(\mathbf{r}',t')]&[\hat{j}^{x}(\mathbf{r},t),\hat{j}^{x}(\mathbf{r}',t')]&[\hat{j}^{x}(\mathbf{r},t),\hat{j}^{y}(\mathbf{r}',t')]\\ [\hat{j}^{y}(\mathbf{r},t),\hat{\rho}(\mathbf{r}',t')]&[\hat{j}^{y}(\mathbf{r},t),\hat{j}^{x}(\mathbf{r}',t')]&[\hat{j}^{y}(\mathbf{r},t),\hat{j}^{y}(\mathbf{r}',t')]\end{bmatrix}\right|\Phi_0\right\rangle$$

$$\times\begin{bmatrix}-e\varphi(\mathbf{r}',t')-e\Delta\varphi(\mathbf{r}',t')\\ \frac{e}{c}A_x(\mathbf{r}',t')+\frac{e}{c}\Delta A_x(\mathbf{r}',t')\\ \frac{e}{c}A_y(\mathbf{r}',t')+\frac{e}{c}\Delta A_y(\mathbf{r}',t')\end{bmatrix}dt'\,d\mathbf{r}'\;,\tag{3.16}$$

which expresses the perturbed response kernel in terms of the unperturbed one. It should be noted that the unperturbed current operator $\mathbf{j}$, rather than the physical current $\mathbf{J}$, appears in Eqs. (3.14)–(3.16). Solving these equations simultaneously for the Fourier-transformed response kernel

$$\mathcal{D}=\begin{bmatrix}\langle\rho_{\mathbf{q}}\rho_{-\mathbf{q}}\rangle_\omega&\langle\rho_{\mathbf{q}}j^{x}_{-\mathbf{q}}\rangle_\omega&\langle\rho_{\mathbf{q}}j^{y}_{-\mathbf{q}}\rangle_\omega\\ \langle j^{x}_{\mathbf{q}}\rho_{-\mathbf{q}}\rangle_\omega&\langle j^{x}_{\mathbf{q}}j^{x}_{-\mathbf{q}}\rangle_\omega&\langle j^{x}_{\mathbf{q}}j^{y}_{-\mathbf{q}}\rangle_\omega\\ \langle j^{y}_{\mathbf{q}}\rho_{-\mathbf{q}}\rangle_\omega&\langle j^{y}_{\mathbf{q}}j^{x}_{-\mathbf{q}}\rangle_\omega&\langle j^{y}_{\mathbf{q}}j^{y}_{-\mathbf{q}}\rangle_\omega\end{bmatrix}\;,\tag{3.17}$$

we obtain

$$\mathcal{D} \cong [1 - \mathcal{D}^0 \mathcal{V}]^{-1} \mathcal{D}^0 , \tag{3.18}$$

where $\mathcal{D}^0$ denotes $\mathcal{D}$ evaluated for the unperturbed system and

$$\mathcal{V} = \begin{bmatrix} \dfrac{N}{m} \left[\dfrac{e}{c}\right]^2 |V(\mathbf{q})|^2 & 0 & -\left[\dfrac{e}{c}\right] V(\mathbf{q}) \\[2ex] 0 & 0 & 0 \\[2ex] \left[\dfrac{e}{c}\right] V(\mathbf{q}) & 0 & 0 \end{bmatrix} . \tag{3.19}$$

We now convert $\mathcal{D}$ to the paramagnetic response kernel Δ defined by Eq. (3.8) by perturbatively accounting for the difference between $\mathbf{j}$ and $\mathbf{J}$. For this, we observe that the $\mathbf{p} = \mathbf{q}$ term in the expression

$$\mathbf{J_q} = \mathbf{j}_q + \frac{e}{mc} \sum_j (\mathbf{A}_j - \overline{\mathbf{A}}_j) e^{-i\mathbf{q} \cdot \mathbf{r}_j}$$

$$= \mathbf{j}_q + \frac{e}{mc} \sum_{\mathbf{p} \neq 0} \mathbf{V}(\mathbf{p}) \rho_{\mathbf{q}-\mathbf{p}} \rho_{\mathbf{p}} , \tag{3.20}$$

obtained from Eqs. (1.13), (1.14), and (3.4) again dominates the sum because it has matrix elements connecting the ground state with itself. Replacing $\rho_{\mathbf{q}-\mathbf{p}}$ in this expression with its ground-state expectation value N, we obtain

$$\mathbf{J}_q^{\mathrm{RPA}} = \mathbf{j}_q + \frac{Ne}{mc} \mathbf{V}(\mathbf{q}) \rho(\mathbf{q}) \tag{3.21}$$

and thus

$$\Delta \cong (1 + \mathcal{U}^\dagger) \mathcal{D} (1 + \mathcal{U}) , \tag{3.22}$$

where

$$\mathcal{U} = -\frac{Ne}{mc} V(\mathbf{q}) \begin{bmatrix} 0 & 0 & 1 \\ 0 & 0 & 0 \\ 0 & 0 & 0 \end{bmatrix} . \tag{3.23}$$

We have, finally,

$$\mathcal{H} \cong \frac{1}{L^2} (1 + \mathcal{U}^\dagger) \{ [1 - \mathcal{D}^0 \mathcal{V}]^{-1} \mathcal{D}^0 \} (1 + \mathcal{U})$$

$$+ \frac{\overline{\rho}}{m} \begin{bmatrix} 0 & 0 & 0 \\ 0 & 1 & 0 \\ 0 & 0 & 1 \end{bmatrix} . \tag{3.24}$$

Let us now explicitly evaluate the unperturbed response kernel $\mathcal{D}^0$ and thereby the RPA response kernel $\mathcal{H}$. For convenience, we shall measure lengths and energies in units of a_0 and $\hbar\omega_c$, as defined by Eqs. (1.5) and (1.6). The ground state $|\Phi_0\rangle$, defined by Eq. (1.3), is the Slater determinant

$$|\Phi_0\rangle = \prod_k \begin{bmatrix} c_{0k}^\dagger |0\rangle, & \nu = 0 \\ c_{1k}^\dagger c_{0k}^\dagger |0\rangle, & \nu = \frac{1}{2} \end{bmatrix} , \tag{3.25}$$

where $c_{nk}^\dagger$ is the operator creating a fermion in the state φ_{nk} defined by Eq. (1.4). The excited states $|l\rangle$ in Eq. (3.8) are the Slater determinants

$$|l\rangle = c_{n'k'}^\dagger c_{nk} |\Phi_0\rangle , \tag{3.26}$$

where φ_{nk} is occupied in the ground state and $\varphi_{n'k'}$ is empty. The energy eigenvalues are

$$\mathcal{H}_0 |\Phi_0\rangle = E_0 |\Phi_0\rangle ,$$

$$\mathcal{H}_0 |l\rangle = (E_0 + n' - n) |l\rangle . \tag{3.27}$$

The matrix elements appearing in Eq. (3.8) are elementary integrals involving φ_{nk} and $\varphi_{n'k'}$, such as

$$\langle l | \rho_\mathbf{q} | \Phi_0 \rangle = \int \varphi_{n'k'}^*(\mathbf{r}) e^{-i\mathbf{q} \cdot \mathbf{r}} \varphi_{nk}(\mathbf{r}) d\mathbf{r} . \tag{3.28}$$

The explicit evaluation of these integrals and the summation over excited states are described in detail in Appendix H. The final result for $\hat{\mathbf{q}} = \hat{\mathbf{x}}$ is

$$\mathcal{D}^0 = \frac{L^2}{2\pi(1-\nu)} \begin{bmatrix} q^2 \Sigma_0 & q\omega\Sigma_0 & -iq\Sigma_1 \\[1ex] \omega q \Sigma_0 & \omega^2 \Sigma_0 - 1 & -i\omega\Sigma_1 \\[1ex] iq\Sigma_1 & i\omega\Sigma_1 & \Sigma_2 \end{bmatrix} , \tag{3.29}$$

where

$$\Sigma_j{}_{(\nu=0)} = \sum_{n=1}^{\infty} \frac{e^{-b} b^{n-1}}{(n-1)![(\omega+i\eta)^2 - n^2]} (n-b)^j \tag{3.30}$$

and

$$\Sigma_j{}_{(\nu=1/2)} = \frac{1}{2} \sum_{n=1}^{\infty} \frac{e^{-b} b^{n-1}}{(n-1)![(\omega+i\eta)^2 - n^2]}$$

$$\times \left[(1 - \delta_{n1})(n-b)^j \right.$$

$$+ \frac{(n+1-b)^{2-j}}{n+1}$$

$$\times [n(n+1) - (2n+3)b + b^2]^j \bigg] , \tag{3.31}$$

with b denoting $\frac{1}{2} q^2$. Because the matrix $[1 - \mathcal{D}^0 \mathcal{V}]$ of Eq. (3.18) is sparse, its inverse has a simple analytic form. Noting that

$$\mathcal{V} = \frac{2\pi(1-\nu)}{L^2} \frac{1}{q^2} \begin{bmatrix} 1 & 0 & iq \\ 0 & 0 & 0 \\ -iq & 0 & 0 \end{bmatrix} , \tag{3.32}$$

$$\mathcal{U} = \frac{i}{q} \begin{bmatrix} 0 & 0 & 1 \\ 0 & 0 & 0 \\ 0 & 0 & 0 \end{bmatrix} , \tag{3.33}$$

and

$$\frac{\overline{\rho}}{m} = \frac{1}{2\pi(1-\nu)} , \tag{3.34}$$

in our preferred units, we obtain

$$\mathcal{D} \cong \frac{L^2}{2\pi(1-\nu)} \frac{1}{D} \begin{bmatrix} q^2 \Sigma_0 & q\omega\Sigma_0 & -iq\Sigma_s \\[1ex] \omega q \Sigma_0 & \omega^2 \Sigma_0 - D & -i\omega\Sigma_s \\[1ex] iq\Sigma_s & i\omega\Sigma_s & \Sigma_2 + \Sigma_1^2 - \Sigma_0\Sigma_2 \end{bmatrix} , \tag{3.35}$$

where

$$D = (1+\Sigma_1)^2 - \Sigma_0(1+\Sigma_2) \tag{3.36}$$

and

$$\Sigma_s = D - 1 - \Sigma_1 + \Sigma_0 , \tag{3.37}$$

and thus

$$\mathcal{H} \cong \frac{1}{2\pi(1-\nu)} \frac{1}{D}$$

$$\times \begin{vmatrix} q^2\Sigma_0 & q\omega\Sigma_0 & -iq(\Sigma_s - \Sigma_0) \\ \omega q\Sigma_0 & \omega^2\Sigma_0 & -i\omega(\Sigma_s - \Sigma_0) \\ iq(\Sigma_s - \Sigma_0) & i\omega(\Sigma_s - \Sigma_0) & 1+\Sigma_2 \end{vmatrix} , \tag{3.38}$$

per Eq. (3.24).

IV. RPA SUPERFLUIDITY

Let us now consider the physical significance of Eq. (3.38). When long-range interparticle potentials are omitted (as they have been in the present work), superfluidity is expected to be manifested in $\mathcal{H}$ in three ways:[6,9] (i) a sharp pole in the longitudinal response, indicating the presence of ordinary compressional sound; (ii) a large static structure factor, indicating particle number uncertainty; and (iii) perfect diamagnetism in the transverse channel, indicating a Meissner effect. In principle, these are all consequences of the superfluid broken symmetry and are thus not independent. Since our calculation demonstrates the broken symmetry only implicitly, however, we shall show that all three occur.

Let us preface our remarks by noting that the first two properties can also be caused by broken translational symmetry. For example, consider the phonon response function of Eq. (2.21) with ρ_q, as defined by Eq. (2.26), substituted for x_q. Expanding the density-density response about $q = 0$, we obtain, for the dynamic structure factor,

$$S(q,\omega) = -\frac{1}{\pi} \text{Im} \langle \rho_q \rho_{-q} \rangle_\omega^P$$

$$= -\frac{1}{\pi} \text{Im} \left[\frac{2}{b_0} \sin \left[\frac{1}{2} q b_0 \right] \right]^2 \frac{N}{M[(\omega + i\eta/\hbar)^2 - \omega_q^2]}$$

$$\cong \frac{Nq}{2Mv_s} \delta(\omega - v_s q) , \tag{4.1}$$

where

$$v_s \equiv \left[\frac{K}{M} \right]^{1/2} b_0 , \tag{4.2}$$

per Eq. (2.6). The δ function in this expression indicates the presence of a longitudinal-acoustic phonon. Integrating over this pole, we obtain

$$S_q = \frac{1}{N} \langle \Phi_P | \rho_q \rho_{-q} | \Phi_P \rangle = \frac{1}{N} \int_0^\infty S(q,\omega) d\omega = \frac{q}{2Mv_s} , \tag{4.3}$$

for the static structure factor. The small-q behavior of S_q, which is also exhibited by superfluids and ordinary metals,[10] indicates quantum-mechanical uncertainty of the particle number at large length scales, as well as the ability of the system to flow. Unlike a superfluid, however, the crystal and ordinary metal do not flow without loss when impurities are present, nor do they exhibit a Meissner effect.

The dynamic structure factor of the anyon gas is predicted by Eq. (3.38) to be

$$S(\mathbf{q},\omega) = -\frac{1}{\pi} \text{Im} \langle \rho_q \rho_{-q} \rangle_\omega$$

$$= -\frac{L^2}{\pi} \frac{1}{2\pi(1-\nu)} \text{Im} \left[\frac{1}{D} q^2 \Sigma_0 \right] . \tag{4.4}$$

Since Σ_j has no imaginary part for frequencies $\omega < 1$, we may identify the longitudinal collective mode as a zero in the determinant D. Expanding Σ_j to lowest order in ω and b, we find

$$\Sigma_j \cong -1 - [\omega + i\eta]^2 + (1 + j - 2^{j-2})b \begin{bmatrix} 1, & \nu=0 \\ 2, & \nu=\frac{1}{2} \end{bmatrix} \tag{4.5}$$

and thus

$$D \cong -[\omega + i\eta]^2 + 2b \begin{bmatrix} 1, & \nu=0 \\ 2, & \nu=\frac{1}{2} \end{bmatrix} . \tag{4.6}$$

For sufficiently small q and ω, the dynamic structure factor is therefore given by

$$S(\mathbf{q},\omega) \cong N\frac{q}{2v_s} \delta(\omega - v_s q) , \tag{4.7}$$

in our preferred units, where

$$v_s = \begin{bmatrix} 1, & \nu=0 \\ \sqrt{2}, & \nu=\frac{1}{2} \end{bmatrix} . \tag{4.8}$$

The similarity of this expression to Eq. (4.1) shows that $\mathcal{H}$ exhibits the first two properties of a superfluid. As remarked in our previous work,[4] the sound speed v_s for $\nu = \frac{1}{2}$ differs by approximately 5% from the $\sqrt{29/16}$ inferred from the Hartree-Fock bulk modulus. The $\nu = 0$ differs by a much larger 40% from the Hartree-Fock value of $\sqrt{2}$. It should be emphasized, however, that both $\nu = 0$ estimates are artifacts of the computational procedure, as the $\nu = 0$ case corresponds to a noninteracting Bose gas, for which the sound speed is zero. The error occurs because the Fermi representation forces the wave function to have nodes at particle coincidences and thus requires high orders in perturbation theory, omitted from this calculation, to reproduce the correct behavior. Our $\nu = 0$ calculation is more appropriate for a fluid, such as ^{4}He, with strong short-range repulsions between particles that suppress the wave function at particle coincidences.[11]

Let us now consider the Meissner effect. Penetration of transverse vector potentials into the sample is described by the response kernel

$$K(q) \equiv \mathcal{H}_{yy}(\mathbf{q},0) = \frac{1}{2\pi(1-v)} \left[\frac{1}{D}(1+\Sigma_2) \right] \Bigg|_{\omega=0} , \qquad (4.9)$$

which limits to a nonzero constant at $q=0$ when Meissner screening occurs. The value of this constant expected at zero temperature is the diamagnetic contribution to $\mathcal{H}$ in Eq. (3.24) or $1/2\pi(1-v)$. Extending the zero-frequency expansions of the summation in Eqs. (3.30) and (3.31) to next order, we obtain

$$D \cong \begin{bmatrix} 2b - \frac{5}{4}b^2, & v=0 \\ 4b - 5b^2, & v=\frac{1}{2} \end{bmatrix} , \qquad (4.10)$$

$$\Sigma_2 \cong \begin{bmatrix} -1+2b-2b^2, & v=0 \\ -1+4b-8b^2, & v=\frac{1}{2} \end{bmatrix} , \qquad (4.11)$$

and thus

$$K(q) \underset{q \to 0}{\cong} \begin{bmatrix} \dfrac{1}{2\pi}\left[1 - \dfrac{3}{16}q^2 \right], & v=0 \\ \dfrac{1}{\pi}\left[1 - \dfrac{3}{8}q^2 \right], & v=\frac{1}{2} \end{bmatrix} . \qquad (4.12)$$

Meissner screening occurs formally in this calculation because the numerator and denominator in Eq. (4.9) are both of order q^2 at long wavelengths. Since this will not occur unless D has a zero-frequency pole, the Meissner effect in our calculations is fundamentally related to the superfluid fluctuations seen in $S(\mathbf{q},\omega)$. The deviation from perfect screening at finite q seen in Eq. (4.12) provides a measure of the superfluid coherence length. For example, the corresponding Pippard kernel $K_p(q)$ is given at small q by[9]

$$K_P(q) \cong K_P(0)[1 - \tfrac{1}{5}(q\xi_0)^2] , \qquad (4.13)$$

where ξ_0 is the Pippard coherence length. A small-q expansion of the BCS kernel yields the same expression with the coefficient $\frac{1}{5}$ replaced by $\pi^2/30$. Taking either of these to define ξ_0 in terms of the coefficient of q^2 in Eq. (4.12), we find that the coherence length of the anyon gas is comparable with the magnetic length and hence with the interparticle separation.

It may be seen from Eq. (3.38) that the response kernel $\mathcal{H}$ is fully gauge invariant:

$$\frac{1}{2\pi(1-v)} \frac{1}{D}$$

$$\times \begin{bmatrix} q^2\Sigma_0 & q\omega\Sigma_0 & -iq(\Sigma_s-\Sigma_0) \\ \omega q\Sigma_0 & \omega^2\Sigma_0 & -i\omega(\Sigma_s-\Sigma_0) \\ iq(\Sigma_s-\Sigma_0) & i\omega(\Sigma_s-\Sigma_0) & 1+\Sigma_2 \end{bmatrix}$$

$$\begin{bmatrix} -\omega \\ q \\ 0 \end{bmatrix} = 0 . \qquad (4.14)$$

That is, the response of the system to any set of vector and scalar potentials corresponding to a pure gauge

transformation, and thus to no physical electric and magnetic fields, is zero. From the transposition symmetry of $\mathcal{H}$, we see that this is equivalent, as expected,[9] to conservation of the current induced by arbitrary vector or scalar potentials. Gauge invariance is achieved intentionally in our calculation as a condition that $\mathcal{H}$ be physically unambiguous. A discussion of the Ward identifies through which this is achieved may be found in Sec. VIII.

The gauge invariance of $\mathcal{H}$ enables us to concisely relate the presence of the collective mode to the occurrence of Meissner screening. Given that $\mathcal{H}_{00}$ has the denominator $\omega^2 - v_s^2 q^2$ at low frequencies and long wavelengths, $\mathcal{H}_{xx}$ must have the same denominator, since

$$\mathcal{H}_{xx} = \left| \frac{\omega}{q} \right|^2 \mathcal{H}_{00} , \qquad (4.15)$$

by gauge invariance. In the present case, they have the specific forms

$$\mathcal{H}_{00} \cong \bar{\rho}\frac{q^2}{\omega^2-v_s^2q^2}, \qquad \mathcal{H}_{xx} \cong \bar{\rho}\frac{\omega^2}{\omega^2-v_s^2q^2} . \qquad (4.16)$$

At $q=0$, however, there is no distinction between longitudinal and transverse. We must therefore have

$$\mathcal{H}_{yy} \cong \bar{\rho}\frac{\omega^2-Cq^2}{\omega^2-v_s^2q^2} , \qquad (4.17)$$

where C is a constant. Setting $\omega=0$ then yields a Meissner effect (unless $C=0$). As discussed previously, our calculation finds $C=v_s^2$ and thus an exact cancellation between the numerator and denominator. This may be attributed to the absence of any natural velocity scale in the problem other than v_s.

Another consequence of gauge invariance is that $\mathcal{H}$ is completely described by three independent functions of q and ω. Two of these have already been discussed. Let us therefore consider the third function, the Hall conductivity, defined by

$$\sigma_{xy} = \frac{1}{i\omega}K_{xy} = \frac{1}{2\pi(1-v)} \frac{1}{D}(\Sigma_0-\Sigma_s) . \qquad (4.18)$$

Expanding this to low order in q and ω, we obtain

$$\sigma_{xy} \cong \frac{1}{2\pi(1-v)} \left[\frac{-\omega^2+\frac{3}{4}v_s^2q^2}{-\omega^2+v_s^2q^2} - 1 \right]$$

$$= \frac{1}{8\pi(1-v)} \frac{v_s^2q^2}{\omega^2-v_s^2q^2} . \qquad (4.19)$$

As noted in our previous work,[4] the Hall conductance is nonzero only because of a suspiciously inexact cancellation, one that requires the existence of a secondary velocity scale at $(\sqrt{3/4})v_s$. Since the true Hall conductance of the $v=0$ case must be exactly zero, there is reason to suspect this result of being an artifact in both cases.

Let us consider finally the screened fractional-statistics interaction, defined by

$$\mathcal{V}^{\text{RPA}} = \mathcal{V}[1 - \mathcal{D}^0 \mathcal{V}]^{-1}$$

$$= \frac{2\pi(1-\nu)}{L^2 q^2 D} \begin{bmatrix} 1+\Sigma_2 & 0 & iq(1+\Sigma_1) \\ 0 & 0 & 0 \\ -iq(1+\Sigma_1) & 0 & q^2\Sigma_0 \end{bmatrix} . \tag{4.20}$$

Comparing Eqs. (4.18) and (4.20), we see that the effective fractional-statistics interaction $\mathcal{V}_{0y}^{\text{RPA}}$ is totally unscreened (equal to $\mathcal{V}_{0y}$) whenever the Hall conductivity becomes negligible, even though the numerator and denominator individually vanish. Furthermore, $\mathcal{V}_{00}^{\text{RPA}}$,

the effective "Coulomb" interaction, is exactly unscreened in the $q \to 0$ limit regardless of the Hall conductivity behavior, as all Σ_j become equal in this limit. This behavior implies that the concept of an anyon remains valid at higher orders in perturbation theory and partially accounts for our success in describing the system with such a simple calculation.

V. PERTURBATION EXPANSION

Let us now proceed with a formal analysis of this problem.[7] We wish to calculate the time-ordered correlation function

$$\langle \Phi | T[\hat{J}^{\mu}(\mathbf{r},t)\hat{J}^{\nu}(0,0)] | \Phi \rangle = \left\langle \Phi \left| \begin{bmatrix} T[\hat{\rho}(\mathbf{r},t)\hat{\rho}(0,0)] & T[\hat{\rho}(\mathbf{r},t)\hat{J}^x(0,0)] & T[\hat{\rho}(\mathbf{r},t)\hat{J}^y(0,0)] \\ T[\hat{J}^x(\mathbf{r},t)\hat{\rho}(0,0)] & T[\hat{J}^x(\mathbf{r},t)\hat{J}^x(0,0)] & T[\hat{J}^x(\mathbf{r},t)\hat{J}^y(0,0)] \\ T[\hat{J}^y(\mathbf{r},t)\hat{\rho}(0,0)] & T[\hat{J}^y(\mathbf{r},t)\hat{J}^x(0,0)] & T[\hat{J}^y(\mathbf{r},t)\hat{J}^y(0,0)] \end{bmatrix} \right| \Phi \right\rangle , \tag{5.1}$$

the time Fourier transform of which is equal to the retarded response function defined in Eq. (3.8) and thus the electromagnetic response kernel $\mathcal{H}$ of Eq. (3.11) for $\omega > 0$. We shall do this by evaluating the perturbation expansion

$$\langle \Phi | T[\hat{J}^{\mu}(\mathbf{r},t)\hat{J}^{\nu}(0,0)] | \Phi \rangle$$

$$= \sum_{m=0}^{\infty} \frac{(i\hbar)^{-m}}{m!} \int_{-\infty}^{\infty} \cdots \int_{-\infty}^{\infty} e^{(-\eta/\hbar)[|t_1| + \cdots + |t_m|]}$$

$$\times \langle \Phi_0 | T[\mathcal{H}_1^I(t_1) \cdots \mathcal{H}_1^I(t_m)\hat{J}^{\mu I}(\mathbf{r},t)\hat{J}^{\nu I}(0,0)] | \Phi_0 \rangle_{\text{connected}} dt_1 \cdots dt_m , \tag{5.2}$$

where

$$\hat{\mathcal{O}}^I(t) = \exp\left[\frac{i}{\hbar}\mathcal{H}_0 t\right] \mathcal{O} \exp\left[-\frac{i}{\hbar}\mathcal{H}_0 t\right] \tag{5.3}$$

is the interaction version of an arbitrary operator $\mathcal{O}$, η is an infinitesimal, and $|\Phi_0\rangle$ is the unperturbed ground state defined by Eq. (3.25).

The first step in our analysis is to second quantize Eq. (5.2). The perturbation Hamiltonian $\mathcal{H}_1$ defined by Eq. (3.2) may be decomposed into one-, two-, and three-body contributions, in the manner

$$\mathcal{H}_1 = \sum_j u(\mathbf{r}_j) + \frac{1}{2}\sum_{j,k}' v(\mathbf{r}_j,\mathbf{r}_k) + \frac{1}{6}\sum_{j,k,l}' w(\mathbf{r}_j,\mathbf{r}_k,\mathbf{r}_l) , \tag{5.4}$$

where the primes indicate that each summation variable runs over all particles, omitting any terms with equal indices. These are given specifically by

$$u(\mathbf{r}_1) = \frac{1}{m}\left\{-\frac{e}{c}\left[\mathbf{P}_1 + \frac{e}{c}\overline{\mathbf{A}}_1\right]\cdot\overline{\mathbf{A}}_1 + \frac{1}{2}\left[\frac{e}{c}\right]^2|\overline{\mathbf{A}}_1|^2\right\} , \tag{5.5}$$

$$v(\mathbf{r}_1,\mathbf{r}_2) = \frac{1}{m}\left\{\frac{e}{c}\left[\left[\mathbf{P}_1 + \frac{e}{c}\overline{\mathbf{A}}_1\right]\cdot\mathbf{A}_{12} + \left[\mathbf{P}_2 + \frac{e}{c}\overline{\mathbf{A}}_2\right]\cdot\mathbf{A}_{21}\right] - \left[\frac{e}{c}\right]^2[\overline{\mathbf{A}}_1\cdot\mathbf{A}_{12} + \overline{\mathbf{A}}_2\cdot\mathbf{A}_{21} - |\mathbf{A}_{12}|^2]\right\} , \tag{5.6}$$

and

$$w(\mathbf{r}_1,\mathbf{r}_2,\mathbf{r}_3) = \frac{1}{m}\left[\frac{e}{c}\right]^2\left\{\mathbf{A}_{12}\cdot\mathbf{A}_{13} + \mathbf{A}_{21}\cdot\mathbf{A}_{23} + \mathbf{A}_{31}\cdot\mathbf{A}_{32}\right\} , \tag{5.7}$$

where $\mathbf{A}_{jk}$ is defined as in Eq. (1.2). These may then be expressed in terms of Fermi operators $\psi(\mathbf{r})$ and $\psi^\dagger(\mathbf{r})$ satisfying the usual anticommutation relations

$$\{\psi(\mathbf{r}),\psi^\dagger(\mathbf{r}')\} = \delta(\mathbf{r}-\mathbf{r}') , \tag{5.8}$$

in the manner

$$\mathcal{H}_1 = \int \psi^\dagger(\mathbf{r}_1) u(\mathbf{r}_1)\psi(\mathbf{r}_1) d\mathbf{r}_1 + \tfrac{1}{2}\int\int \psi^\dagger(\mathbf{r}_1)\psi^\dagger(\mathbf{r}_2) v(\mathbf{r}_1,\mathbf{r}_2)\psi(\mathbf{r}_2)\psi(\mathbf{r}_1) d\mathbf{r}_1 d\mathbf{r}_2$$

$$+ \tfrac{1}{6}\int\int\int \psi^\dagger(\mathbf{r}_1)\psi^\dagger(\mathbf{r}_2)\psi^\dagger(\mathbf{r}_3) w(\mathbf{r}_1,\mathbf{r}_2,\mathbf{r}_3)\psi(\mathbf{r}_3)\psi(\mathbf{r}_2)\psi(\mathbf{r}_1) d\mathbf{r}_1 d\mathbf{r}_2 d\mathbf{r}_3 , \tag{5.9}$$

provided that terms containing momentum operators are understood to be point split. For example, the one-body term written out explicitly is

$$\int \psi^\dagger(\mathbf{r}) u(\mathbf{r})\psi(\mathbf{r}) d\mathbf{r}$$

$$= \frac{1}{m}\int \psi^\dagger(\mathbf{r})\left\{ -\frac{e}{c}\frac{\hbar}{i}\overline{\mathbf{A}}(\mathbf{r})\cdot\nabla \right.$$

$$\left. -\frac{1}{2}\left[\frac{e}{c}\right]^2 |\overline{\mathbf{A}}(\mathbf{r})|^2 \right\}\psi(\mathbf{r}) d\mathbf{r} . \tag{5.10}$$

The density

$$\rho(\mathbf{r}) = \psi^\dagger(\mathbf{r}_1)\psi(\mathbf{r}_1) , \tag{5.11}$$

and current-density operators defined by Eqs. (1.7) and (1.8) may be expressed similarly. Following Eq. (3.20), we shall decompose the latter into mean-field and correction current operators, in the manner

$$\mathbf{J}(\mathbf{r}) = \mathbf{j}(\mathbf{r}) + \delta\mathbf{J}(\mathbf{r}) , \tag{5.12}$$

where

$$\mathbf{j}(\mathbf{r}_1) = \lim_{\mathbf{r}_2\to\mathbf{r}_1}\frac{1}{m}\left\{ \frac{1}{2}[\mathbf{P}_1 - \mathbf{P}_2] + \frac{e}{c}\overline{\mathbf{A}}(\mathbf{r}_1) \right\}\psi^\dagger(\mathbf{r}_2)\psi(\mathbf{r}_1)$$

$$\tag{5.13}$$

and

$$\delta\mathbf{J}(\mathbf{r}_1) = \frac{e}{mc}\left\{ \int \psi^\dagger(\mathbf{r}_1)\psi^\dagger(\mathbf{r}_2)\, \mathbf{A}_{12}\psi(\mathbf{r}_2)\psi(\mathbf{r}_1) d\mathbf{r}_2 \right.$$

$$\left. -\psi^\dagger(\mathbf{r}_1)\overline{\mathbf{A}}(\mathbf{r}_1)\psi(\mathbf{r}_1) \right\} . \tag{5.14}$$

The next step is to evaluate all relevant matrix elements by normal-ordering the Fermi operators and contracting using Wick's theorem. For this purpose we introduce the usual Fermi time-ordering operator

$$T\{\hat{O}_1^I(t_1)\ \cdots\ \hat{O}_n^I(t_n)\}$$

$$= \mathrm{sgn}(p)\hat{O}_{p(1)}^I(t_{p(1)})\ \cdots\ \hat{O}_{p(n)}^I(t_{p(n)}) , \tag{5.15}$$

where O_j is either $\psi(\mathbf{r}_j)$ or $\psi^\dagger(\mathbf{r}_j)$, p is the permutation satisfying

$$t_{p(1)} > \cdots > t_{p(n)} , \tag{5.16}$$

and $\mathrm{sgn}(p)$ is the sign of p. This is equivalent to the definition of Eq. (5.2), provided that an operator pair at equal times, such as that appearing in Eq. (5.11), is interpreted with the annihilation operator infinitesimally retarded. With T thus defined, we specialize to the case of an equal number n of creation and annihilation operators. With p denoting one of the $n!$ permutations of the creation operators, we have

$$\langle\Phi_0|T\{\hat{\psi}^I(\mathbf{r}_1 t_1)\ \cdots\ \hat{\psi}^I(\mathbf{r}_n t_n)\hat{\psi}^{\dagger I}(\mathbf{r}_{n+1} t_{n+1})\ \cdots\ \hat{\psi}^{\dagger I}(\mathbf{r}_{2n} t_{2n})\}|\Phi_0\rangle$$

$$= (-1)^{n(n-1)/2}\sum_p \mathrm{sgn}(p)[iG^0(\mathbf{r}_1 t_1|\mathbf{r}_{p(n+1)} t_{p(n+1)})]\times \cdots \times[iG^0(\mathbf{r}_n t_n|\mathbf{r}_{p(2n)} t_{p(2n)})] , \tag{5.17}$$

where G^0 is the unperturbed propagator, defined by

$$G^0(\mathbf{r}_1 t_1|\mathbf{r}_2 t_2) = -i\langle\Phi_0|T\{\hat{\psi}^I(\mathbf{r}_1,t_1)\hat{\psi}^{\dagger I}(\mathbf{r}_2,t_2)\}|\Phi_0\rangle . \tag{5.18}$$

The next step is to illustrate the perturbative procedure by writing out a few terms in the series explicitly. Let us begin by considering terms not containing the correction current operator $\delta\mathbf{J}(\mathbf{r})$ as defined by Eq. (5.14), which we note is equivalent to substituting $\mathbf{j}$ for $\mathbf{J}$ in Eq. (5.1). From the $m = 0$ term in Eq. (5.2) we obtain

$$\langle\Phi_0|T[\hat{j}^{\mu I}(\mathbf{r}_1,t_1)\hat{j}^{\nu I}(\mathbf{r}_2,t_2)]|\Phi_0\rangle = \mathcal{G}_1 + \mathcal{G}_2 , \tag{5.19}$$

where

$$\mathcal{G}_1 = j^\mu(\mathbf{r}_1)[iG^0(\mathbf{r}_1 t_1|\mathbf{r}_1 t_1)]j^\nu(\mathbf{r}_2)[iG^0(\mathbf{r}_2 t_2|\mathbf{r}_2 t_2)] , \tag{5.20}$$

$$\mathcal{G}_2 = -j^\mu(\mathbf{r}_1)[iG^0(\mathbf{r}_1 t_1|\mathbf{r}_2 t_2)]j^\nu(\mathbf{r}_2)[iG^0(\mathbf{r}_2 t_2|\mathbf{r}_1 t_1)] , \tag{5.21}$$

and $j^\mu(\mathbf{r})$ is shorthand for the one-body versions of the operators ρ and $\mathbf{j}$. These graphs assume the point-splitting convention of Eq. (5.10), which written out explicitly gives

$$j^x(\mathbf{r})[iG^0(\mathbf{r}t|\mathbf{r}t)] = \lim_{\mathbf{r}'\to\mathbf{r}}\lim_{\varepsilon\to 0}\frac{1}{m}\left[\frac{1}{2}\frac{\hbar}{i}\left[\frac{\partial}{\partial x} - \frac{\partial}{\partial x'}\right] + \frac{e}{c}\overline{A}_x(\mathbf{r})\right][iG^0(\mathbf{r}t|\mathbf{r}'t+\varepsilon)] , \tag{5.22}$$

and

$$j^x(\mathbf{r}_1)[iG^0(\mathbf{r}_1 t_1|\mathbf{r}_2 t_2)]j^y(\mathbf{r}_2)[iG^0(\mathbf{r}_2 t_2|\mathbf{r}_1 t_1)]$$

$$= \lim_{\mathbf{r}_1' \to \mathbf{r}_1} \lim_{\mathbf{r}_2' \to \mathbf{r}_2} \frac{1}{m^2} \left[\frac{1}{2} \frac{\hbar}{i} \left[\frac{\partial}{\partial x_1} - \frac{\partial}{\partial x_1'} \right] + \frac{e}{c} \overline{A}_x(\mathbf{r}_1) \right]$$

$$\times \left[\frac{1}{2} \frac{\hbar}{i} \left[\frac{\partial}{\partial y_2} - \frac{\partial}{\partial y_2'} \right] + \frac{e}{c} \overline{A}_y(\mathbf{r}_2) \right] [iG^0(\mathbf{r}_1 t_1|\mathbf{r}_2' t_2)][iG^0(\mathbf{r}_2 t_2|\mathbf{r}_1' t_1)] . \tag{5.23}$$

Equations (5.20) and (5.21) are illustrated in Fig. 1. Each dot in the figure represents a space-time point. The labels μ and ν indicate the insertion of current operators j^μ and j^ν at these points. Each line represents a factor of iG^0, the arguments of which are the points at either end of the line. The arrow distinguishes the left and right arguments of G^0. Each dot must connect to two fermion lines, one entering and one leaving. There is an overall minus sign for each closed fermion loop, of which there are two in $\mathscr{G}_1$ and one in $\mathscr{G}_2$. Turning now to the case of $m = 1$, we obtain

$$(i\hbar)^{-1} \int e^{(-\eta/\hbar)|t|} \langle \Phi_0 | T[\widehat{\mathscr{H}}_1^I(t) \widehat{j}^{\,\mu I}(\mathbf{r}_1, t_1) \widehat{j}^{\,\nu I}(\mathbf{r}_2, t_2)] | \Phi_0 \rangle dt = \sum_{i=3}^{50} \mathscr{G}_i , \tag{5.24}$$

where the graphs $\mathscr{G}_i$ are illustrated in Figs. 2–4. The dashed boxes in these figures indicate disconnected graphs, which are formally excluded from Eq. (5.2). The solid dots not labeled by μ or ν represent space-time points over which integration is performed. The dashed lines in Fig. 2, the wavy lines in Fig. 3, and the wavy symbol with a node in Fig. 4 represent factors of u, v, and w, respectively, as defined by Eqs. (5.5)–(5.7). The time variables associated with a given interaction line are constrained to be equal and are therefore not independent. The graph $\mathscr{G}_3$, for example, is given by

$$\mathscr{G}_3 = -(i\hbar)^{-1} \int_{-\infty}^{\infty} \int j^\mu(\mathbf{r}_1)[iG^0(\mathbf{r}_1 t_1|\mathbf{r}_2 t_2)]j^\nu(\mathbf{r}_2)[iG^0(\mathbf{r}_2 t_2|\mathbf{r}t)]u(\mathbf{r})[iG^0(\mathbf{r}t|\mathbf{r}_1 t_1)]d\mathbf{r}\,dt , \tag{5.25}$$

which, per the point-splitting convention, is evaluated in the manner

$$[iG^0(\mathbf{r}_2 t_2|\mathbf{r}t)]u(\mathbf{r})[iG^0(\mathbf{r}t|\mathbf{r}_1 t_1)] = \lim_{\mathbf{r}' \to \mathbf{r}} \frac{1}{m} \left\{ -\frac{1}{2} \frac{e}{c}(\mathbf{P} - \mathbf{P}') \cdot \overline{\mathbf{A}}(\mathbf{r}) - \frac{1}{2} \left[\frac{e}{c} \right]^2 |\overline{\mathbf{A}}(\mathbf{r})|^2 \right\} [iG^0(\mathbf{r}_2 t_2|\mathbf{r}'t)][iG^0(\mathbf{r}t|\mathbf{r}_1 t_1)] . \tag{5.26}$$

The graph $\mathscr{G}_{13}$ is given by

$$\mathscr{G}_{13} = -(i\hbar)^{-1} \int_{-\infty}^{\infty} \int \int j^\mu(\mathbf{r}_1)[iG^0(\mathbf{r}_1 t_1|\mathbf{r}_3 t)][iG^0(\mathbf{r}_3 t|\mathbf{r}_2 t_2)]$$

$$\times j^\nu(\mathbf{r}_2)[iG^0(\mathbf{r}_2 t_2|\mathbf{r}_4 t)][iG^0(\mathbf{r}_4 t|\mathbf{r}_1 t_1)]\tfrac{1}{2}v(\mathbf{r}_3, \mathbf{r}_4)d\mathbf{r}_3 d\mathbf{r}_4 dt + [3 \leftrightarrow 4] , \tag{5.27}$$

where $[3 \leftrightarrow 4]$ indicates the same integral with the dummy variables $\mathbf{r}_3$ and $\mathbf{r}_4$ reversed. This reflects the usual rule associated with pair potentials that the two-fold degeneracy required by Eq. (5.2) is cancelled by the $\frac{1}{2}$ in the definition of v. We note that the number in parentheses below each of the connected graphs in Fig. 3, which indicates the number of distinct contractions leading to the graph, is always 2. The three-body graph $\mathscr{G}_{24}$ is given by

$$\mathscr{G}_{24} = -(i\hbar)^{-1} \int_{-\infty}^{\infty} \int \int \int j^\mu(\mathbf{r}_1)[iG^0(\mathbf{r}_1 t_1|\mathbf{r}_2 t_2)]j^\nu(\mathbf{r}_2)[iG^0(\mathbf{r}_2 t_2|\mathbf{r}_3 t)][iG^0(\mathbf{r}_3 t|\mathbf{r}_4 t)][iG^0(\mathbf{r}_4 t|\mathbf{r}_5 t)][iG^0(\mathbf{r}_5 t|\mathbf{r}_1 t_1)]$$

$$\times \tfrac{1}{6}w(\mathbf{r}_3, \mathbf{r}_4, \mathbf{r}_5)d\mathbf{r}_3 d\mathbf{r}_4 d\mathbf{r}_5 dt + [\text{permutations of (345)}] . \tag{5.28}$$

In this case the total number of distinct contractions is 6, which cancels the factor of $\frac{1}{6}$ in the definition of w. However, some of the connected three-body graphs, those for which two of the three space-time points connected by the interaction are indistinguishable, correspond to only three contractions. The factor of w in these graphs is thus effectively halved. We consider finally the correction $\delta J(\mathbf{r})$ defined by Eq. (5.14). From the $m = 0$ term in Eq. (5.2), we have

$$\langle \Phi_0 | T[\delta \widehat{j}^{\,\mu I}(\mathbf{r}_1, t_1) \widehat{j}^{\,\nu I}(\mathbf{r}_2, t_2)] | \Phi_0 \rangle = \sum_{i=51}^{58} \mathscr{G}_i , \tag{5.29}$$

where the graphs $\mathscr{G}_i$ are illustrated in Fig. 5. The dotted and dashed lines in this figure represent effective one-body

$$\overline{u}(\mathbf{r}_1) = -\frac{1}{m} \frac{e}{c} \overline{\mathbf{A}}(\mathbf{r}_1) \tag{5.30}$$
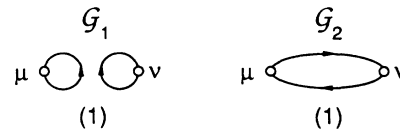
and two-body

FIG. 1. $m = 0$ graphs defined by Eq. (5.19). The dots represent space-time points. The labels μ and ν indicate the insertion of current operators j^μ and j^ν at these points. The lines represent factors of iG^0, as defined by Eq. (5.18). The number in parentheses indicates the number of distinct contractions leading to a graph. The total number of contractions in the figure is 2!.
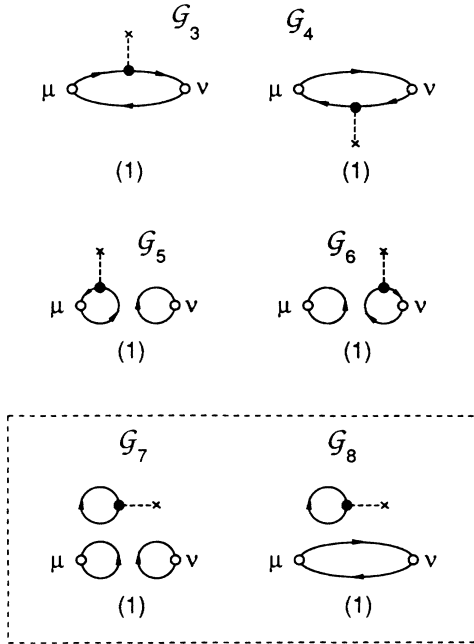
FIG. 2. One-body contributions to the $m = 1$ graphs defined by Eq. (5.24). The internal dot represents a space-time integration variable. The dashed line represents a factor of u, as defined by Eq. (5.5). The dashed box identifies the disconnected graphs, which do not contribute to Eq. (5.2). The number in parentheses indicates the number of distinct contractions leading to a graph. The total number of contractions in the figure is 3!.

$$\bar{v}(\mathbf{r}_1, \mathbf{r}_2) = \frac{1}{m} \frac{e}{c} \mathbf{A}_{12} \tag{5.31}$$

interactions analogous to those defined in Eqs. (5.5) and (5.6). However, these potentials are associated only with the points labeled μ and ν and replace the current operators j^μ and j^ν normally inserted at these points. For example, the graphs $\mathcal{G}_{52}$ and $\mathcal{G}_{54}$ are given by

$$\mathcal{G}_{52} = -\bar{u}^{\,\mu}(\mathbf{r}_1)[iG^0(\mathbf{r}_1 t_1 | \mathbf{r}_2 t_2)]j^\nu(\mathbf{r}_2)[iG^0(\mathbf{r}_2 t_2 | \mathbf{r}_1 t_1)] \tag{5.32}$$

and

$$\mathcal{G}_{54} = -\int \bar{v}^{\,\mu}(\mathbf{r}_1, \mathbf{r})[iG^0(\mathbf{r} t_1 | \mathbf{r} t_1)][iG^0(\mathbf{r}_1 t_1 | \mathbf{r}_2 t_2)]$$
$$\times j^\nu(\mathbf{r}_2)[iG^0(\mathbf{r}_2 t_2 | \mathbf{r}_1 t_1)]d\mathbf{r} . \tag{5.33}$$

Note that the time components of $\bar{u}$ and $\bar{v}$ are zero, so that only the spatial components are affected by the correction.

The final step is to generalize these results to higher values of m. As was the case with $m = 1$, each higher-order term in Eq. (5.2) may be expanded into a sum of graphs containing m interaction lines and up to two current correction lines, which must be summed. The graphs of order m implicitly contain an $m!$-fold degeneracy, associated with relabeling of the dummy integration variables, which exactly cancels the $m!$ in the denominator in Eq. (5.2). The disconnected graphs sum to an unphysical overall phase and are thus excluded. The Feynman rules for this problem are therefore the following.
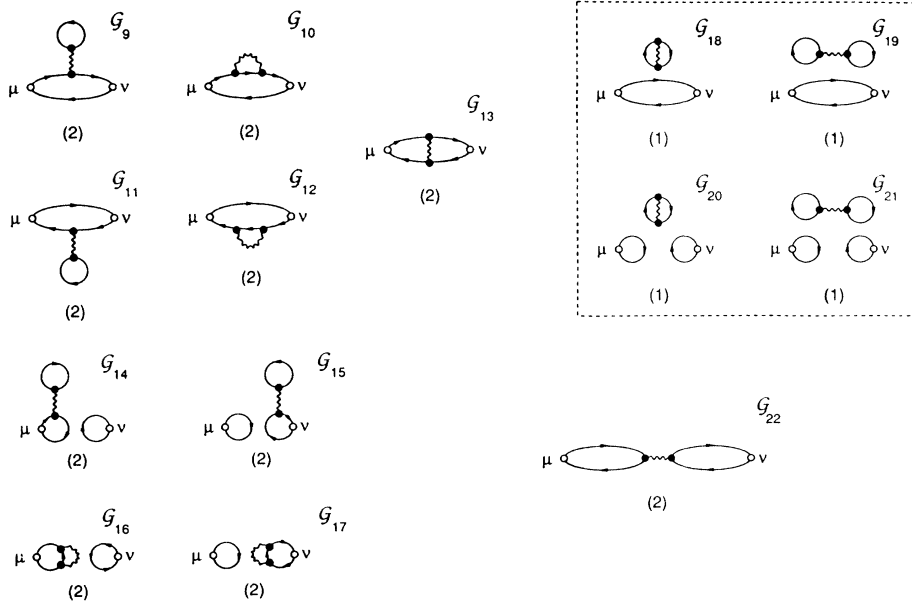
(1) Draw all distinct graphs beginning and ending at

FIG. 3. Two-body contributions to the $m = 1$ graphs defined by Eq. (5.24). The internal dots represent space-time integration variables constrained to occur at equal times. The wavy line represents a factor of v, as defined by Eq. (5.6). The dashed box identifies the disconnected graphs, which do not contribute to Eq. (5.2). The number in parentheses indicates the number of distinct contractions leading to a graph. The total number of contractions in the figure is 4!.

QUANTUM MECHANICS OF THE FRACTIONAL-STATISTICS . . .

points labeled μ and ν. Each point connects to two fermion lines, one entering and one leaving. Points other than μ and ν also connect to one interaction line. μ and ν have either two fermion lines only or two fermion lines and one current correction line, as illustrated in Fig. 5.

(2) Assign a space-time location to every point.

(3) Assign a factor iG^0 to each directed fermion line, taking the arguments of G^0 to be the points at either end of the line. Infinitesimally retard the creation operator in G^0 if its time arguments are equal.

(4) Assign factors u, v, and w to the one-, two-, and three-body interaction lines. If two of the three vertices of a three-body line are indistinguishable, assign an additional factor of $\frac{1}{2}$.

(5) Assign factors of $\bar{u}$ and $\bar{v}$ to current-correction lines, if present.

(6) Insert a current operator j^μ or j^ν at the points μ or ν if a current-correction line is absent.

(7) Constrain all times associated with a given interaction line to be equal. Assign a factor $(i\hbar)^{-1}$ for each distinct integrated time variable.

(8) Assign a factor -1 for each closed fermion loop.

(9) Integrate over all distinct internal space and time variables.

The use of these rules is considerably simplified by the systematic cancellation of the terms in u, v, and $\bar{u}$ involving a freestanding factor of $\bar{\mathbf{A}}$. Consider, for example, the graphs shown in Fig. 6(a). Integrating on the space-time points 2 and 3 first and noting that the last graph has an extra factor of $\frac{1}{2}$ per our Feynman rule (4), we find that the sum reduces to the effective one-body interaction

$$u_{\mathrm{eff}}(\mathbf{r}_1) = \frac{1}{m}\left[\frac{e}{c}\right]^2 \bar{\rho}\int d2|\,\mathbf{A}_{12}|^2 \ . \tag{5.34}$$

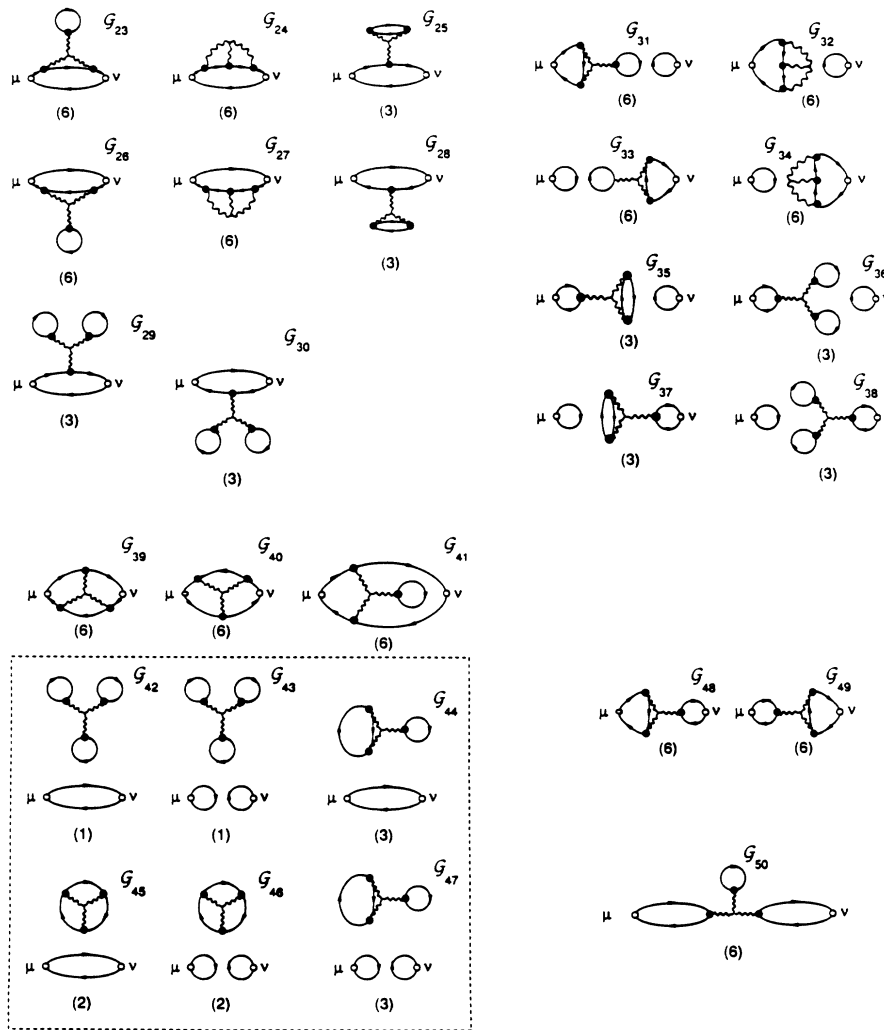This may be substituted for u in the diagrammatic expan-

FIG. 4. Three-body contributions to the $m=1$ graphs defined by Eq. (5.24). The internal dots represent space-time integration variables constrained to occur at equal times. The three wavy lines meeting at a node represents a factor of w, as defined in Eq. (5.7). The dashed box identifies the disconnected graphs, which do not contribute to Eq. (5.2). The number in parentheses indicates the number of distinct contractions leading to a graph. The total number of contractions in the figure is 5!.
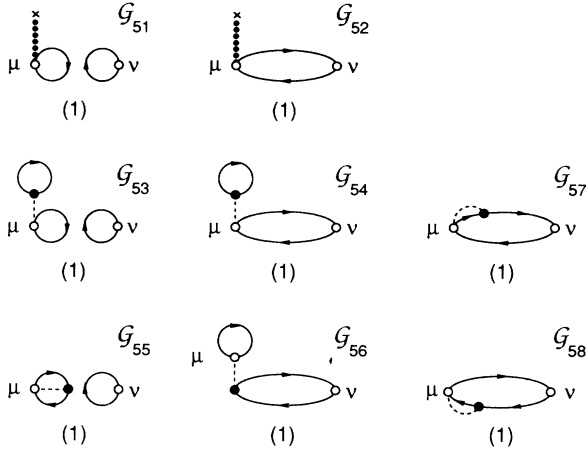
FIG. 5. $m = 0$ graphs defined by Eq. (5.29). The dotted and dashed lines correspond to factors of $\bar{u}$ and $\bar{v}$, as defined by Eqs. (5.30) and (5.31), respectively. The number in parentheses indicates the number of distinct contractions leading to a graph. The total number of contractions in the figure is $2! + 3!$.

FIG. 6. Illustration of cancellation of terms in u, v, and w involving a freestanding factor of $\bar{\mathbf{A}}$: (a) Diagrams defining effective one-body interaction $u_{\mathrm{eff}}(\mathbf{r}_1)$ of Eq. (5.34), (b) diagrams defining effective two-body interaction $v_{\mathrm{eff}}(\mathbf{r}_1,\mathbf{r}_2)$ of Eq. (5.35), and (c) diagrams defining effective one-body current-correction factor $\bar{u}_{\mathrm{eff}}(\mathbf{r}_1)$ of Eq. (5.36).

sion, provided that the Hartree diagrams involving v and w (namely, those containing $\mathscr{G}_{62}$ and $\mathscr{G}_{63}$ as insertions) are systematically excluded. Similarly, the graphs shown in Fig. 6(b), the latter of which lacks the factor of $\frac{1}{2}$, reduce to the effective two-body interaction

$$
\begin{aligned}
v_{\mathrm{eff}}(\mathbf{r}_1,\mathbf{r}_2) \\
= \frac{1}{m} \left\{ \frac{e}{c} \left[\left[\mathbf{P}_1 + \frac{e}{c}\overline{\mathbf{A}}_1 \right] \cdot \mathbf{A}_{12} + \left[\mathbf{P}_2 + \frac{e}{c}\overline{\mathbf{A}}_2 \right] \cdot \mathbf{A}_{21} \right] \right. \\
\left. + \left[\frac{e}{c} \right]^2 \left[|\mathbf{A}_{12}|^2 + \bar{\rho}\int d3\ \mathbf{A}_{13}\cdot\mathbf{A}_{23} \right] \right\} .
\end{aligned}
\tag{5.35}
$$

This may be substituted for v, provided that the corresponding two-body Hartree graphs are systematically excluded. The current-correction graphs shown in Fig. 6(c)
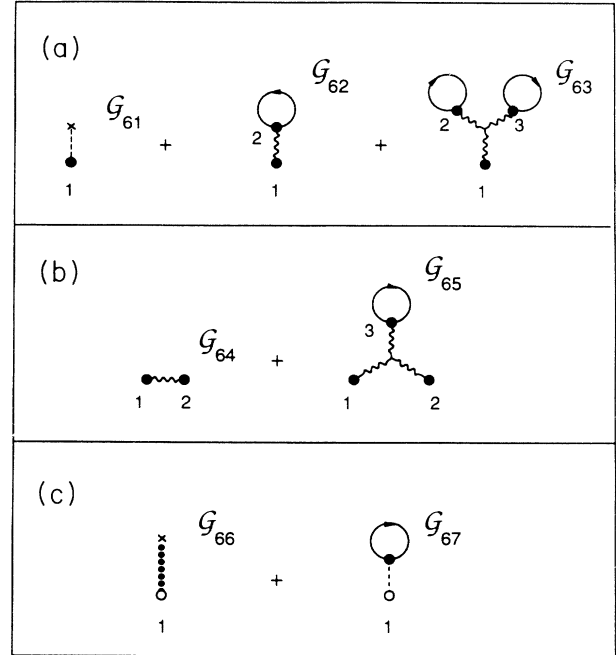
sum to zero. We may write

$$
\bar{u}_{\mathrm{eff}}(\mathbf{r}_1) = 0 .
\tag{5.36}
$$

VI. HARTREE-FOCK PROPAGATOR

Let us now identify the sum of graphs equivalent to our previous variational Hartree-Fock work.[1] We begin by explicitly evaluating the unperturbed propagator defined by Eq. (5.18). As before, we shall use lengths and energies in units of a_0 and $\hbar\omega_c$, as defined by Eqs. (1.5) and (1.6). Since all the wave functions φ_{nk} defined by Eq. (1.4) with the same value of n are eigenstates of $\mathscr{H}_0$ with eigenvalues $n + \frac{1}{2}$, it is convenient to first combine them into the nth Landau-level projector, defined by

$$
\Pi_n(\mathbf{r}_1,\mathbf{r}_2) = \sum_k \varphi_{nk}(z_1)\varphi_{nk}^*(z_2) = \frac{1}{2\pi 2^n n!} \left[2\frac{\partial}{\partial z_2} - \frac{1}{2}z_2^* \right]^n \left[2\frac{\partial}{\partial z_1^*} - \frac{1}{2}z_1 \right]^n e^{-[|z_1|^2 + |z_2|^2]/4} e^{z_1^* z_2/2} ,
\tag{6.1}
$$

where $z = x + iy$ is again $\mathbf{r}$ expressed as a complex number. In terms of this we then have

$$
G_0(\mathbf{r}_1 t_1 | \mathbf{r}_2 t_2) = \frac{1}{2\pi}\int_{-\infty}^{\infty} \sum_{n=0}^{\infty} \frac{\Pi_n(\mathbf{r}_1,\mathbf{r}_2)}{E - (n + \frac{1}{2}) + i\eta_n} e^{i(E/\hbar)(t_2 - t_1)} dE ,
\tag{6.2}
$$

where the infinitesimal η_n is positive for empty Landau levels and negative for filled ones.

The Hartree-Fock propagator is the diagrammatic sum illustrated in Fig. 7. It is given by[1]

$$
G_{\mathrm{HF}}(\mathbf{r}_1 t_1 | \mathbf{r}_2 t_2) = \frac{1}{2\pi}\int_{-\infty}^{\infty} \sum_{n=0}^{\infty} \frac{\Pi_n(\mathbf{r}_1,\mathbf{r}_2)}{E - \varepsilon_n + i\eta_n} e^{i(E/\hbar)(t_2 - t_1)} dE ,
\tag{6.3}
$$

where ε_n is the Hartree-Fock self-energy, given by

$$\varepsilon_{n\ (\nu=0)} = \left[-\frac{1}{2}E_R\right]\delta_{n0} + \left[n+\frac{1}{4}-\frac{1}{4n(n+1)}+\frac{1}{2}\sum_{k=1}^{n}\frac{1}{k}+\frac{1}{2}E_R\right](1-\delta_{n0}) \tag{6.4}$$

and

$$\varepsilon_{n\ (\nu=1/2)} = [\tfrac{1}{8}-\tfrac{1}{4}E_R]\delta_{n0}+[\tfrac{11}{8}-\tfrac{1}{4}E_R]\delta_{n1}+\left[n+\frac{5}{16}-\frac{1}{2(n^2-1)}+\frac{1}{4}\sum_{k=1}^{n}\frac{1}{k}+\frac{1}{4}E_R\right](1-\delta_{n0}-\delta_{n1}) , \tag{6.5}$$

where

$$E_R = \int_0^R dr\frac{1}{r}(1-e^{-r^2/2}) \underset{(R\to\infty)}{=} \ln(R)+\tfrac{1}{2}[\gamma-\ln(2)] , \tag{6.6}$$

with R denoting the sample radius, measured in units of a_0, and $\gamma=0.577\cdots$ denoting Euler's constant.

In our previous work,[1] ε_n was divided into 12 parts $\varepsilon_n^{(i)}$, which are reproduced for convenience in Appendixes A and B. As is indicated in Table I, each of these corresponds to a specific graph in Fig. 7. For example, $\varepsilon_n^{(6)}$, which is a constant that diverges as $\ln(R)$, is the Hartree energy deriving from the effective one-body interaction $u_{\rm eff}$ defined by Eq. (5.34). We note in Eqs. (A6) and (B6) that the weak divergence in $\varepsilon_n^{(6)}$ at small values of the integration variable r is exactly canceled by a similar divergence in $\varepsilon_n^{(7)}$. The latter is part of the exchange energy deriving from the effective two-body interaction $v_{\rm eff}$ defined by Eq. (5.35). This cancellation occurs because $\varepsilon^{(6)}$ includes a contribution from $\mathcal{G}_{63}$ in Fig. 6(a), which is the Hartree diagram corresponding to $\mathcal{G}_{65}$. Such cancellations occur commonly in Hartree-Fock calculations whenever the Hartree and exchange diagrams corresponding to a weakly singular two-body interaction are added. The reason is that antisymmetry of the many-body wave function prevents the particles from ever getting close enough to feel the singularity. The long-range part of $\varepsilon^{(6)}$, which is not canceled, adds to $\varepsilon^{(5)}$ and $\varepsilon^{(11)}$, the three-body Hartree energies corresponding to $\mathcal{G}_{75}$ in Fig. 7, to give an overall constant of $\frac{1}{2}(1-\nu)E_R$. This is very important, for it identifies a divergent energy cost to inject an extra particle into the system. As remarked previously, this occurs because the long-range potentials attached to the injected particle polarize the surrounding fluid into a current vortex, thus causing a $\ln(R)$ increase in the total kinetic energy. The long-range part of $\mathcal{G}_{74}$, given by $\varepsilon^{(12)}$, acts only on the occupied Landau levels and causes the energy cost to inject a *hole* also to be $\frac{1}{2}(1-\nu)E_R$. This occurs because the long-range potentials attached to the injected hole also polarize the fluid into a vortex, although in the opposite direction. Thus the energy cost to make a particle-hole pair is twice this value or $(1-\nu)E_R$. The absence of this energy is the most serious shortcoming of the simple RPA calculation described in Sec. III.
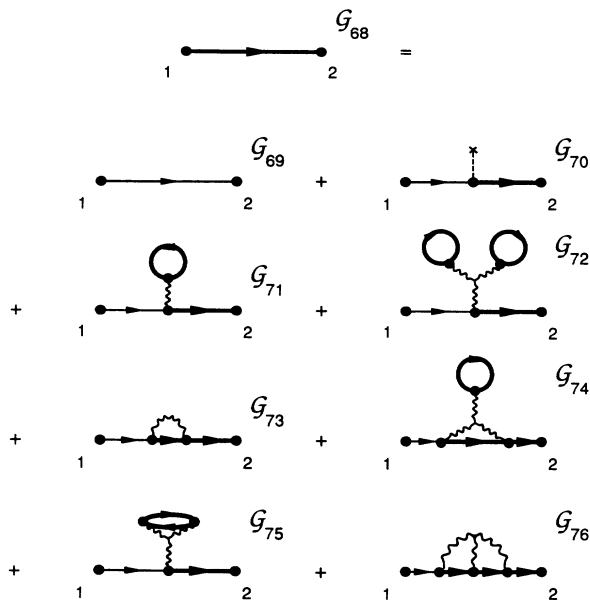

FIG. 7. Diagrammatic definition of the Hartree-Fock propagator, given by Eq. (6.3).

TABLE I. Twelve families of Hartree-Fock self-energies $\varepsilon^{(i)}$ and two-particle matrix elements $\mathcal{W}^{(i)}$ leading to gauge-invariant response kernel $\mathcal{H}$. The graphs associated with each family are listed to the right. The asterisk by the fourth family indicates that exchange current corrections are also required for gauge invariance, per Fig. 10(c).

1	$\varepsilon^{(2)}\cdots\varepsilon^{(6)}$	$\mathcal{G}_{70}\cdots\mathcal{G}_{72}$		
2	$\varepsilon^{(5)}$	$\mathcal{G}_{75}$		
3	$\varepsilon^{(11)}$			
4*	$\varepsilon^{(3)},\varepsilon^{(4)}$		$\mathcal{W}^{(3)},\mathcal{W}^{(4)}$	
5	$\varepsilon^{(7)}$	$\mathcal{G}_{73},\mathcal{G}_{74}$	$\mathcal{W}^{(6)}$	$\mathcal{G}_{79},\mathcal{G}_{80}$
6	$\varepsilon^{(12)}$		$\mathcal{W}^{(7)}$	
7	$\varepsilon^{(8)}\cdots\varepsilon^{(10)}$	$\mathcal{G}_{76}$	$\mathcal{W}^{(15)}\cdots\mathcal{W}^{(20)}$	$\mathcal{G}_{81},\mathcal{G}_{82}$
8			$\mathcal{W}^{(1)},\mathcal{W}^{(2)}$	
9			$\mathcal{W}^{(5)}$	$\mathcal{G}_{83},\mathcal{G}_{84}$
10			$\mathcal{W}^{(14)}$	
11			$\mathcal{W}^{(12)}\cdots\mathcal{W}^{(13)}$	$\mathcal{G}_{85},\mathcal{G}_{86}$
12			$\mathcal{W}^{(8)}\cdots\mathcal{W}^{(11)}$	

VII. VERTEX CORRECTION

Let us now consider the evaluation of the Bethe-Salpeter equation illustrated in Fig. 8, which includes two classes of graph. The first is the set of ladder diagrams required for maintaining compatibility of the response function with particle conservation,[12] per Eq. (1.9). These may also be viewed as accounting for the strong attractive potential between particles and holes associated

with their tendency to polarize the background fluid into vortices. The second is the set of bubble diagrams required to implement the RPA.

It may be seen from Fig. 8 that, despite the presence of three-body interactions, summation of the series still only requires knowledge of the four-point function at space-time configurations for which $t_1 = t_4$ and $t_2 = t_3$. Thus our first step is to identify the time variables in the Hartree-Fock four-point function $\mathcal{G}_{78}$, obtaining

$$[iG_{HF}(\mathbf{r}_1 t_1|\mathbf{r}_2 t_2)][iG_{HF}(\mathbf{r}_3 t_2|\mathbf{r}_4 t_1)] = \frac{\hbar}{2\pi i}\int_{-\infty}^{\infty}\mathcal{F}^0(\mathbf{r}_1,\mathbf{r}_4|\mathbf{r}_2,\mathbf{r}_3)e^{i\omega(t_1-t_2)}d\omega \ , \tag{7.1}$$

where

$$\mathcal{F}^0(\mathbf{r}_1,\mathbf{r}_4|\mathbf{r}_2,\mathbf{r}_3) = \sum_{\substack{n\,\text{empty}\\n'\,\text{filled}}}\left\{\frac{\Pi_n(\mathbf{r}_1,\mathbf{r}_2)\Pi_{n'}(\mathbf{r}_3,\mathbf{r}_4)}{\hbar\omega-(\varepsilon_n-\varepsilon_{n'})+i\eta} + \frac{\Pi_{n'}(\mathbf{r}_1,\mathbf{r}_2)\Pi_n(\mathbf{r}_3,\mathbf{r}_4)}{-\hbar\omega-(\varepsilon_n-\varepsilon_{n'})+i\eta}\right\} \ . \tag{7.2}$$

$\mathcal{F}^0$ corresponds approximately to the unperturbed response function $\mathcal{D}^0$ given by Eq. (3.29).

Our next step is to observe that summation is simplified by working in the basis of "magnetoexciton" basis wave functions, defined by[2]

$$\psi_{n\alpha}^{n'}(\mathbf{r}_1,\mathbf{r}_2) \equiv \frac{(-1)^n}{L}\frac{1}{(2\pi 2^{n+n'}n!n'!)^{1/2}}\left[2\frac{\partial}{\partial z_1^*}-\frac{1}{2}z_1\right]^n\left[2\frac{\partial}{\partial z_2}-\frac{1}{2}z_2^*\right]^{n'}e^{-[|z_1|^2+|z_2|^2+|z_\alpha|^2]/4}e^{[z_1^*z_2+z_1^*z_\alpha-z_2z_\alpha^*]/2} \ , \tag{7.3}$$

where $z = x + iy$ is again $\mathbf{r}$ expressed as a complex number, discussed in our previous work. These have a well-defined center-of-mass momentum $\mathbf{q}$, defined by

$$z_\alpha = iq_x - q_y \ , \tag{7.4}$$

which is conserved in this problem, even though the momentum of an isolated particle or hole is not, and are complete and orthonormal. Projecting $\mathcal{F}^0$ onto this basis, we obtain

$$\langle{}_m^{m'}|\mathcal{F}^0|{}_n^{n'}\rangle \equiv \int\int\int\int[\psi_{m\alpha}^{m'*}(\mathbf{r}_1,\mathbf{r}_4)]\mathcal{F}^0(\mathbf{r}_1,\mathbf{r}_4|\mathbf{r}_2,\mathbf{r}_3)\psi_{n\beta}^{n'}(\mathbf{r}_2,\mathbf{r}_3)d\mathbf{r}_1 d\mathbf{r}_2 d\mathbf{r}_3 d\mathbf{r}_4$$

$$= \delta_{\alpha\beta}\delta_{mn}\delta_{m'n'}\begin{bmatrix}[\hbar\omega-(\varepsilon_n-\varepsilon_{n'})+i\eta]^{-1}, & n \text{ empty}, \ n' \text{ occupied}\\[-\hbar\omega-(\varepsilon_{n'}-\varepsilon_n)+i\eta]^{-1}, & n' \text{ empty}, \ n \text{ occupied}\\0, & \text{otherwise}\end{bmatrix} \ . \tag{7.5}$$

We note that the only magnetoexciton wave functions not destroyed by $\mathcal{F}^0$ are those consisting of a hole in a filled Landau level and a particle in an empty one or the reverse, namely, a hole in an empty Landau level and a particle in a filled one. The latter makes no sense for a Hartree-Fock ground state, but is meaningful for a ground state in which particle-hole excitations of the Hartree-Fock vacuum are virtually present, as occurs in the RPA.

Our next step is to observe that all the interactions in Fig. 8, including the three-body terms, reduce to an effective pair interaction $\mathcal{W}(\mathbf{r}_1\mathbf{r}_2|\mathbf{r}_3\mathbf{r}_4)$ between the particle and hole. This is because all the internal Hartree-Fock lines have their time arguments constrained by the

Feynman rules to be equal and thus contain only information about the Hartree-Fock ground state, which is the same as the unperturbed ground state. The Bethe-Salpeter equation may therefore be solved by taking matrix elements of both $\mathcal{F}^0$ and the two-particle interaction $\mathcal{W}$ in the magnetoexciton basis and evaluating the matrix expression

$$\mathcal{F} \cong [1-\mathcal{F}^0\mathcal{W}]^{-1}\mathcal{F}^0 \ , \tag{7.6}$$

analogous to Eq. (3.18). Referring now to our second paper, we find that the matrix elements of $\mathcal{W}$, like those of $\mathcal{F}^0$, are zero unless the momentum quantum number z_α is the same for the initial and final states. The momentum-conserving matrix elements

$$\langle{}_m^{m'}|\mathcal{W}|{}_n^{n'}\rangle \equiv \int\int\int\int\psi_{m\alpha}^{m'*}(\mathbf{r}_1,\mathbf{r}_4)\mathcal{W}(\mathbf{r}_1,\mathbf{r}_4|\mathbf{r}_2,\mathbf{r}_3)\psi_{n\alpha}^{n'}(\mathbf{r}_2,\mathbf{r}_3)d\mathbf{r}_1 d\mathbf{r}_2 d\mathbf{r}_3 d\mathbf{r}_4 \ , \tag{7.7}$$

are given, with ψ_A and ψ_B shorthand for $\psi_{m\alpha}^{m'}$ and $\psi_{n\alpha'}^{n'}$, by

$$\mathcal{W} = \sum_{i=1}^{20} \mathcal{W}^{(i)} , \tag{7.8}$$

where

$$\mathcal{W}^{(1)} = \lim_{3 \to 1} \int d1 \int d2 \, \psi_B(2,2)[\, \mathbf{A}_{12} \cdot (\mathbf{P}_1 + \overline{\mathbf{A}}_1)]\psi_A^*(3,1) , \tag{7.9}$$

$$\mathcal{W}^{(2)} = \lim_{3 \to 1} \int d1 \int d2 \, \psi_A^*(2,2)[\, \mathbf{A}_{12} \cdot (\mathbf{P}_1 + \overline{\mathbf{A}}_1)]\psi_B(1,3) , \tag{7.10}$$

$$\mathcal{W}^{(3)} = - \int d1 \int d2 \, \psi_B(2,1)[\, \mathbf{A}_{12} \cdot (\mathbf{P}_1 + \overline{\mathbf{A}}_1)]\psi_A^*(2,1) , \tag{7.11}$$

$$\mathcal{W}^{(4)} = - \int d1 \int d2 \, \psi_A^*(1,2)[\, \mathbf{A}_{12} \cdot (\mathbf{P}_1 + \overline{\mathbf{A}}_1)]\psi_B(1,2) , \tag{7.12}$$

$$\mathcal{W}^{(5)} = \int d1 \int d2 |\, \mathbf{A}_{12}|^2 \psi_A^*(2,2)\psi_B(1,1) , \tag{7.13}$$

$$\mathcal{W}^{(6)} = - \int d1 \int d2 |\, \mathbf{A}_{12}|^2 \psi_A^*(1,2)\psi_B(1,2) , \tag{7.14}$$

$$\mathcal{W}^{(7)} = - \int d1 \int d2 \int d3 \, \mathbf{A}_{12} \cdot \mathbf{A}_{13} \Pi(1,1)\psi_A^*(2,3)\psi_B(2,3) , \tag{7.15}$$

$$\mathcal{W}^{(8)} = - \int d1 \int d2 \int d3 \, \mathbf{A}_{12} \cdot \mathbf{A}_{13} \Pi(1,3)\psi_A^*(1,3)\psi_B(2,2) , \tag{7.16}$$

$$\mathcal{W}^{(9)} = - \int d1 \int d2 \int d3 \, \mathbf{A}_{12} \cdot \mathbf{A}_{13} \Pi(3,1)\psi_A^*(2,2)\psi_B(1,3) , \tag{7.17}$$

$$\mathcal{W}^{(10)} = - \int d1 \int d2 \int d3 \, \mathbf{A}_{12} \cdot \mathbf{A}_{13} \Pi(1,2)\psi_A^*(3,3)\psi_B(2,1) , \tag{7.18}$$

$$\mathcal{W}^{(11)} = - \int d1 \int d2 \int d3 \, \mathbf{A}_{12} \cdot \mathbf{A}_{13} \Pi(2,1)\psi_A^*(2,1)\psi_B(3,3) , \tag{7.19}$$

$$\mathcal{W}^{(12)} = - \int d1 \int d2 \int d3 \, \mathbf{A}_{12} \cdot \mathbf{A}_{13} \Pi(3,2)\psi_A^*(1,1)\psi_B(2,3) , \tag{7.20}$$

$$\mathcal{W}^{(13)} = - \int d1 \int d2 \int d3 \, \mathbf{A}_{12} \cdot \mathbf{A}_{13} \Pi(2,3)\psi_A^*(2,3)\psi_B(1,1) , \tag{7.21}$$

$$\mathcal{W}^{(14)} = \int d1 \int d2 \int d3 \, \mathbf{A}_{12} \cdot \mathbf{A}_{13} \Pi(1,1)\psi_A^*(3,3)\psi_B(2,2) , \tag{7.22}$$

$$\mathcal{W}^{(15)} = \int d1 \int d2 \int d3 \, \mathbf{A}_{12} \cdot \mathbf{A}_{13} \Pi(1,3)\psi_A^*(2,3)\psi_B(2,1) , \tag{7.23}$$

$$\mathcal{W}^{(16)} = \int d1 \int d2 \int d3 \, \mathbf{A}_{12} \cdot \mathbf{A}_{13} \Pi(3,1)\psi_A^*(2,1)\psi_B(2,3) , \tag{7.24}$$

$$\mathcal{W}^{(17)} = \int d1 \int d2 \int d3 \, \mathbf{A}_{12} \cdot \mathbf{A}_{13} \Pi(1,2)\psi_A^*(1,3)\psi_B(2,3) , \tag{7.25}$$

$$\mathcal{W}^{(18)} = \int d1 \int d2 \int d3 \, \mathbf{A}_{12} \cdot \mathbf{A}_{13} \Pi(2,1)\psi_A^*(2,3)\psi_B(1,3) , \tag{7.26}$$

$$\mathcal{W}^{(19)} = \int d1 \int d2 \int d3 \, \mathbf{A}_{12} \cdot \mathbf{A}_{13} \Pi(3,2)\psi_A^*(1,2)\psi_B(1,3) , \tag{7.27}$$

and

$$\mathcal{W}^{(20)} = \int d1 \int d2 \int d3 \, \mathbf{A}_{12} \cdot \mathbf{A}_{13} \Pi(3,2)\psi_A^*(3,1)\psi_B(2,1) , \tag{7.28}$$

with $\mathbf{A}_{ij}$ defined as in Eq. (1.2), $\overline{\mathbf{A}}_j$ given by Eq. (1.11), and

$$\Pi(\mathbf{r}_1, \mathbf{r}_2) \equiv \sum_{\substack{n \\ \text{filled}}} \Pi_n(\mathbf{r}_1, \mathbf{r}_2) . \tag{7.29}$$

The dimensioned quantities e, m, c, and $\hbar$ have been set to 1 in these expressions, as appropriate for measuring lengths and energies in units of a_0 and $\hbar\omega_c$. Because $\mathcal{F}^0$ is qualitatively different for the particle-hole and hole-particle channels, it is helpful to divide the relevant matrix elements of $\mathcal{F}^0$ and $\mathcal{W}$ into four blocks. Thus, restricting m and n to *empty* Landau levels and m' and n' to *filled* ones, we define

$$\langle {}^{m'}_m | \mathcal{W} | {}^{n'}_n \rangle \equiv \langle {}^{m'}_m | \mathcal{E} | {}^{n'}_n \rangle , \tag{7.30}$$

and

$$\langle {}^{m'}_m | \mathcal{W} | {}^{n}_{n'} \rangle \equiv \langle {}^{m'}_m | \mathcal{A} | {}^{n}_{n'} \rangle . \tag{7.31}$$

Since the remaining matrix elements of $\mathcal{W}$ are related to these by

$$\langle {}^{m}_{m'} | \mathcal{W} | {}^{n'}_n \rangle = \langle {}^{m'}_m | \mathcal{E} | {}^{n'}_n \rangle^* \tag{7.32}$$

and

$$\langle {}^{m}_{m'}|\mathcal{W}|{}^{n'}_{n}\rangle = \langle {}^{m'}_{m}|\mathcal{A}|{}^{n'}_{n}\rangle^* \ , \tag{7.33}$$

we have, with the matrix $\Delta\varepsilon$ defined by

$$\langle {}^{m'}_{m}|\Delta\varepsilon|{}^{n'}_{n}\rangle \equiv \delta_{mn}\delta_{m'n'}(\varepsilon_n - \varepsilon_{n'}) \ , \tag{7.34}$$

and n, n', m, and m' now allowed to represent both filled and empty Landau levels,

$$\langle {}^{m'}_{m}|\mathcal{F}|{}^{n'}_{n}\rangle \equiv \int \int \int \int \psi^{m'}_{m\alpha}{}^{*}(\mathbf{r}_1,\mathbf{r}_4)\mathcal{F}(\mathbf{r}_1,\mathbf{r}_4|\mathbf{r}_2,\mathbf{r}_3)\psi^{n'}_{n\alpha}(\mathbf{r}_2,\mathbf{r}_3)d\mathbf{r}_1 d\mathbf{r}_2 d\mathbf{r}_3 d\mathbf{r}_4$$

$$= \left\langle {}^{m'}_{m}\right| \left[\begin{array}{cc} \hbar\omega - \Delta\varepsilon - \mathcal{E} + i\eta & -\mathcal{A} \\ -\mathcal{A}^\dagger & -\hbar\omega - \Delta\varepsilon - \mathcal{E}^* + i\eta \end{array} \right]^{-1} \left|{}^{n'}_{n}\right\rangle \ . \tag{7.35}$$

The contributions of the potentials $\mathcal{W}^{(i)}$ to the matrices $\mathcal{E}$ and $\mathcal{A}$ are listed in Appendixes D–G.

As was the case with the decomposed Hartree-Fock energies $\varepsilon_n^{(i)}$, the two-particle matrix elements $\mathcal{W}^{(i)}$ defined by Eqs. (7.9)–(7.28) correspond to specific graphs in Fig. 8, as is indicated in Table I. For example, $\mathcal{W}^{(6)}$ and $\mathcal{W}^{(7)}$ are the long-range potential contributions to the ladder graphs $\mathcal{G}_{79}$ and $\mathcal{G}_{80}$. $\mathcal{W}^{(12)}$ and $\mathcal{W}^{(13)}$ correspond to the three-body RPA graphs $\mathcal{G}_{85}$ and $\mathcal{G}_{86}$ neglected in our previous work. It may be seen from Appendixes D and F that the diagonal contributions $\mathcal{E}^{(6)}$, $\mathcal{E}^{(7)}$, $\mathcal{E}^{(12)}$, and $\mathcal{E}^{(13)}$ deriving from these together diverge as $-(1-v)E_R$ and thus exactly cancel the similar divergence in $\Delta\varepsilon$. This behavior, also seen in our variational work, occurs because these graphs account for the large attractive potential between particles and holes caused by the net cancellation of their vortex fields at infinity. These energies also contain a short-range divergence that is exactly canceled by $\mathcal{W}^{(5)}$, which is part of the two-body RPA contributions corresponding to $\mathcal{G}_{83}$ and $\mathcal{G}_{84}$. As was the case with the Hartree-Fock energy contributions, this cancellation may be attributed to the antisymmetry of the many-body wave function in the Fermi representation.

VIII. WARD IDENTITIES

Let us now consider the full electromagnetic response kernel $\mathcal{H}$ defined by Eqs. (3.11) and (3.8) using our approximate evaluation of the perturbative expansion in Eq. (5.2). We shall first do this by identifying the space-time points on either side of the four-point function $\mathcal{F}$, as illustrated by graph $\mathcal{G}_{87}$ in Fig. 9, and then Fourier transforming. We obtain
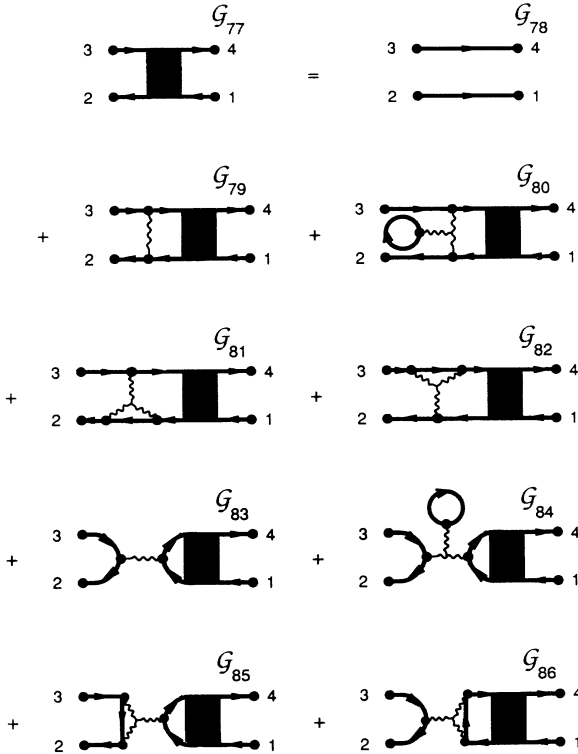

FIG. 8. Illustration of self-consistent four-point function defined by Eq. (7.7) and given explicitly by Eq. (7.36).
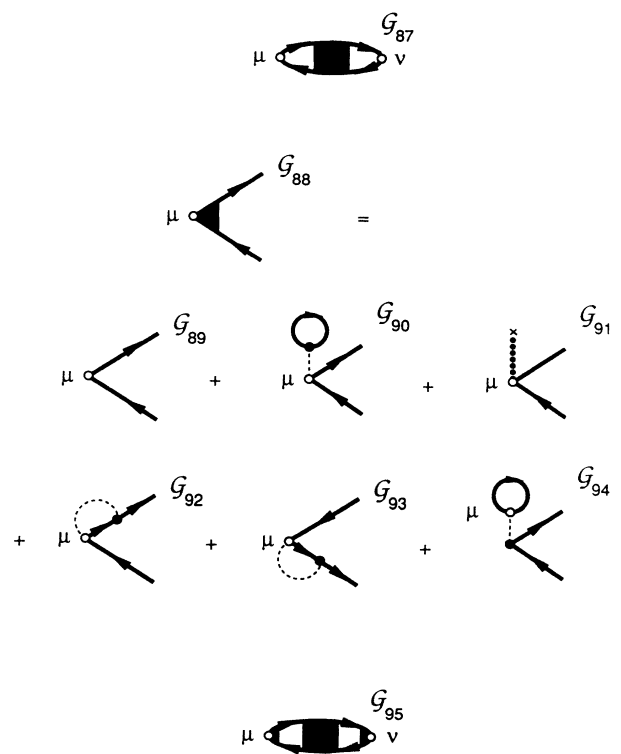

FIG. 9. Illustration of paramagnetic response kernels $\mathcal{D}$ and Δ as defined by Eqs. (8.1) and (8.4).

$$\mathcal{D}_{\mu\nu} = L^2 \int (i\hbar)^{-1} \int_{-\infty}^{\infty} e^{-i(\mathbf{q}\cdot\mathbf{r}_{12}-\omega t_{12})} e^{(-\eta/\hbar)|t_{12}|} j_\mu(1)\mathcal{F}(1,1|2,2) j_\nu(2) dt_1 d\mathbf{r}_1$$

$$= \sum_{mm'} \sum_{nn'} \langle j_\mu|_m^{m'}\rangle\langle_m^{m'}|\mathcal{F}|_n^{n'}\rangle\langle j_\nu|_n^{n'}\rangle^* ,$$
(8.1)

where the matrix elements $\langle j_\mu|_n^{n'}\rangle$ are defined by

$$\langle\rho|_n^{n'}\rangle = \int d1\, \psi_{n\alpha}^{n'}(1,1)e^{-i\mathbf{q}\cdot\mathbf{r}_1}$$
(8.2)

and

$$\langle\mathbf{j}|_n^{n'}\rangle = \int d1 \lim_{1\to 2} \left[\frac{1}{2}\left\{(\mathbf{P}_1+\overline{\mathbf{A}}_1)-(\mathbf{P}_2-\overline{\mathbf{A}}_2)\right\}\psi_{n\alpha}^{n'}(1,2)\right]e^{-i\mathbf{q}\cdot\mathbf{r}_1} .$$
(8.3)

Specific expressions for these matrix elements are listed in Appendix H. We then correct the current operators as we did in Eq. (3.22), but with the inclusion of exchange corrections required for maintaining gauge invariance. We have
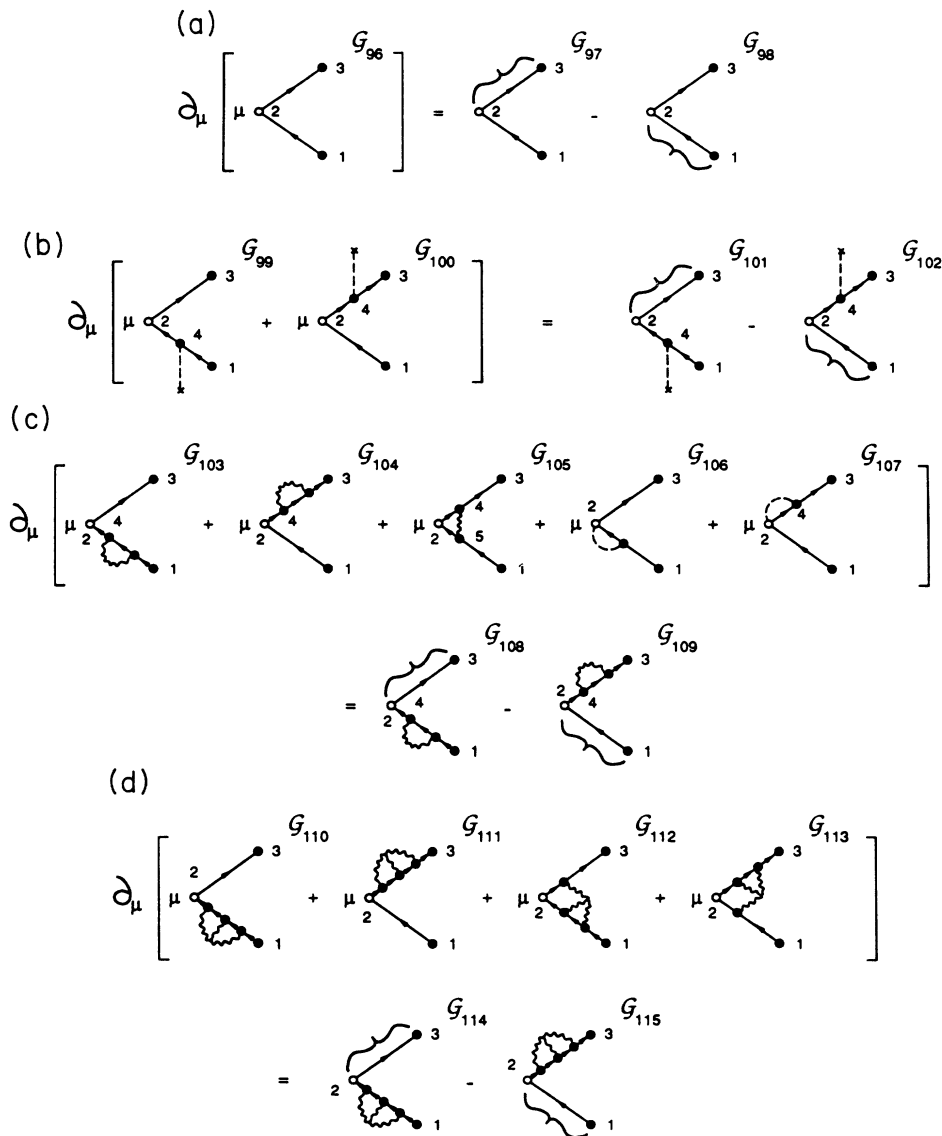
FIG. 10. Illustration of Ward identity for corrected current vertex: (a) Ward identity for unperturbed system described by Eq. (8.6), (b) typical one-body contribution, (c) two-body contribution involving spatial derivatives, and (d) three-body contribution. The curly bracket indicates the substitution of a three-dimensional δ function for the relevant Green's-function factor, per Eq. (8.6).

$$\Delta_{\mu\nu} = \sum_{mm'} \sum_{nn'} \langle j_\mu + \delta j_\mu |^{m'}_m \rangle \langle {}^{m'}_m | \mathcal{F} |^{n'}_n \rangle \langle j_\nu + \delta j_\nu |^{n'}_n \rangle^* \ , \tag{8.4}$$

where

$$\langle \delta j |^{n'}_n \rangle = \int d2 \, e^{-i\mathbf{q}\cdot\mathbf{r}_2} \int d1 \ \mathbf{A}_{21} \{ \Pi(2,2)\psi^{n'}_{n\alpha}(1,1) - \Pi(2,1)\psi^{n'}_{n\alpha}(1,2) - \Pi(1,2)\psi^{n'}_{n\alpha}(2,1) \} \ . \tag{8.5}$$

Note that the first term in this expression is equivalent to the matrix $\mathcal{U}$ defined by Eq. (3.23). Specific expressions for these matrix elements are also listed in Appendix H. Equation (8.4) corresponds to graph $\mathcal{G}_{95}$ in Fig. 9, with the definition of $\mathcal{G}_{88} - \mathcal{G}_{94}$. We then convert Δ to $\mathcal{H}$ by means of Eq. (3.11).

Gauge invariance of $\mathcal{H}$, as defined by Eq. (4.14), may be demonstrated by means of the Ward identity

$$\partial_\mu \{ [iG_0(1,2)]j^\mu(2)[iG_0(2,3)] \} = \frac{\partial}{\partial t_2} \{ [iG_0(1,2)][iG_0(2,3)] \} + \nabla_2 \cdot \{ [iG_0(1,2)]\mathbf{j}(2)[iG_0(2,3)] \}$$

$$= \{ [iG_0(1,2)]\delta^3(2,3) - \delta^3(1,2)[iG_0(2,3)] \} \ , \tag{8.6}$$

following the convention of Eq. (5.23), which is illustrated in Fig. 10. This follows from current conservation in the $\mathcal{H}_1 \to 0$ limit, which we may write

$$[\mathcal{H}_0, \rho(\mathbf{r})] = i\hbar \nabla \cdot \mathbf{j}(\mathbf{r}) \ , \tag{8.7}$$

per Eq. (1.9). Gauge invariance of the perturbed response kernel is demonstrated by identifying space-time points 1 and 3 in this expression, obtaining

$$\partial_\mu \{ [iG_0(1,2)]j^\mu(2)[iG_0(2,1)] \} = 0 \tag{8.8}$$

and

$$\partial_\mu \{ [iG_0(1,2)]j^\mu(2)[iG_0(2,1)]j^x(1) \} = -\frac{\hbar}{m} G_0(2,2) \frac{\partial}{\partial x_1} \delta^3(1,2) \ . \tag{8.9}$$

The right-hand side of Eq. (8.9) is canceled by the diamagnetic correction in Eq. (3.11). Our expression for the perturbed response kernel is gauge invariant because it effectively substitutes G_{HF} for G_0 on the right-hand side of Eq. (8.6). To see this let us consider the graphs in Fig. 10(b). Application of Eq. (8.6) to $\mathcal{G}_{99}$ and $\mathcal{G}_{100}$ produces terms proportional to $\delta^3(2,3)$ and $\delta^3(1,2)$, which are indicated as $\mathcal{G}_{101}$ and $\mathcal{G}_{102}$ in the figure, and two terms proportional to $\delta^3(2,4)$, which cancel exactly. Continuing this to higher order, we find that the only nonzero contributions come from graphs with *no* interaction line on at least one leg, and these contribute a δ function for this leg. Similar cancellations occur in Figs. 10(c) and 10(d), except for $\mathcal{G}_{106}$ and $\mathcal{G}_{107}$, which are required by the presence of spatial derivatives in the pair interaction v defined by Eq. (5.6). These effectively point-split the ends of the pair interaction lines in $\mathcal{G}_{103} - \mathcal{G}_{105}$, causing the extra contributions of these graphs to cancel incompletely. We note that the current corrections $\mathcal{G}_{90}$, $\mathcal{G}_{91}$, and $\mathcal{G}_{94}$ in Fig. 9 have no effect on the gauge invariance of $\mathcal{H}$.

The cancellation of specific contributions to the Fock and ladder sums in pairs, as occurs in Figs. 10(c) and 10(d), may be conveniently exploited to check the calculation for errors. In Table I we have organized the Hartree-Fock self-energy contributions $\varepsilon^{(i)}$ and the two-particle matrix elements $\mathcal{W}^{(i)}$ listed in the Appendixes into families representing subsets of diagrams leading to a gauge-invariant response kernel $\mathcal{H}$. If, for example, Eqs. (7.34) and (8.1) are evaluated with all the $\varepsilon^{(i)}$ and $\mathcal{W}^{(i)}$ set to zero except $\varepsilon^{(1)}$, $\varepsilon^{(12)}$, and $\mathcal{W}^{(7)}$, the result will be gauge invariant, although unphysical. This is also the case with the other 11 families, although a fourth of these requires the use of Eq. (8.4) rather than (8.1), as the latter includes the exchange current corrections shown in Fig. 10(c).

IX. BOSE FLUID

Let us now consider the results of our calculations for $\nu = 0$. The purpose of this is to test the reliability of the formalism in a case for which the answer is known. Our procedure is to truncate the basis of Eq. (7.3) to the states for which n and n' are no greater than a value n_c and then perform the matrix inversion of Eq. (7.35) numerically. The result is then substituted into Eqs. (8.4) and (3.11) to generate the electromagnetic response kernel $\mathcal{H}$.

In Fig. 11 we show the $\omega \to 0$ limit of the longitudinal response $\mathcal{H}_{xx}$, which is required by gauge invariance to be zero. These results show that the calculation converges rapidly with n_c, that it is accurately gauge invariant, and that the range of momentum over which it is valid increases with n_c. We have also performed, but not displayed in the figure, tests of the other two rows of $\mathcal{H}$, as well as tests of all three rows at finite ω, all of which are consistent with these results. The calculations reported in this paper are computed with $n_c = 30$ and are thus fully converged for $q \leq 5$.

In Fig. 12 we compare the longitudinal collective-mode frequency ω_q, defined as the low-frequency pole of $\mathcal{H}_{00}$, with the old RPA result obtained using Eq. (3.38). While the two calculations are qualitatively similar at small q, we observe that the sound speed is reduced from the value 1 given by Eq. (4.8) to the value $1/\sqrt{2}$ predicted by
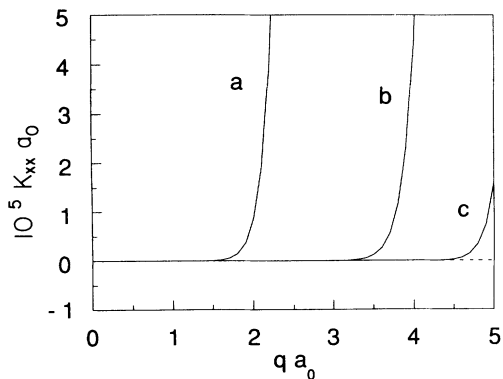
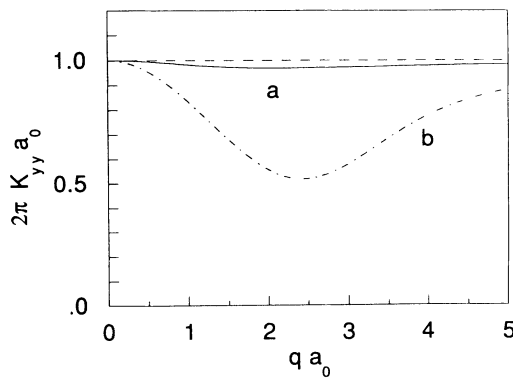FIG. 11. Gauge invariance test for $v=0$: (a) $n_c=10$, (b) $n_c=20$, and (c) $n_c=30$.

FIG. 13. Meissner kernel $\mathcal{K}_{yy}$ at $\omega=0$ for $v=0$: (a) present result and (b) previous RPA.

the Hartree-Fock bulk modulus.[1] This is not surprising in retrospect because the graphs we have included constitute a conserving approximation.[12] However, the old RPA calculation fails to find the logarithmic behavior at large q predicted by our previous variational study.[2] In contrast, the full calculation reported here agrees to within the line thickness with the variational work for $q \geq 2$. As remarked previously,[2] the variational calculation correctly describes the motion of a vortex pair in a fluid such as helium, but does not correctly describe the decay of such pairs into phonons. The latter effect would cause the collective mode to lose its sharpness at large q. The results at large q show that the ground state $|\Phi\rangle$ implicit in this calculation differs significantly from the unperturbed ground state $|\Phi_0\rangle$ only at long length scales. Quantities determined by the short-range behavior, such as the compressibility, may thus be calculated equally well with $|\Phi\rangle$ or $|\Phi_0\rangle$.

In Fig. 13 we compare the present Meissner kernel $\mathcal{K}_{yy}$ for $\omega=0$ with the old RPA result. The convergence of both curves to 1 as $q \to 0$ shows a perfect Meissner effect in either case. However, the present calculation shows screening that is much more pointlike. The coherence length, measured by the curvature at $q=0$, is one order of magnitude smaller. The coherence length is in either
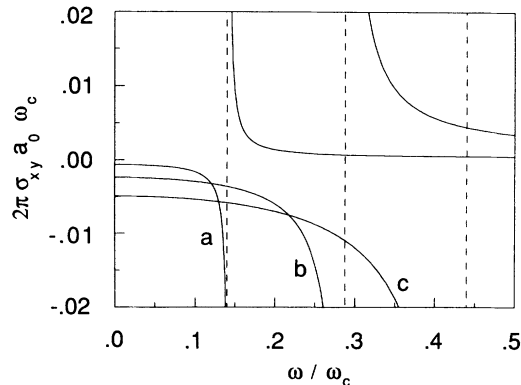

FIG. 14. Real part of Hall conductivity, as defined by Eq. (4.18) for $v=0$: (a) $q=0.2$, (b) $q=0.4$, and (c) $q=0.6$. The vertical lines mark the location of the sound pole for each value of q.
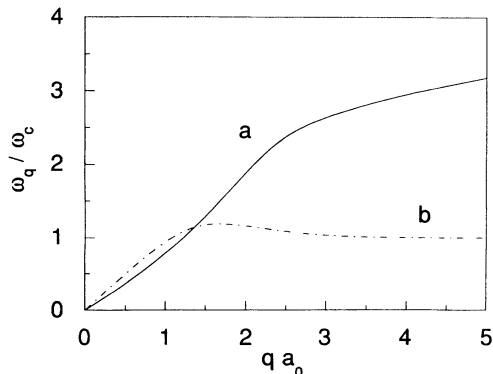

FIG. 12. Collective-mode frequency ω_q for $v=0$: (a) present result and (b) previous RPA.
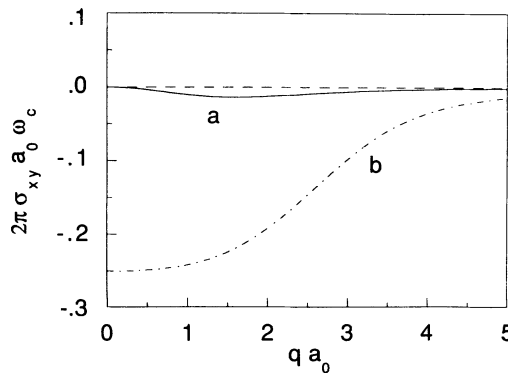

FIG. 15. Real part of Hall conductivity, as defined by Eq. (4.18) for $v=0$ in the $\omega \to 0$ limit: (a) present result and (b) previous RPA.

case unusually short. The convergence of both calcula-
tions to 1 at large values of q is a general feature of any
system of particles with finite-range interactions.

In Fig. 14 we show the frequency dependence of the
Hall conductivity σ_{xy} defined by Eq. (4.18). We see that
the present calculation, like the old RPA, predicts a
nonzero value of σ_{xy} and a singularity at the sound pole.
However, in contrast to our previous result, the present
one predicts the strength of this pole to vanish as q^2,
causing the pole to become irrelevant at small q. This is
shown more explicitly in Fig. 15, where the $\omega \rightarrow 0$ Hall
conductivity is plotted as a function of q. The present
calculation is identically zero at $q = 0$, and its maximum
excursion at $q \cong 1.5$ is only $\frac{1}{20}$ times the old RPA value.
We conclude from this that this computational technique
effectively eliminates the spurious Hall effect of the old
RPA (Ref. 4) for $v = 0$.

X. ONE-HALF FRACTIONAL-STATISTICS FLUID

Let us now consider the results for $v = \frac{1}{2}$. As we did in
Fig. 11, we show in Fig. 16 the gauge-invariance test
based on the longitudinal response $\mathcal{H}_{xx}$ in the $\omega \rightarrow 0$ limit.
The parameter n_c has the same formal definition as be-
fore, but the number of channels is effectively $2n_c$ because
two Landau levels are filled. The behavior is qualitatively
the same as in Fig. 11 and has the same significance.

In Fig. 17 we compare the collective-mode frequency,
defined as in Fig. 12, with that given by the old RPA.
The effect of the Fock and ladder diagrams is similar to
that seen in Fig. 12. The sound speed in this case is re-
duced from its RPA value of $\sqrt{2}$ to the $\sqrt{29/16}$ predict-
ed from the Hartree-Fock bulk modulus.[1,12] The behav-
ior for $q \geq 2$ is identical to within the line thickness with
the result obtained by setting the d matrices in Eq. (7.35)
to zero. This is equivalent to the variational calculation
performed by us previously for the $v = 0$ case and results
in the opening of a gap of $\frac{1}{2}$ at $q = 0$. The positions of the
peak and "roton" minimum are also in good agreement.
Also reproduced in this figure are the numerical results of
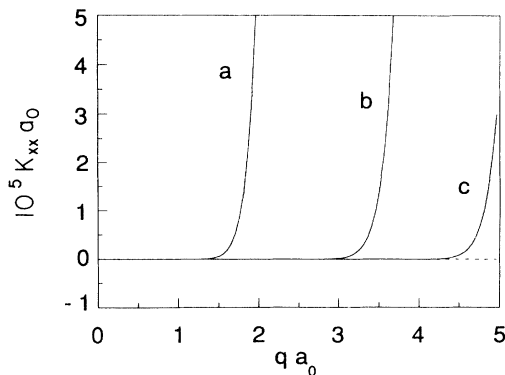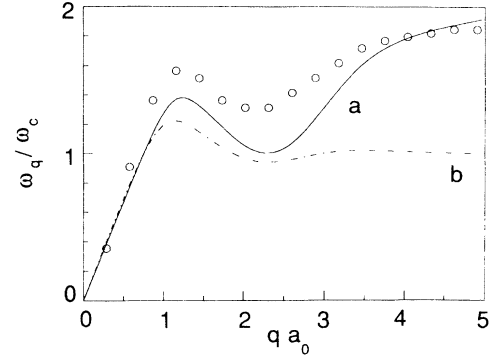Xie, He, and Das Sarma,[13] which are based on studies of

FIG. 17. Collective-mode frequency ω_q for $v = \frac{1}{2}$: (a) present
result and (b) previous RPA. The circles are the numerical re-
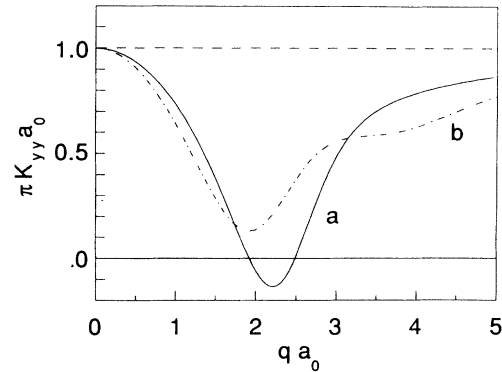sult from Ref. 13.

FIG. 18. Meissner kernel $\mathcal{H}_{yy}$ at $\omega = 0$ for $v = \frac{1}{2}$: (a) present
result and (b) previous RPA.

FIG. 16. Gauge-invariance test for $v = \frac{1}{2}$: (a) $n_c = 10$, (b)
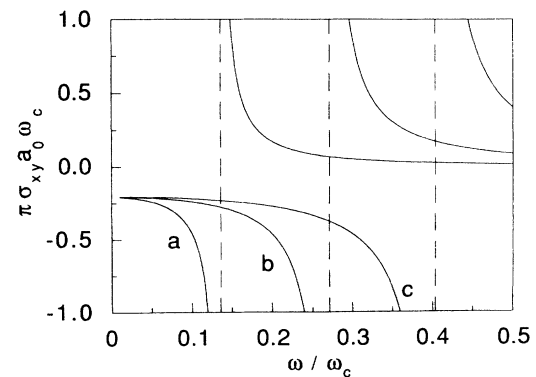$n_c = 20$, and (c) $n_c = 30$.

FIG. 19. Real part of Hall conductivity, as defined by Eq.
(4.18) for $v = \frac{1}{2}$: (a) $q = 0.1$, (b) $q = 0.2$, and (c) $q = 0.3$. The
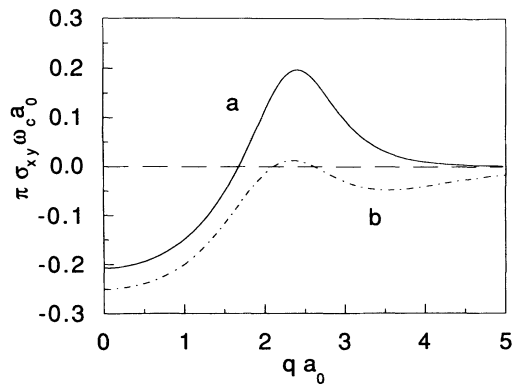vertical lines mark the location of the sound pole for each value
of q.

FIG. 20. Real part of Hall conductivity, as defined by Eq. (4.18) for $\nu=\frac{1}{2}$ in the $\omega\to0$ limit: (a) present result and (b) previous RPA.

small clusters. We note particularly the good agreement between the computed sound speeds and the position and depth of the roton.

In Fig. 18 we compare the Meissner kernel $\mathcal{H}_{yy}$ at $\omega=0$ with that of the old RPA. The behavior is qualitatively similar, including complete Meissner screening at $q\to0$, a deep minimum at $q\cong2$, and a gradual return to 1 at large q. In contrast to the $\nu=0$ case, however, we find no significant modification of the coherence length by the Fock and ladder diagrams. This strongly suggests that the structure in $\mathcal{H}_{yy}$ is given correctly by both calculations.

In Fig. 19 we plot the real part of the Hall conductivity, defined as in Eq. (4.18), as we did in Fig. 14. We again see resonant structure at the sound pole associated with a nonzero value of σ_{xy} in the $\omega\to0$ limit. However, in this case the full calculation is in qualitative agreement with the old RPA. This is shown explicitly in Fig. 20, where we compare the momentum dependence of the two calculations. The $q\to0$ limit may be seen to be finite and large in either case. In light of the ability of the Fock and ladder diagrams to counteract the spurious Hall effect in the $\nu=0$ case, this result suggests that the Hall effect is not spurious for $\nu=\frac{1}{2}$, but is a characteristic property of the fractional-statistics gas.

XI. DISCUSSION

The most surprising result of the calculations described in this paper is the disappearance of the Hall-effect pole for $\nu=0$ and its persistence for $\nu=\frac{1}{2}$. Since $\nu=0$ is a more severe perturbation from noninteracting fermions than $\nu=\frac{1}{2}$, this implies that inclusion of Fock and ladder diagrams is sufficient to describe the Hall effect correctly at long wavelengths and that the $\nu=\frac{1}{2}$ anomaly is not an artifact. Per our discussion of Eq. (4.19), this is very disturbing because it implies the existence of more than one velocity scale for the problem. For this reason we are reluctant to state categorically that this effect is real without study of the problem to higher order in perturbation theory. Given that it is correct, the persistence of

the anomaly may be related to the recent finding of Rojo and Canright[14] that the system acquires a magnetic moment at high temperatures.

Another unexpected result is the broad corroboration of the old RPA results for the $\nu=\frac{1}{2}$ fluid. Since this did not occur for $\nu=0$, it cannot be dismissed as an automatic consequence of the formalism. It is apparently the case that the fractional-statistics fluid is described fairly well by the RPA.

A critical difference between the full calculation and the old RPA is the effect of finite temperature. It has been discovered by several authors[15] that finite-temperature perturbation theory applied to the class of diagrams included in the old RPA predicts the destruction of the superfluidity at any finite temperature. This behavior is quite violent and not to be confused with the destruction of long-range coherence due to the Mermin-Wagner theorem.[16] While it is formally correct, the prediction is unphysical. The calculated low-energy excitation spectrum of the system at zero temperature is qualitatively similar to that of ^{4}He.[11] The effect of finite temperature must therefore be the same as that in ^{4}He, which is to thermally populate the $q\to0$ collective modes, lower the superfluid density by means of scatterings among these modes, and eventually cause a Kosterlitz-Thouless transition.[17] However, application of finite-temperature perturbation theory to the present calculation leads to no temperature dependence at all. This is equally unphysical and thus warrants discussion.

Let us first consider why finite temperature destroys the superfluidity in the old RPA. Substituting Matsubara sums[7] for energy integrals in the unperturbed polarizability $\mathcal{D}^0$ defined by Eq. (3.29) merely thermally repopulates the Landau levels in the unperturbed propagator G_0. This causes the Hall conductance of Σ_1 to have a value different from -1 at small q and ω and thus causes the collective mode, defined as the zero of D in Eq. (3.38), to acquire a gap. This is physically incorrect because particles and holes obeying fractional statistics are also vortices and antivortices. A dilute gas of particles cannot actually form at low temperatures because vortices and antivortices are tightly bound. Since this binding energy is formally absent in the old RPA, the calculation effectively forces Kosterlitz-Thouless unbinding of vortex-antivortex pairs to occur prematurely.

Let us now consider the absence of temperature dependence in the present calculation. The effect of finite temperature on the Hartree-Fock graphs of Fig. 7 is also thermal repopulation of the Landau levels of G_{HF}. However, in contrast to the old RPA calculation, the gap between the lowest empty Landau level and the highest filled one is $(1-\nu)E_R$, as defined by Eq. (6.6), which is formally infinite in the thermodynamic limit. Thus G_{HF} has no temperature dependence in the thermodynamic limit. Since the graphs of Figs. 8 and 9 have no temperature dependence of their own, $\mathcal{H}$ has no temperature dependence either. As remarked previously,[1] $\frac{1}{2}(1-\nu)E_R$ corresponds to the energy for making an isolated vortex. Thus superfluidity persists in this calculation because vortex-antivortex pairs are always tightly bound and, in

particular, do not screen each other out. Kosterlitz-Thouless unbinding is therefore precluded.

It was recently shown by Kitazawa and Murayama[18] that a Kosterlitz-Thouless transition occurs in a calculation in which a renormalized fractional-statistics interaction is substituted for the bare one. This result suggests that the correct temperature dependence will be produced by a calculation that includes RPA graphs on every interaction line, so as to self-consistently screen the interaction. Assuming that this is the case, we may ask why the zero-temperature properties are described so well without including these graphs. The reason suggested by Eq. (4.20) is that the fractional-statistics interaction is effectively unscreened at zero temperature. In particular, $\mathcal{V}_{00}^{RPA}$, the "Coulomb" interaction between particles responsible for the logarithmic gap $(1-v)E_R$, exactly equals $\mathcal{V}_{00}$. While the effects of retardation in the other elements of $\mathcal{V}^{RPA}$ on a fully self-consistent calculation have yet to be worked out, the good agreement in Fig. 17 suggests that they are unimportant at zero temperature. As the temperature is raised, however, the Coulomb interaction is expected to become dielectrically screened by the gas of tightly bound particle-hole pairs in the sample. This will change the magnitude of $\mathcal{V}_{00}^{RPA}$, but not its functional form at $q \rightarrow 0$, thus causing E_R to decrease in magnitude while maintaining its logarithmic dependence on R. Above the Kosterlitz-Thouless temperature, however, when the pairs unbind to form a particle-hole plasma, $\mathcal{V}_{00}^{RPA}$ should switch over to Debye screening, and E_R should lose its dependence and become finite.

We note finally that the tendency for the statistical interaction to remain unscreened in a many-body calculation has precedent in the high-energy literature[19] and is therefore more general than our calculation would suggest. However, the principles causing it to occur are poorly understood.

ACKNOWLEDGMENTS

APPENDIX A

Contributions $\varepsilon_n^{(i)}$ to the Hartree-Fock self-energy ε_n given by Eq. (6.4) for the case of $v=0$. E_R is defined as in Eq. (6.6). The specific graphs to which these correspond are indicated in Table I.

$$\varepsilon_n^{(1)} = (n + \tfrac{1}{2}) , \tag{A1}$$

$$\varepsilon_n^{(2)} = 0 , \tag{A2}$$

$$\varepsilon_n^{(3)} = \varepsilon_n^{(4)} = -\tfrac{1}{2}\delta_{n0} , \tag{A3}$$

$$\varepsilon_n^{(5)} = -\tfrac{1}{4} , \tag{A4}$$

$$\varepsilon_n^{(6)} = \lim_{\eta \to 0} \int_0^R dr \frac{1}{r+\eta} , \tag{A5}$$

$$\varepsilon_n^{(7)} = -\lim_{\eta \to 0} \int_0^R dr \frac{1}{r+\eta} e^{-r^2/2} + \frac{1}{2}(1-\delta_{n0}) \sum_{k=1}^{n} \frac{1}{k} , \tag{A6}$$

$$\varepsilon_n^{(8)} = \varepsilon_n^{(9)} = \tfrac{1}{4}\delta_{n0} , \tag{A7}$$

$$\varepsilon_n^{(10)} = \frac{1}{4}\delta_{n0} + \frac{1}{4}(1-\delta_{n0}) \left[\frac{1}{n+1} + \frac{1}{n} \right] , \tag{A8}$$

$$\varepsilon_n^{(11)} = -\tfrac{1}{2}E_R , \tag{A9}$$

$$\varepsilon_n^{(12)} = -E_R\delta_{n0} - \frac{1}{2}(1-\delta_{n0})\frac{1}{n} . \tag{A10}$$

APPENDIX B

Contributions $\varepsilon_n^{(i)}$ to the Hartree-Fock self-energy ε_n given by Eq. (6.5) for the case of $v=\tfrac{1}{2}$. E_R is defined as in Eq. (6.6). The specific graphs to which these correspond are indicated in Table I.

$$\varepsilon_n^{(1)} = (n + \tfrac{1}{2}) , \tag{B1}$$

$$\varepsilon_n^{(2)} = 0 , \tag{B2}$$

$$\varepsilon_n^{(3)} = \varepsilon_n^{(4)} = -\tfrac{1}{4}(\delta_{n0} + \delta_{n1}) , \tag{B3}$$

$$\varepsilon_n^{(5)} = -\tfrac{1}{8} , \tag{B4}$$

$$\varepsilon_n^{(6)} = \frac{1}{2} \lim_{\eta \to 0} \int_0^R dr \frac{1}{r+\eta} , \tag{B5}$$

$$\varepsilon_n^{(7)} = -\frac{1}{2} \lim_{\eta \to 0} \int_0^R dr \frac{1}{r+\eta} e^{-r^2/2} , + \frac{1}{8}\delta_{n0} + \frac{1}{4}\delta_{n1} + \frac{1}{4}(1-\delta_{n0}-\delta_{n1}) \sum_{k=1}^{n} \frac{1}{k} , \tag{B6}$$

$$\varepsilon_n^{(8)} = \varepsilon_n^{(9)} = \tfrac{3}{16}\delta_{n0} + \tfrac{1}{16}\delta_{n1} , \tag{B7}$$

$$\varepsilon_n^{(10)} = \tfrac{1}{16}\delta_{n0} + \tfrac{3}{16}\delta_{n1} + \frac{1}{4}(1-\delta_{n0}-\delta_{n1}) \left[\frac{1}{n+1} + \frac{1}{n} \right] , \tag{B8}$$

$$\varepsilon_n^{(11)} = -\tfrac{1}{16} - \tfrac{1}{4}E_R , \tag{B9}$$

$$\varepsilon_n^{(12)} = -(\tfrac{1}{4} + \tfrac{1}{2}E_R)\delta_{n0} - \tfrac{1}{2}E_R\delta_{n1} - \frac{1}{4}(1-\delta_{n0}-\delta_{n1}) \left[\frac{1}{n} + \frac{1}{n-1} \right] . \tag{B10}$$

APPENDIX C

Glossary of symbols used in Appendixes D–G. With z_α related to the momentum q as in Eq. (7.4), we have

$$c = \left| \begin{array}{ll} \dfrac{(-z_\alpha^*)^m(-z_\alpha)^n}{(2^{m+n}m!n!)^{1/2}}, & \nu=0 \\[12pt] \dfrac{(-z_\alpha^*)^{m-m'}(-z_\alpha)^{n-n'}}{(2^{m+n-m'-n'}m!n!)^{1/2}}, & \nu=\tfrac{1}{2} \end{array} \right|, \quad \text{(C1)}$$

$$d = \left| \begin{array}{ll} \dfrac{(-z_\alpha^*)^{m+n}}{(2^{m+n}m!n!)^{1/2}}, & \nu=0 \\[12pt] \dfrac{(-z_\alpha^*)^{m+n-m'-n'}}{(2^{m+n-m'-n'}m!n!)^{1/2}}, & \nu=\tfrac{1}{2} \end{array} \right|, \quad \text{(C2)}$$

$$b = \tfrac{1}{2}|z_\alpha|^2 , \quad \text{(C3)}$$

$$f_n = e^{-b} \sum_{k=0}^{n} \frac{b^k}{k!} , \quad \text{(C4)}$$

$$g_n = \sum_{k=0}^{n} \frac{k!}{b^{k+1}} f_k , \quad \text{(C5)}$$

$$h_n = \sum_{k=0}^{n} \frac{k!}{b^{k+1}} [1 - f_k] . \quad \text{(C6)}$$

We also define two formally divergent integrals

$$I_1 = e^{-b} \lim_{\eta \to 0} \int_0^\infty dr \frac{r}{r^2+\eta^2} J_0(qr) , \quad \text{(C7)}$$

where $q = |z_\alpha|$ and J_0 is a Bessel function and

$$I_2 = e^{-b} \lim_{\eta \to 0} \int_0^\infty dr \frac{r}{r^2+\eta^2} e^{-r^2/2} , \quad \text{(C8)}$$

which cancel from the final result, and three versions of the exponential-integral function

$$E_b = \frac{1}{2} \int_0^b dx \frac{1}{x}(1-e^{-x}) = -\frac{1}{2} \sum_{p=1}^{\infty} \frac{(-b)^p}{p!p} , \quad \text{(C9)}$$

$$X = e^{-b} \int_0^b dx \frac{1}{x}(e^x - 1) = e^{-b} \sum_{p=1}^{\infty} \frac{b^p}{p!p} , \quad \text{(C10)}$$

$$Y_{m,n} = m!n!e^{-b} \sum_{p=1}^{\infty} \frac{(p-1)!}{(p+m)!(p+n)!} b^p$$

$$\underset{n \geq m}{=} \sum_{k=0}^{m} \frac{1}{k!} \frac{m!n!}{(m-k)!(n-k)!}(-b)^{-k}$$

$$\times \left\{ \left[\sum_{j=1}^{n} \frac{1}{j} + \sum_{j=k+1}^{m+1} \frac{1}{j} - \frac{1}{m+1} \right] e^{-b} \right.$$

$$\left. + X - h_{m+n-k-1} \right\} . \quad \text{(C11)}$$

The quantity E_R is defined as in Eq. (6.6).

APPENDIX D

Matrix elements $\langle {}^0_m | \mathscr{E} | {}^0_n \rangle$ defined by Eq. (7.30), decomposed per Eqs. (7.9)–(7.28), for the case of $\nu=0$. Symbols are defined as in Appendix C. Note that $m, n > 0$.

$$\mathscr{E}^{(1)} = -\frac{c}{2} e^{-b} \left[\frac{m}{b} - 1 \right] , \quad \text{(D1)}$$

$$\mathscr{E}^{(2)} = -\frac{c}{2} e^{-b} \left[\frac{n}{b} - 1 \right] , \quad \text{(D2)}$$

$$\mathscr{E}^{(3)} = -\frac{c}{2} e^{-b} , \quad \text{(D3)}$$

$$\mathscr{E}^{(4)} \underset{n \geq m}{=} -\frac{c}{2} \left\{ e^{-b} - \frac{n!}{b^n}[(1-\delta_{mn}) - f_{n-1}] + \frac{m!}{b^m} f_{m-1} \right\} , \quad \text{(D4)}$$

$$\mathscr{E}^{(5)} = cI_1 , \quad \text{(D5)}$$

$$\mathscr{E}^{(6)} \underset{n \geq m}{=} -\frac{c}{2} \{ 2I_2 + X + g_{m-1} - h_{n-1} \} , \quad \text{(D6)}$$

$$\mathscr{E}^{(7)} \underset{n \geq m}{=} \left\{ E_b - E_R + \frac{1}{2} e^{-b} \sum_{p=0}^{n-1} \left[\sum_{k=p+1}^{n} \frac{1}{k} \right] \frac{b^p}{p!} \right\}$$

$$- (1 - \delta_{mn}) \frac{c}{2} \frac{1}{n-m}$$

$$\times \left\{ \frac{m!}{b^m} f_{m-1} + \frac{n!}{b^n}[1 - f_{n-1}] \right\} , \quad \text{(D7)}$$

$$\mathscr{E}^{(8)} = \frac{c}{4} e^{-b} \left[\frac{m}{b} - 1 \right] , \quad \text{(D8)}$$

$$\mathscr{E}^{(9)} = \frac{c}{4} e^{-b} \left[\frac{n}{b} - 1 \right] , \quad \text{(D9)}$$

$$\mathscr{E}^{(10)} = -\frac{c}{4} e^{-b} \left[\frac{1}{b} + \frac{1}{n+1} \right] , \quad \text{(D10)}$$

$$\mathscr{E}^{(11)} = -\frac{c}{4} e^{-b} \left[\frac{1}{b} + \frac{1}{m+1} \right] , \quad \text{(D11)}$$

$$\mathscr{E}^{(12)} = -\frac{c}{2}(I_1 - I_2) - \frac{c}{4} e^{-b} \sum_{k=1}^{n} \frac{1}{k} , \quad \text{(D12)}$$

$$\mathscr{E}^{(13)} = -\frac{c}{2}(I_1 - I_2) - \frac{c}{4} e^{-b} \sum_{k=1}^{m} \frac{1}{k} , \quad \text{(D13)}$$

$$\mathscr{E}^{(14)} = \frac{c}{2} e^{-b} \frac{1}{b} , \quad \text{(D14)}$$

$$\mathscr{E}^{(15)} = \frac{c}{4} e^{-b} , \quad \text{(D15)}$$

$$\mathscr{E}^{(16)} = \frac{c}{4} e^{-b} , \quad \text{(D16)}$$

$$\mathscr{E}^{(17)} \underset{n \geq m}{=} \frac{c}{4} \left\{ \frac{1}{n} \frac{n!}{b^n}[(1-\delta_{mn}) - f_{n-1}] + \frac{1}{n+1} \frac{m!}{b^m} f_m \right\} , \quad \text{(D17)}$$

$$\mathscr{E}^{(18)} \underset{n \geq m}{=} \frac{c}{4} \left\{ -\frac{1}{m} \frac{m!}{b^m} f_{m-1} \right.$$

$$\left. - \frac{1}{m+1} \frac{n!}{b^n}[(1-\delta_{mn}) - f_n] \right\} , \quad \text{(D18)}$$

$$\mathscr{E}^{(19)} \underset{n \geq m}{=} \frac{c}{4} \left\{ X + g_{m-1} \right.$$

$$\left. - h_{n-1} + \frac{m!n!}{b^{m+n+1}} f_m [1 - f_n] e^b \right\} , \quad (D19)$$

$$\mathscr{E}^{(20)} = \frac{c}{4} \left\{ \frac{1}{b} e^{-b} + Y_{m,n} \right\} . \quad (D20)$$

APPENDIX E

Matrix elements $\langle {}^{0}_{m} | \mathscr{A} | {}^{0}_{n} \rangle$ defined by Eq. (7.31), decomposed per Eqs. (7.9)–(7.28), for the case of $v=0$. Symbols are defined as in Appendix C. Note that $m, n > 0$.

$$\mathscr{A}^{(1)} = -\frac{d}{2} e^{-b} \left[\frac{m}{b} - 1 \right] , \quad (E1)$$

$$\mathscr{A}^{(2)} = -\frac{d}{2} e^{-b} \left[\frac{n}{b} - 1 \right] , \quad (E2)$$

$$\mathscr{A}^{(3)} = -\frac{d}{2} \left\{ e^{-b} - m \frac{(m+n-1)!}{b^{m+n}} [1 - f_{m+n-1}] \right\} , \quad (E3)$$

$$\mathscr{A}^{(4)} = -\frac{d}{2} \left\{ e^{-b} - n \frac{(n+m-1)!}{b^{n+m}} [1 - f_{n+m-1}] \right\} , \quad (E4)$$

$$\mathscr{A}^{(5)} = d I_1 , \quad (E5)$$

$$\mathscr{A}^{(6)} = -\frac{d}{2} \{ 2 I_2 + X - h_{m+n-1} \} , \quad (E6)$$

$$\mathscr{A}^{(7)} = -\frac{d}{2} \frac{(m+n-1)!}{b^{m+n}} [1 - f_{m+n-1}] , \quad (E7)$$

$$\mathscr{A}^{(8)} = -\frac{d}{4} e^{-b} \left[\frac{1}{b} + \frac{1}{m+1} \right] , \quad (E8)$$

$$\mathscr{A}^{(9)} = \frac{d}{4} e^{-b} \left[\frac{n}{b} - 1 \right] , \quad (E9)$$

$$\mathscr{A}^{(10)} = -\frac{d}{4} e^{-b} \left[\frac{1}{b} + \frac{1}{n+1} \right] , \quad (E10)$$

$$\mathscr{A}^{(11)} = \frac{d}{4} e^{-b} \left[\frac{m}{b} - 1 \right] , \quad (E11)$$

$$\mathscr{A}^{(12)} = -\frac{d}{2} (I_1 - I_2) - \frac{d}{4} e^{-b} \sum_{k=1}^{n} \frac{1}{k} , \quad (E12)$$

$$\mathscr{A}^{(13)} = -\frac{d}{2} (I_1 - I_2) - \frac{d}{4} e^{-b} \sum_{k=1}^{m} \frac{1}{k} , \quad (E13)$$

$$\mathscr{A}^{(14)} = \frac{d}{2} e^{-b} \frac{1}{b} , \quad (E14)$$

$$\mathscr{A}^{(15)} = \frac{d}{4} \left\{ \frac{1}{m+1} e^{-b} + \frac{(m+n-1)!}{b^{m+n}} [1 - f_{m+n-1}] \right\} , \quad (E15)$$

$$\mathscr{A}^{(16)} = \frac{d}{4} \left\{ e^{-b} - m \frac{(m+n-1)!}{b^{m+n}} [1 - f_{m+n-1}] \right\} , \quad (E16)$$

$$\mathscr{A}^{(17)} = \frac{d}{4} \left\{ \frac{1}{n+1} e^{-b} + \frac{(m+n-1)!}{b^{m+n}} [1 - f_{m+n-1}] \right\} , \quad (E17)$$

$$\mathscr{A}^{(18)} = \frac{d}{4} \left\{ e^{-b} - n \frac{(m+n-1)!}{b^{m+n}} [1 - f_{m+n-1}] \right\} , \quad (E18)$$

$$\mathscr{A}^{(19)} = \frac{d}{4} \left\{ X - h_{m+n-1} + e^{-b} \sum_{k=1}^{m} \frac{1}{k} \right\} , \quad (E19)$$

$$\mathscr{A}^{(20)} = \frac{d}{4} \left\{ X - h_{m+n-1} + e^{-b} \sum_{k=1}^{n} \frac{1}{k} \right\} . \quad (E20)$$

APPENDIX F

Matrix elements $\langle {}^{m'}_{m} | \mathscr{E} | {}^{n'}_{n} \rangle$ defined by Eq. (7.30), decomposed per Eqs. (7.9)–(7.28), for the case of $v = \frac{1}{2}$. Symbols are defined as in Appendix C. Note that $m, n > 1$ and that m' and n' are indicated by $[\mathscr{E}]^{m'n'}$.

$$[\mathscr{E}^{(1)}]^{00} = -\frac{c}{4} e^{-b} \left[\frac{m}{b} - 1 \right] , \quad (F1a)$$

$$[\mathscr{E}^{(1)}]^{10} = -\frac{c}{4} e^{-b} \left\{ (b-m) \left[\frac{m-1}{b} - 1 \right] + 2 \right\} , \quad (F1b)$$

$$[\mathscr{E}^{(1)}]^{01} = -\frac{c}{4} e^{-b} (b-n) \left[\frac{m}{b} - 1 \right] , \quad (F1c)$$

$$[\mathscr{E}^{(1)}]^{11} = -\frac{c}{4} e^{-b} (b-n) \left\{ (b-m) \left[\frac{m-1}{b} - 1 \right] + 2 \right\} , \quad (F1d)$$

$$[\mathscr{E}^{(2)}]^{00} = -\frac{c}{4} e^{-b} \left[\frac{n}{b} - 1 \right] , \quad (F2a)$$

$$[\mathscr{E}^{(2)}]^{10} = -\frac{c}{4} e^{-b} (b-m) \left[\frac{n}{b} - 1 \right] , \quad (F2b)$$

$$[\mathscr{E}^{(2)}]^{01} = -\frac{c}{4} e^{-b} \left\{ (b-n) \left[\frac{n-1}{b} - 1 \right] + 2 \right\} , \quad (F2c)$$

$$[\mathscr{E}^{(2)}]^{11} = -\frac{c}{4} e^{-b} (b-m) \left\{ (b-n) \left[\frac{n-1}{b} - 1 \right] + 2 \right\} , \quad (F2d)$$

$$[\mathscr{E}^{(3)}]^{00} = -\frac{c}{4} e^{-b} , \quad (F3a)$$

$$[\mathscr{E}^{(3)}]^{10} \underset{n \geq m}{=} \frac{c}{4} \left\{ (m-b) e^{-b} + \frac{n!}{b^n} [1 - f_n] \right\} , \quad (F3b)$$

$$[\mathscr{E}^{(3)}]^{01} \underset{n \geq m}{=} \frac{c}{4} \left\{ (n-b) e^{-b} + \frac{m!}{b^m} [\delta_{mn} - f_m] \right\} , \quad (F3c)$$

$$[\mathscr{E}^{(3)}]^{11}_{\substack{=\\n\geq m}} = -\frac{c}{4}\{(b-m)(b-n)+2b\}e^{-b} , \qquad \text{(F3d)}$$

$$[\mathscr{E}^{(4)}]^{00}_{\substack{=\\n\geq m}} = -\frac{1}{4}\delta_{mn} - \frac{c}{4}\left\{\frac{m!}{b^m}f_m - \frac{n!}{b^n}[1-f_{n-1}]\right\} , \qquad \text{(F4a)}$$

$$[\mathscr{E}^{(4)}]^{10}_{\substack{=\\n\geq m}} = -\frac{c}{4}\left\{be^{-b} - \frac{n!}{b^n}(n[1-f_n]\right. \\ \left. -m[1-f_{n-1}])\right\} , \qquad \text{(F4b)}$$

$$[\mathscr{E}^{(4)}]^{01}_{\substack{=\\n\geq m}} = -\frac{c}{4}\left\{be^{-b} + \frac{m!}{b^m}[mf_m - nf_{m-1}]\right\} , \qquad \text{(F4c)}$$

$$[\mathscr{E}^{(4)}]^{11}_{\substack{=\\n\geq m}} = -\frac{c}{4}\left\{(b^2-2b-mn)e^{-b}\right. \\ -\frac{n!}{b^{n-1}}[(1-\delta_{mn})-f_n] \\ \left. +\frac{m!}{b^{m-1}}f_m\right\} , \qquad \text{(F4d)}$$

$$[\mathscr{E}^{(5)}]^{00} = \frac{c}{4}I_1 , \qquad \text{(F5a)}$$

$$[\mathscr{E}^{(5)}]^{10} = \frac{c}{4}(b-m)I_1 , \qquad \text{(F5b)}$$

$$[\mathscr{E}^{(5)}]^{01} = \frac{c}{4}(b-n)I_1 , \qquad \text{(F5c)}$$

$$[\mathscr{E}^{(5)}]^{11} = \frac{c}{4}(b-m)(b-n)I_1 , \qquad \text{(F5d)}$$

$$[\mathscr{E}^{(6)}]^{00}_{\substack{=\\n\geq m}} = -\frac{c}{8}\{2I_2 + X + g_{m-1} - h_{n-1}\} , \qquad \text{(F6a)}$$

$$[\mathscr{E}^{(6)}]^{10}_{\substack{=\\n\geq m}} = -\frac{c}{8}\left[(b-m)\{2I_2+X+g_{m-1}-h_n\} - m\left\{\frac{n!}{b^{n+1}}[1-f_n] - \frac{(m-1)!}{b^m}f_{m-1}\right\}\right] , \qquad \text{(F6b)}$$

$$[\mathscr{E}^{(6)}]^{01}_{\substack{=\\n\geq m}} = -\frac{c}{8}\left[(b-n)\{2I_2+X+g_m-h_{n-1}\} + \frac{nm!}{b^{m+1}}f_m - \frac{n!}{b^n}[1-f_{n-1}]\right] , \qquad \text{(F6c)}$$

$$[\mathscr{E}^{(6)}]^{11}_{\substack{=\\n\geq m}} = -\frac{c}{8}\left[(b-m)(b-n)\{2I_2+X+g_{m-1}-h_{n-1}\} - b^2\left\{\frac{n!}{b^{n+1}}[1-f_n] - \frac{m!}{b^{m+1}}f_m\right\}\right. \\ \left. +nm\left\{\frac{(n-1)!}{b^n}[1-f_{n-1}] - \frac{(m-1)!}{b^m}f_{m-1}\right\}\right] , \qquad \text{(F6d)}$$

$$[\mathscr{E}^{(7)}]^{00}_{\substack{=\\n\geq m}} = \frac{1}{2}\delta_{mn}\left\{-E_R+E_b+\frac{1}{2}e^{-b}\sum_{p=0}^{n-1}\frac{b^p}{p!}\left[\sum_{k=p+1}^n\frac{1}{k}\right]\right\} - (1-\delta_{mn})\frac{c}{4}\frac{1}{n-m}\left\{\frac{m!}{b^m}f_{m-1} + \frac{n!}{b^n}[1-f_{n-1}]\right\} , \qquad \text{(F7a)}$$

$$[\mathscr{E}^{(7)}]^{10}_{\substack{=\\n\geq m}} = -\frac{c}{4}\frac{n!}{b^n}[1-f_n] , \qquad \text{(F7b)}$$

$$[\mathscr{E}^{(7)}]^{01}_{\substack{=\\n\geq m}} = -\frac{c}{4}\frac{m!}{b^m}[\delta_{mn}-f_m] , \qquad \text{(F7c)}$$

$$[\mathscr{E}^{(7)}]^{11}_{\substack{=\\n\geq m}} = \frac{1}{2}\delta_{mn}\left\{-E_R+E_b+\frac{1}{2}e^{-b}\sum_{p=0}^{n-1}\frac{b^p}{p!}\left[\sum_{k=p+1}^n\frac{1}{k}\right]+\frac{1}{2}\frac{b^n}{n!}e^{-b}\right\} \\ -(1-\delta_{mn})\frac{c}{4}\left[\frac{1}{n-m}\left\{\frac{m!}{b^{m-1}}f_{m-1} + \frac{n!}{b^{n-1}}[1-f_{n-1}]\right\} - be^{-b}\right] , \qquad \text{(F7d)}$$

$$[\mathscr{E}^{(8)}]^{00} = \frac{c}{16}e^{-b}\left[\frac{m}{b}-1\right] , \qquad \text{(F8a)}$$

$$[\mathscr{E}^{(8)}]^{10} = -\frac{c}{16}e^{-b}\left[b-2m+1+\frac{m(m-1)}{b}\right] , \qquad \text{(F8b)}$$

$$[\mathscr{E}^{(8)}]^{01} = \frac{c}{16}e^{-b}(b-n)\left[\frac{m}{b}-1\right] , \qquad \text{(F8c)}$$

$$[\mathscr{E}^{(8)}]^{11} = -\frac{c}{16}e^{-b}(b-n)\left[b-2m+1+\frac{m(m-1)}{b}\right] , \qquad \text{(F8d)}$$

$$[\mathscr{E}^{(9)}]^{00} = \frac{c}{16}e^{-b}\left[\frac{n}{b}-1\right] , \qquad \text{(F9a)}$$

$$[\mathscr{E}^{(9)}]^{10} = \frac{c}{16} e^{-b}(b-m)\left[\frac{n}{b} - 1\right] , \qquad \text{(F9b)}$$

$$[\mathscr{E}^{(9)}]^{01} = -\frac{c}{16} e^{-b}\left[b - 2n + 1 + \frac{n(n-1)}{b}\right] , \qquad \text{(F9c)}$$

$$[\mathscr{E}^{(9)}]^{11} = -\frac{c}{16} e^{-b}(b-m)\left[b - 2n + 1 + \frac{n(n-1)}{b}\right] , \qquad \text{(F9d)}$$

$$[\mathscr{E}^{(10)}]^{00} = -\frac{c}{8} e^{-b}\left\{\frac{1}{n+1} + \frac{1}{b}\right\} , \qquad \text{(F10a)}$$

$$[\mathscr{E}^{(10)}]^{10} = -\frac{c}{8} e^{-b}(b-m)\left\{\frac{1}{n+1} + \frac{1}{b}\right\} , \qquad \text{(F10b)}$$

$$[\mathscr{E}^{(10)}]^{01} = -\frac{c}{8} e^{-b}\left\{\frac{b}{n+1} + \frac{1-n}{b}\right\} , \qquad \text{(F10c)}$$

$$[\mathscr{E}^{(10)}]^{11} = -\frac{c}{8} e^{-b}(b-m)\left\{\frac{b}{n+1} + \frac{1-n}{b}\right\} , \qquad \text{(F10d)}$$

$$[\mathscr{E}^{(11)}]^{00} = -\frac{c}{8} e^{-b}\left\{\frac{1}{m+1} + \frac{1}{b}\right\} , \qquad \text{(F11a)}$$

$$[\mathscr{E}^{(11)}]^{10} = -\frac{c}{8} e^{-b}\left\{\frac{b}{m+1} + \frac{1-m}{b}\right\} , \qquad \text{(F11b)}$$

$$[\mathscr{E}^{(11)}]^{01} = -\frac{c}{8} e^{-b}(b-n)\left\{\frac{1}{m+1} + \frac{1}{b}\right\} , \qquad \text{(F11c)}$$

$$[\mathscr{E}^{(11)}]^{11} = -\frac{c}{8} e^{-b}(b-n)\left\{\frac{b}{m+1} + \frac{1-m}{b}\right\} , \qquad \text{(F11d)}$$

$$[\mathscr{E}^{(12)}]^{00} = -\frac{c}{16}\left\{2(I_1 - I_2) + e^{-b}\sum_{k=1}^{n}\frac{1}{k}\right\} , \qquad \text{(F12a)}$$

$$[\mathscr{E}^{(12)}]^{10} = -\frac{c}{16}(b-m)\left\{2(I_1 - I_2) + e^{-b}\sum_{k=1}^{n}\frac{1}{k}\right\} , \qquad \text{(F12b)}$$

$$[\mathscr{E}^{(12)}]^{01} = -\frac{c}{16}(b-n)\left\{2(I_1 - I_2) + e^{-b}\sum_{k=1}^{n}\frac{1}{k}\right\} , \qquad \text{(F12c)}$$

$$[\mathscr{E}^{(12)}]^{11} = -\frac{c}{16}(b-m)(b-n)$$
$$\times\left\{2(I_1 - I_2) + e^{-b}\sum_{k=1}^{n}\frac{1}{k}\right\} , \qquad \text{(F12d)}$$

$$[\mathscr{E}^{(13)}]^{00} = -\frac{c}{16}\left\{2(I_1 - I_2) + e^{-b}\sum_{k=1}^{m}\frac{1}{k}\right\} , \qquad \text{(F13a)}$$

$$[\mathscr{E}^{(13)}]^{10} = -\frac{c}{16}(b-m)\left\{2(I_1 - I_2) + e^{-b}\sum_{k=1}^{m}\frac{1}{k}\right\} , \qquad \text{(F13b)}$$

$$[\mathscr{E}^{(13)}]^{01} = -\frac{c}{16}(b-n)\left\{2(I_1 - I_2) + e^{-b}\sum_{k=1}^{m}\frac{1}{k}\right\} , \qquad \text{(F13c)}$$

$$[\mathscr{E}^{(13)}]^{11} = -\frac{c}{16}(b-n)(b-m)$$
$$\times\left\{2(I_1 - I_2) + e^{-b}\sum_{k=1}^{m}\frac{1}{k}\right\} , \qquad \text{(F13d)}$$

$$[\mathscr{E}^{(14)}]^{00} = \frac{c}{4} e^{-b}\frac{1}{b} , \qquad \text{(F14a)}$$

$$[\mathscr{E}^{(14)}]^{10} = \frac{c}{4} e^{-b}\frac{1}{b}(b-m) , \qquad \text{(F14b)}$$

$$[\mathscr{E}^{(14)}]^{01} = \frac{c}{4} e^{-b}\frac{1}{b}(b-n) , \qquad \text{(F14c)}$$

$$[\mathscr{E}^{(14)}]^{11} = \frac{c}{4} e^{-b}\frac{1}{b}(b-m)(b-n) , \qquad \text{(F14d)}$$

$$[\mathscr{E}^{(15)}]^{00} \underset{n\geq m}{=} \frac{c}{16} e^{-b} , \qquad \text{(F15a)}$$

$$[\mathscr{E}^{(15)}]^{10} \underset{n\geq m}{=} \frac{c}{16}\left\{(b-m)e^{-b} + \frac{n!}{b^n}[1-f_n]\right\} , \qquad \text{(F15b)}$$

$$[\mathscr{E}^{(15)}]^{01} \underset{n\geq m}{=} \frac{c}{16}\left\{(b-n)e^{-b} - \frac{m!}{b^m}[\delta_{mn} - f_m]\right\} , \qquad \text{(F15c)}$$

$$[\mathscr{E}^{(15)}]^{11} \underset{n\geq m}{=} \frac{c}{16}(b-m)(b-n)e^{-b} , \qquad \text{(F15d)}$$

$$[\mathscr{E}^{(16)}]^{00} \underset{n\geq m}{=} \frac{c}{16} e^{-b} , \qquad \text{(F16a)}$$

$$[\mathscr{E}^{(16)}]^{10} \underset{n\geq m}{=} \frac{c}{16}\left\{(b-m)e^{-b} - \frac{n!}{b^n}[1-f_n]\right\} , \qquad \text{(F16b)}$$

$$[\mathscr{E}^{(16)}]^{01} \underset{n\geq m}{=} \frac{c}{16}\left\{(b-n)e^{-b} + \frac{m!}{b^m}[\delta_{mn} - f_m]\right\} , \qquad \text{(F16c)}$$

$$[\mathscr{E}^{(16)}]^{11} \underset{n\geq m}{=} \frac{c}{16}(b-m)(b-n)e^{-b} , \qquad \text{(F16d)}$$

$$[\mathscr{E}^{(17)}]^{00} \underset{n\geq m}{=} \frac{c}{8}\left\{\frac{(n-1)!}{b^n}[(1-\delta_{mn}) - f_{n-1}] + \frac{1}{n+1}\frac{m!}{b^m}f_m\right\} , \qquad \text{(F17a)}$$

$$[\mathscr{E}^{(17)}]^{10} \underset{n\geq m}{=} \frac{c}{8}\left\{(n-m)\frac{(n-1)!}{b^n}[1-f_{n-1}] + \left[\frac{b}{n+1} - 1\right]e^{-b}\right\} , \qquad \text{(F17b)}$$

$$[\mathcal{E}^{(17)}]^{01} \underset{n \geq m}{=} \frac{c}{8}\left\{\frac{(m-n)}{n+1}\frac{m!}{b^m}f_m + \left[\frac{b}{n+1}-1\right]e^{-b}\right\},$$

(F17c)

$$[\mathcal{E}^{(17)}]^{11} \underset{n \geq m}{=} \frac{c}{8}\left\{\frac{1}{n+1}\frac{m!}{b^{m-1}}f_m + \frac{(n-1)!}{b^{n-1}}[(1-\delta_{mn})-f_{n-1}] + \left[\frac{b^2}{n+1}-2b+m\right]e^{-b}\right\},$$

(F17d)

$$[\mathcal{E}^{(18)}]^{00} \underset{n \geq m}{=} \frac{c}{8}\left\{-\frac{(m-1)!}{b^m}f_{m-1} - \frac{1}{m+1}\frac{n!}{b^n}[(1-\delta_{mn})-f_n]\right\},$$

(F18a)

$$[\mathcal{E}^{(18)}]^{10} \underset{n \geq m}{=} \frac{c}{8}\left\{\frac{(m-n)}{m+1}\frac{n!}{b^n}[1-f_n] + \left[\frac{b}{m+1}-1\right]e^{-b}\right\},$$

(F18b)

$$[\mathcal{E}^{(18)}]^{01} \underset{n \geq m}{=} \frac{c}{8}\left\{(n-m)\frac{(m-1)!}{b^m}f_{m-1} + \left[\frac{b}{m+1}-1\right]e^{-b}\right\},$$

(F18c)

$$[\mathcal{E}^{(18)}]^{11} \underset{n \geq m}{=} \frac{c}{8}\left\{-\frac{1}{m+1}\frac{n!}{b^{n-1}}[(1-\delta_{mn})-f_n] - \frac{(m-1)!}{b^{m-1}}f_{m-1} + \left[\frac{b^2}{m+1}-2b+n\right]e^{-b}\right\},$$

(F18d)

$$[\mathcal{E}^{(19)}]^{00} \underset{n \geq m}{=} \frac{c}{16}\left\{X-h_{n-1}+g_{m-1} + \left[2+\frac{1}{b}(b-m-1)(b-n-1)\right]\frac{m!n!}{b^{m+n+1}}f_m[1-f_n]e^b \right.$$
$$\left. -(b-n-1)\frac{n!}{b^{n+1}}[1-f_n] + (b-m-1)\frac{m!}{b^{m+1}}f_m\right\},$$

(F19a)

$$[\mathcal{E}^{(19)}]^{10} \underset{n \geq m}{=} \frac{c}{16}\left\{(b-m)[X-h_{n-1}+g_{m-1}]-(b-n-1)\frac{m!n!}{b^{m+n+1}}f_m[1-f_n]e^b+(b-m-1)e^{-b}\right\},$$

(F19b)

$$[\mathcal{E}^{(19)}]^{01} \underset{n \geq m}{=} \frac{c}{16}\left\{(b-n)[X-h_{n-1}+g_{m-1}]-(b-m-1)\frac{m!n!}{b^{m+n+1}}f_m[1-f_n]e^b+(b-n-1)e^{-b}\right\},$$

(F19c)

$$[\mathcal{E}^{(19)}]^{11} \underset{n \geq m}{=} \frac{c}{16}\left\{b^2[X-h_n+g_m]-(m+n)b[X-h_{n-1}+g_{m-1}]\right.$$
$$\left. +mn[X-h_{n-2}+g_{m-2}]+\frac{m!n!}{b^{m+n}}f_m[1-f_n]e^b+[(b-m)(b-n)-b]e^{-b}\right\},$$

(F19d)

$$[\mathcal{E}^{(20)}]^{00} = \frac{c}{16}\left\{Y_{m,n}+\frac{mn}{b}Y_{m-1,n-1} + \left[\left(1+\frac{1}{b}\right)^2-2\right]e^{-b}\right\},$$

(F20a)

$$[\mathcal{E}^{(20)}]^{10} = \frac{c}{16}\left\{bY_{m,n+1}+mnY_{m-1,n} + \left[(2-m)\left(1+\frac{1}{b}\right)^2-\frac{1}{b}-(b-m)-\frac{b}{n+1}\right]e^{-b}\right\},$$

(F20b)

$$[\mathcal{E}^{(20)}]^{01} = \frac{c}{16}\left\{bY_{m+1,n}+mnY_{m,n-1} + \left[(2-n)\left(1+\frac{1}{b}\right)^2-\frac{1}{b}-(b-n)-\frac{b}{m+1}\right]e^{-b}\right\},$$

(F20c)

$$[\mathcal{E}^{(20)}]^{11} = \frac{c}{16}\left\{b(b-m-n+mn)Y_{m,n}+[mn(2b+1)-(m+n)(2b^2+3b+2)-(b^4-4b^3-5b^2-6b-4)]\frac{1}{b^2}e^{-b}\right\}.$$

(F20d)

APPENDIX G

Matrix elements $\langle\begin{smallmatrix}m'\\m\end{smallmatrix}|\mathcal{A}|\begin{smallmatrix}n'\\n\end{smallmatrix}\rangle$ defined by Eq. (7.31), decomposed per Eqs. (7.9)–(7.28), for the case of $\nu=\frac{1}{2}$. Symbols are defined as in Appendix C. Note that $m,n > 1$ and that m' and n' are indicated by $[\mathcal{A}]^{m'n'}$.

$$[\mathcal{A}^{(1)}]^{00} = \frac{d}{4}\frac{1}{b}(b-m)e^{-b},$$

(G1a)

$$[\mathcal{A}^{(1)}]^{10} = \frac{d}{4}\left\{\frac{1}{b}(b-m)(b-m+1)-2\right\}e^{-b},$$

(G1b)

$$[\mathcal{A}^{(1)}]^{01} = \frac{d}{4}(b-n)\left\{\frac{1}{b}(b-m)\right\}e^{-b} , \tag{G1c}$$

$$[\mathcal{A}^{(1)}]^{11} = \frac{d}{4}(b-n)\left\{\frac{1}{b}(b-m)(b-m+1)-2\right\}e^{-b} , \tag{G1d}$$

$$[\mathcal{A}^{(2)}]^{00} = \frac{d}{4}\frac{1}{b}(b-n)e^{-b} , \tag{G2a}$$

$$[\mathcal{A}^{(2)}]^{10} = \frac{d}{4}(b-m)\left\{\frac{1}{b}(b-n)\right\}e^{-b} , \tag{G2b}$$

$$[\mathcal{A}^{(2)}]^{01} = \frac{d}{4}\left\{\frac{1}{b}(b-n)(b-n+1)-2\right\}e^{-b} , \tag{G2c}$$

$$[\mathcal{A}^{(2)}]^{11} = \frac{d}{4}(b-m)\left\{\frac{1}{b}(b-n)(b-n+1)-2\right\}e^{-b} , \tag{G2d}$$

$$[\mathcal{A}^{(3)}]^{00} = -\frac{d}{4}\left\{e^{-b}-m\frac{(m+n-1)!}{b^{m+n}}[1-f_{m+n-1}]\right\} , \tag{G3a}$$

$$[\mathcal{A}^{(3)}]^{10} = -\frac{d}{4}\left\{be^{-b}-mn\frac{(m+n-2)!}{b^{m+n-1}}[1-f_{m+n-2}]\right\} , \tag{G3b}$$

$$[\mathcal{A}^{(3)}]^{01} = -\frac{d}{4}\left\{(b+m-n+1)e^{-b}-m(m-1)\frac{(m+n-2)!}{b^{m+n-1}}[1-f_{m+n-2}]\right\} , \tag{G3c}$$

$$[\mathcal{A}^{(3)}]^{11} = -\frac{d}{4}\left\{[(b-m)(b-n)+(1+m)b+(1-m)]e^{-b}-nm(m-1)\frac{(m+n-3)!}{b^{m+n-2}}[1-f_{m+n-3}]\right\} , \tag{G3d}$$

$$[\mathcal{A}^{(4)}]^{00} = -\frac{d}{4}\left\{e^{-b}-n\frac{(m+n-1)!}{b^{m+n}}[1-f_{m+n-1}]\right\} , \tag{G4a}$$

$$[\mathcal{A}^{(4)}]^{10} = -\frac{d}{4}\left\{(b+n-m+1)e^{-b}-n(n-1)\frac{(m+n-2)!}{b^{m+n-1}}[1-f_{m+n-2}]\right\} , \tag{G4b}$$

$$[\mathcal{A}^{(4)}]^{01} = -\frac{d}{4}\left\{be^{-b}-mn\frac{(m+n-2)!}{b^{m+n-1}}[1-f_{m+n-2}]\right\} , \tag{G4c}$$

$$[\mathcal{A}^{(4)}]^{11} = -\frac{d}{4}\left\{[(b-m)(b-n)+(1+n)b+(1-n)]e^{-b}-mn(n-1)\frac{(m+n-3)!}{b^{m+n-2}}[1-f_{m+n-3}]\right\} , \tag{G4d}$$

$$[\mathcal{A}^{(5)}]^{00} = \frac{d}{4}I_1 , \tag{G5a}$$

$$[\mathcal{A}^{(5)}]^{10} = \frac{d}{4}(b-m)I_1 , \tag{G5b}$$

$$[\mathcal{A}^{(5)}]^{01} = \frac{d}{4}(b-n)I_1 , \tag{G5c}$$

$$[\mathcal{A}^{(5)}]^{00} = \frac{d}{4}(b-m)(b-n)I_1 , \tag{G5d}$$

$$[\mathcal{A}^{(6)}]^{00} = -\frac{d}{8}\{2I_2+X-h_{m+n-1}\} , \tag{G6a}$$

$$[\mathcal{A}^{(6)}]^{10} = -\frac{d}{8}\{(b-m)[2I_2+X]-bh_{m+n-1}+mh_{m+n-2}+e^{-b}\} , \tag{G6b}$$

$$[\mathcal{A}^{(6)}]^{01} = -\frac{d}{8}\{(b-n)[2I_2+X]-bh_{m+n-1}+nh_{m+n-2}+e^{-b}\} , \tag{G6c}$$

$$[\mathscr{A}^{(6)}]^{11} = -\frac{d}{8}\{(b-m)(b-n)[2I_2+X]-b^2h_{m+n-1}+(m+n)bh_{m+n-2}-mnh_{m+n-3}+[(b-m)+(b-n)+1]e^{-b}\} ,$$

(G6d)

$$[\mathscr{A}^{(7)}]^{00} = -\frac{d}{4}\frac{(m+n-1)!}{b^{m+n}}[1-f_{m+n-1}] ,$$

(G7a)

$$[\mathscr{A}^{(7)}]^{10} = -\frac{d}{4}\left\{-e^{-b}+n\frac{(m+n-2)!}{b^{m+n-1}}[1-f_{m+n-2}]\right\} ,$$

(G7b)

$$[\mathscr{A}^{(7)}]^{01} = -\frac{d}{4}\left\{-e^{-b}+m\frac{(m+n-2)!}{b^{m+n-1}}[1-f_{m+n-2}]\right\} ,$$

(G7c)

$$[\mathscr{A}^{(7)}]^{11} = -\frac{d}{4}\left\{-(1+b)e^{-b}+mn\frac{(m+n-3)!}{b^{m+n-2}}[1-f_{m+n-3}]\right\} ,$$

(G7d)

$$[\mathscr{A}^{(8)}]^{00} = -\frac{d}{8}e^{-b}\left\{\frac{1}{m+1}+\frac{1}{b}\right\} ,$$

(G8a)

$$[\mathscr{A}^{(8)}]^{10} = -\frac{d}{8}e^{-b}\left\{\frac{b}{m+1}+\frac{1-m}{b}\right\} ,$$

(G8b)

$$[\mathscr{A}^{(8)}]^{01} = -\frac{d}{8}e^{-b}(b-n)\left[\frac{1}{m+1}+\frac{1}{b}\right] ,$$

(G8c)

$$[\mathscr{A}^{(8)}]^{11} = -\frac{d}{8}e^{-b}(b-n)\left\{\frac{b}{m+1}+\frac{1-m}{b}\right\} ,$$

(G8d)

$$[\mathscr{A}^{(9)}]^{00} = -\frac{d}{16}\frac{1}{b}(b-n)e^{-b} ,$$

(G9a)

$$[\mathscr{A}^{(9)}]^{10} = -\frac{d}{16}\frac{1}{b}(b-m)(b-n)e^{-b} ,$$

(G9b)

$$[\mathscr{A}^{(9)}]^{01} = -\frac{d}{16}\frac{1}{b}(b-n)(b-n+1)e^{-b} ,$$

(G9c)

$$[\mathscr{A}^{(9)}]^{11} = -\frac{d}{16}\frac{1}{b}(b-m)(b-n)(b-n+1)e^{-b} ,$$

(G9d)

$$[\mathscr{A}^{(10)}]^{00} = -\frac{d}{8}e^{-b}\left\{\frac{1}{n+1}+\frac{1}{b}\right\} ,$$

(G10a)

$$[\mathscr{A}^{(10)}]^{10} = -\frac{d}{8}(b-m)e^{-b}\left\{\frac{1}{n+1}+\frac{1}{b}\right\} ,$$

(G10b)

$$[\mathscr{A}^{(10)}]^{01} = -\frac{d}{8}e^{-b}\left\{\frac{b}{n+1}+\frac{1-n}{b}\right\} ,$$

(G10c)

$$[\mathscr{A}^{(10)}]^{11} = -\frac{d}{8}e^{-b}(b-m)\left\{\frac{b}{n+1}+\frac{1-n}{b}\right\} ,$$

(G10d)

$$[\mathscr{A}^{(11)}]^{00} = -\frac{d}{16}\frac{1}{b}(b-m)e^{-b} ,$$

(G11a)

$$[\mathscr{A}^{(11)}]^{10} = -\frac{d}{16}\frac{1}{b}(b-m)(b-m+1)e^{-b} ,$$

(G11b)

$$[\mathscr{A}^{(11)}]^{01} = -\frac{d}{16}\frac{1}{b}(b-n)(b-m)e^{-b} ,$$

(G11c)

$$[\mathscr{A}^{(11)}]^{11} = -\frac{d}{16}\frac{1}{b}(b-n)(b-m)(b-m+1)e^{-b} ,$$

(G11d)

$$[\mathscr{A}^{(12)}]^{00} = -\frac{d}{16}\left\{2(I_1-I_2)+e^{-b}\sum_{k=1}^{n}\frac{1}{k}\right\} ,$$

(G12a)

$$[\mathscr{A}^{(12)}]^{10} = -\frac{d}{16}(b-m)\left\{2(I_1-I_2)+e^{-b}\sum_{k=1}^{n}\frac{1}{k}\right\} ,$$

(G12b)

$$[\mathscr{A}^{(12)}]^{01} = -\frac{d}{16}(b-n)\left\{2(I_1-I_2)+e^{-b}\sum_{k=1}^{n}\frac{1}{k}\right\} ,$$

(G12c)

$$[\mathscr{A}^{(12)}]^{11}$$

$$= -\frac{d}{16}(b-m)(b-n)\left\{2(I_1-I_2)+e^{-b}\sum_{k=1}^{n}\frac{1}{k}\right\} ,$$

(G12d)

$$[\mathscr{A}^{(13)}]^{00} = -\frac{d}{16}\left\{2(I_1-I_2)+e^{-b}\sum_{k=1}^{m}\frac{1}{k}\right\} ,$$

(G13a)

$$[\mathscr{A}^{(13)}]^{10} = -\frac{d}{16}(b-m)\left\{2(I_1-I_2)+e^{-b}\sum_{k=1}^{m}\frac{1}{k}\right\} ,$$

(G13b)

$$[\mathscr{A}^{(13)}]^{01} = -\frac{d}{16}(b-n)\left\{2(I_1-I_2)+e^{-b}\sum_{k=1}^{m}\frac{1}{k}\right\} ,$$

(G13c)

$$[\mathscr{A}^{(13)}]^{11} = -\frac{d}{16}(b-n)(b-m)$$

$$\times\left\{2(I_1-I_2)+e^{-b}\sum_{k=1}^{m}\frac{1}{k}\right\} ,$$

(G13d)

$$[\mathscr{A}^{(14)}]^{00} = \frac{d}{4}\frac{1}{b}e^{-b} ,$$

(G14a)

$$[\mathscr{A}^{(14)}]^{10} = \frac{d}{4}\frac{1}{b}(b-m)e^{-b} ,$$

(G14b)

$$[\mathscr{A}^{(14)}]^{01} = \frac{d}{4}\frac{1}{b}(b-n)e^{-b} ,$$

(G14c)

$$[\mathscr{A}^{(14)}]^{11} = \frac{d}{4}\frac{1}{b}(b-m)(b-n)e^{-b} ,$$

(G14d)

$$[\mathscr{A}^{(15)}]^{00} = \frac{d}{8}\left\{\frac{1}{m+1}e^{-b} + \frac{(m+n-1)!}{b^{m+n}}[1-f_{m+n-1}]\right\},$$ (G15a)

$$[\mathscr{A}^{(15)}]^{10} = \frac{d}{8}\left\{\left[\frac{b-m}{m+1}-1\right]e^{-b} + n\frac{(m+n-2)!}{b^{m+n-1}}[1-f_{m+n-2}]\right\},$$ (G15b)

$$[\mathscr{A}^{(15)}]^{01} = \frac{d}{8}\left\{\left[\frac{b-n+1}{m+1}-1\right]e^{-b} + (m-1)\frac{(m+n-2)!}{b^{m+n-1}}[1-f_{m+n-2}]\right\},$$ (G15c)

$$[\mathscr{A}^{(15)}]^{11} = \frac{d}{8}\left\{\left[(b-m)\frac{b-n+1}{m+1}+\frac{1}{m+1}-b\right]e^{-b} + n(m-1)\frac{(m+n-3)!}{b^{m+n-2}}[1-f_{m+n-3}]\right\},$$ (G15d)

$$[\mathscr{A}^{(16)}]^{00} = \frac{d}{16}\left\{e^{-b} - m\frac{(m+n-1)!}{b^{m+n}}[1-f_{m+n-1}]\right\},$$ (G16a)

$$[\mathscr{A}^{(16)}]^{10} = \frac{d}{16}\left\{be^{-b} - mn\frac{(m+n-2)!}{b^{m+n-1}}[1-f_{m+n-2}]\right\},$$ (G16b)

$$[\mathscr{A}^{(16)}]^{01} = \frac{d}{16}\left\{[(b-n)+(m-1)]e^{-b} - m(m-1)\frac{(m+n-2)!}{b^{m+n-1}}[1-f_{m+n-2}]\right\}$$ (G16c)

$$[\mathscr{A}^{(16)}]^{11} = \frac{d}{16}\left\{[(b-m)(b-n)+(m-1)(b+1)]e^{-b} - nm(m-1)\frac{(m+n-3)!}{b^{m+n-2}}[1-f_{m+n-3}]\right\},$$ (G16d)

$$[\mathscr{A}^{(17)}]^{00} = \frac{d}{8}\left\{\frac{1}{n+1}e^{-b} + \frac{(m+n-1)!}{b^{m+n}}[1-f_{m+n-1}]\right\},$$ (G17a)

$$[\mathscr{A}^{(17)}]^{10} = \frac{d}{8}\left\{\left[\frac{b-m+1}{n+1}-1\right]e^{-b} + (n-1)\frac{(m+n-2)!}{b^{m+n-1}}[1-f_{m+n-2}]\right\},$$ (G17b)

$$[\mathscr{A}^{(17)}]^{01} = \frac{d}{8}\left\{\left[\frac{b-n}{n+1}-1\right]e^{-b} + m\frac{(m+n-2)!}{b^{m+n-1}}[1-f_{m+n-2}]\right\},$$ (G17c)

$$[\mathscr{A}^{(17)}]^{11} = \frac{d}{8}\left\{\left[(b-n)\frac{b-m+1}{n+1}+\frac{1}{n+1}-b\right]e^{-b} + m(n-1)\frac{(m+n-3)!}{b^{m+n-2}}[1-f_{m+n-3}]\right\},$$ (G17d)

$$[\mathscr{A}^{(18)}]^{00} = \frac{d}{16}\left\{e^{-b} - n\frac{(m+n-1)!}{b^{m+n}}[1-f_{m+n-1}]\right\},$$ (G18a)

$$[\mathscr{A}^{(18)}]^{10} = \frac{d}{16}\left\{[(b-m)+(n-1)]e^{-b} - n(n-1)\frac{(m+n-2)!}{b^{m+n-1}}[1-f_{m+n-2}]\right\}$$ (G18b)

$$[\mathscr{A}^{(18)}]^{01} = \frac{d}{16}\left\{be^{-b} - mn\frac{(m+n-2)!}{b^{m+n-1}}[1-f_{m+n-2}]\right\},$$ (G18c)

$$[\mathscr{A}^{(18)}]^{11} = \frac{d}{16}\left\{[(b-m)(b-n)+(n-1)(b+1)]e^{-b} - mn(n-1)\frac{(m+n-3)!}{b^{m+n-2}}[1-f_{m+n-3}]\right\},$$ (G18d)

$$[\mathscr{A}^{(19)}]^{00} = \frac{d}{16}\left\{X - h_{m+n-1} + e^{-b}\sum_{k=1}^{m}\frac{1}{k}\right\},$$ (G19a)

$$[\mathscr{A}^{(19)}]^{10} = \frac{d}{16}\left\{b[X-h_{m+n-1}] - m[X-h_{m+n-2}] + e^{-b}\left[(b-m)\sum_{k=1}^{m}\frac{1}{k}+1\right]\right\},$$ (G19b)

$$[\mathscr{A}^{(19)}]^{01} = \frac{d}{16}\left\{b[X-h_{m+n-1}] - n[X-h_{m+n-2}] + e^{-b}\left[(b-n)\sum_{k=1}^{m}\frac{1}{k}+1\right]\right\},$$ (G19c)

$$[\mathcal{A}^{(19)}]^{11} = \frac{d}{16} \left\{ b^2 [X - h_{m+n-1}] - (m+n)b[X - h_{m+n-2}] \right.$$

$$\left. + mn[X - h_{m+n-3}] + \left[(b-m)(b-n) \sum_{k=1}^{m} \frac{1}{k} + (2b - m - n + 1) \right] e^{-b} \right\} , \tag{G19d}$$

$$[\mathcal{A}^{(20)}]^{00} = \frac{d}{16} \left\{ X - h_{m+n-1} + e^{-b} \sum_{k=1}^{n} \frac{1}{k} \right\} , \tag{G20a}$$

$$[\mathcal{A}^{(20)}]^{10} = \frac{d}{16} \left\{ b[X - h_{m+n-1}] - m[X - h_{m+n-2}] + \left[(b-m) \sum_{k=1}^{n} \frac{1}{k} + 1 \right] e^{-b} \right\} , \tag{G20b}$$

$$[\mathcal{A}^{(20)}]^{01} = \frac{d}{16} \left\{ b[X - h_{m+n-1}] - n[X - h_{m+n-2}] + \left[(b-n) \sum_{k=1}^{n} \frac{1}{k} + 1 \right] e^{-b} \right\} , \tag{G20c}$$

$$[\mathcal{A}^{(20)}]^{11} = \frac{d}{16} \left\{ b^2 [X - h_{m+n-1}] - (m+n)b[X - h_{m+n-2}] \right.$$

$$\left. + mn[X - h_{m+n-3}] + \left[(b-m)(b-n) \sum_{k=1}^{n} \frac{1}{k} + (2b - m - n + 1) \right] e^{-b} \right\} . \tag{G20d}$$

APPENDIX H

The matrix elements $\langle j_\mu |_n^{n'} \rangle$ defined by Eq. (8.2) and (8.3) are zero unless z_α and q correspond per Eq. (7.4). The temporal components are given by

$$\langle \rho |_n^{n'} \rangle = \frac{L}{(2\pi 2^{n+n'} n! n'!)^{1/2}} e^{|z_\alpha|^2/4} \left[2 \frac{\partial}{\partial z_\alpha} \right]^{n'} \left[2 \frac{\partial}{\partial z_\alpha^*} \right]^n e^{-|z_\alpha|^2/2}$$

$$\underset{n \geq n'}{=} (-1)^{n'} L \left[\frac{n'!}{2\pi n!} \right]^{1/2} (-z_\alpha/\sqrt{2})^{n-n'} L_{n'}^{n-n'} (\tfrac{1}{2} |z_\alpha|^2) e^{-|z_\alpha|^2/4} , \tag{H1}$$

where the associated Laguerre polynomial is defined as usual by

$$L_n^m(x) = \frac{1}{n!} e^x x^{-m} \left[\frac{\partial}{\partial x} \right]^n [x^{n+m} e^{-x}] . \tag{H2}$$

The spatial components are given in terms of these by

$$\langle j_x |_n^{n'} \rangle = \frac{1}{\sqrt{8} i} \{ -\sqrt{n+1} \langle \rho |_{n+1}^{n'} \rangle + \sqrt{n} \langle \rho |_{n-1}^{n'} \rangle - \sqrt{n'+1} \langle \rho |_n^{n'+1} \rangle + \sqrt{n'} \langle \rho |_n^{n'-1} \rangle \} , \tag{H3}$$

and

$$\langle j_y |_n^{n'} \rangle = \frac{1}{\sqrt{8}} \{ \sqrt{n+1} \langle \rho |_{n+1}^{n'} \rangle + \sqrt{n} \langle \rho |_{n-1}^{n'} \rangle - \sqrt{n'+1} \langle \rho |_n^{n'+1} \rangle - \sqrt{n'} \langle \rho |_n^{n'-1} \rangle \} . \tag{H4}$$

The six matrix elements relevant to the calculations in this paper are given explicitly, with $b = \frac{1}{2} |z_\alpha|^2$, by

$$\langle \rho |_n^0 \rangle = \frac{L}{\sqrt{2\pi n!}} (-z_\alpha/\sqrt{2})^n e^{-b/2} , \tag{H5}$$

$$\langle j_x |_n^0 \rangle = \frac{L}{\sqrt{2\pi n!}} \frac{1}{\sqrt{8} i} \{ -(-z_\alpha/\sqrt{2})^{n+1} + [2n-b](-z_\alpha/\sqrt{2})^{n-1} \} e^{-b/2} , \tag{H6}$$

$$\langle j_y |_n^0 \rangle = \frac{L}{\sqrt{2\pi n!}} \frac{1}{\sqrt{8}} \{ (-z_\alpha/\sqrt{2})^{n+1} + [2n-b](-z_\alpha/\sqrt{2})^{n-1} \} e^{-b/2} , \tag{H7}$$

$$\langle \rho |_n^1 \rangle = -\frac{L}{\sqrt{2\pi n!}} (-z_\alpha/\sqrt{2})^{n-1} [n-b] e^{-b/2} , \tag{H8}$$

$$\langle j_x |_n^1 \rangle = \frac{L}{\sqrt{2\pi n!}} \frac{1}{\sqrt{8} i} \{ [n+2-b](-z_\alpha/\sqrt{2})^n - [2n(n-1) - 3nb + b^2](-z_\alpha/\sqrt{2})^{n-2} \} e^{-b/2} , \tag{H9}$$

and

$$\langle j_y |^1_n \rangle = \frac{L}{\sqrt{2\pi n!}} \frac{1}{\sqrt{8}} \{ -[n+2-b](-z_\alpha/\sqrt{2})^n - [2n(n-1)-3nb+b^2](-z_\alpha/\sqrt{2})^{n-2} \} e^{-b/2} \ . \tag{H10}$$

The matrix elements $\langle j_\mu |^{n'}_n \rangle$ may be used to generate a simple derivation of Eq. (3.29). Because the magnetoexciton basis is complete over the set of particle-hole pair excitations, we may write

$$\sum_k \sum_{k'} \varphi^*_{n'k'}(\mathbf{r}_2)\varphi_{nk}(\mathbf{r}_1) = \sum_\alpha \psi^{n'}_{n\alpha}(\mathbf{r}_1,\mathbf{r}_2) \ . \tag{H11}$$

Substituting this into Eq. (3.9), we obtain

$$\langle j^\mu_q j^\nu_{-q} \rangle_\omega = \sum_{\substack{n',k' \\ \text{filled}}} \sum_{\substack{n,k \\ \text{empty}}} \int \int \varphi^*_{n'k'}(1)\varphi^*_{nk}(2) \left\{ \frac{j^\mu(1)j^\nu(2)}{\omega-(n-n')+i\eta} + \frac{j^\nu(1)j^\mu(2)}{-\omega-(n-n')-i\eta} \right\} \varphi_{nk}(1)\varphi_{n'k'}(2)e^{i\mathbf{q}\cdot(\mathbf{r}_1-\mathbf{r}_2)} d1\, d2$$

$$= \sum_{\substack{n \text{ empty} \\ n' \text{ filled}}} \left\{ \frac{\langle j^\mu |^{n'}_n \rangle \langle j^\nu |^{n'}_n \rangle^*}{\omega-(n-n')+i\eta} + \frac{\langle j^\nu |^n_{n'} \rangle \langle j^\mu |^n_{n'} \rangle^*}{-\omega-(n-n')-i\eta} \right\} \ . \tag{H12}$$

Evaluation is further simplified by means of the relations

$$\langle \rho |^n_{n'} \rangle = \langle \rho |^{n'}_n \rangle^* \ , \tag{H13a}$$

$$\langle j^x |^n_{n'} \rangle = -\langle j^x |^{n'}_n \rangle^* , \quad \langle j^x |^n_{n'} \rangle = -\langle j^x |^{n'}_n \rangle^* \ . \tag{H13b}$$

The current-correction matrix elements defined by Eq. (8.5) are given for the case of $v=0$ by

$$\langle \delta j_x |^0_n \rangle_{(v=0)} = \frac{1}{\sqrt{2\pi n!}} \frac{1}{\sqrt{8}i} \left\{ \left[\frac{1}{n+1} - \frac{1}{b} \right] (-z_\alpha/\sqrt{2})^{n+1} + (b-n)(-z_\alpha/\sqrt{2})^{n-1} \right\} e^{-b/2} \ , \tag{H14}$$

$$\langle \delta j_y |^0_n \rangle_{(v=0)} = \frac{L}{\sqrt{2\pi n!}} \frac{1}{\sqrt{8}} \left\{ - \left[\frac{1}{n+1} - \frac{1}{b} \right] (-z_\alpha/\sqrt{2})^{n+1} + (b-n)(-z_\alpha/\sqrt{2})^{n-1} \right\} e^{-b/2} \ , \tag{H15}$$

and for the case of $v=\frac{1}{2}$ by

$$\langle \delta j_x |^0_n \rangle_{(v=\frac{1}{2})} = \frac{L}{\sqrt{2\pi n!}} \frac{1}{\sqrt{8}i} \left\{ \left[\frac{1}{n+1} - \frac{1}{b} \right] (-z_\alpha/\sqrt{2})^{n+1} + \frac{1}{2}(b-n)(-z_\alpha/\sqrt{2})^{n-1} \right\} e^{-b/2} \ , \tag{H16}$$

$$\langle \delta j_y |^0_n \rangle_{(v=\frac{1}{2})} = \frac{L}{\sqrt{2\pi n!}} \frac{1}{\sqrt{8}} \left\{ - \left[\frac{1}{n+1} - \frac{1}{b} \right] (-z_\alpha/\sqrt{2})^{n+1} + \frac{1}{2}(b-n)(-z_\alpha/\sqrt{2})^{n-1} \right\} e^{-b/2} \ , \tag{H17}$$

$$\langle \delta j_x |^1_n \rangle_{(v=\frac{1}{2})} = \frac{L}{\sqrt{2\pi n!}} \frac{1}{\sqrt{8}i} \left\{ \left[\frac{n}{b} + \frac{b}{n+1} - \frac{3}{2} \right] (-z_\alpha/\sqrt{2})^n \right.$$

$$\left. + \left[\frac{1}{2}b^2 - nb + \frac{1}{2}n(n-1)+1 \right] (-z_\alpha/\sqrt{2})^{n-2} \right\} e^{-b/2} \ , \tag{H18}$$

$$\langle \delta j_y |^1_n \rangle_{(v=\frac{1}{2})} = \frac{L}{\sqrt{2\pi n!}} \frac{1}{\sqrt{8}i} \left\{ - \left[\frac{n}{b} + \frac{b}{n+1} - \frac{3}{2} \right] (-z_\alpha/\sqrt{2})^n \right.$$

$$\left. + \left[\frac{1}{2}b^2 - nb + \frac{1}{2}n(n-1)+1 \right] (-z_\alpha/\sqrt{2})^{n-2} \right\} e^{-b/2} \ . \tag{H19}$$

The current-correction matrix elements also obey Eq. (H13b).

---

[1] C. B. Hanna, R. B. Laughlin, and A. L. Fetter, Phys. Rev. B **40**, 8745 (1989).

[2] C. B. Hanna, R. B. Laughlin, and A. L. Fetter, Phys. Rev. B **43**, 309 (1991).

[3] P. M. Platzman and P. A. Wolff, in *Solid State Physics*, edited by H. Ehrenreich, F. Seitz, and D. Turnbull (Academic, New York, 1973), Suppl. 13, p. 1.

[4] A. L. Fetter, C. B. Hanna, and R. B. Laughlin, Phys. Rev. B **39**, 9679 (1989).

[5] S. Doniach, *Green's Functions for Solid State Physicists* (Benjamin, Reading, MA, 1974).

[6] P. W. Anderson, Phys. Rev. **112**, 1900 (1958).

[7] A. L. Fetter and J. D. Walecka, *Quantum Theory of Many-Particle Systems* (McGraw-Hill, New York, 1971).

[8] A. L. Fetter, C. B. Hanna, and R. B. Laughlin, Int. J. Mod. Phys. 85, 2751 (1991); A. L. Fetter and C. B. Hanna, Phys. Rev. B 45, 2335 (1992).

[9] J. R. Schrieffer, *Theory of Superconductivity* (Benjamin, Reading, MA, 1964).

[10] D. Pines and P. Nozieres, *The Theory of Quantum Liquids* (Benjamin, New York, 1966).

[11] E. Feenberg, *Theory of Quantum Fluids* (Academic, New York, 1969).

[12] G. Baym and L. P. Kadanoff, Phys. Rev. 124, 287 (1961).

[13] X. C. Xie, Song He, and S. Das Sarma, Phys. Rev. Lett. 65, 649 (1990).

[14] A. G. Rojo and G. S. Canright, in *The Physics and Mathematics of Anyons*, edited by S. S. Chern, C. W. Chu, and C. S. Ting (World Scientific, Singapore, 1991), p. 65.

[15] J. D. Lykken, J. Sonnenschein, and N. Weiss, Phys. Rev. D 42, 2161 (1990); J. E. Hetrick, Y. Hosotani, and B.-H. Lee, Ann. Phys. (N.Y.) 209, 151 (1991).

[16] N. D. Mermin and H. Wagner, Phys. Rev. Lett. 17, 1133 (1966).

[17] J. M. Kosterlitz and D. J. Thouless, Prog. Low Temp. Phys. B 7, 371 (1978).

[18] Y. Kitazawa and H. Murayama, Phys. Rev. B 41, 11 101 (1990).

[19] G. Semenoff, Phys. Rev. Lett. 62, 715 (1989); S. Coleman and B. Hill, Phys. Lett. 159B, 1984 (1985).